UNCLASSIFIED

AD **273 876**

UNCLASSIFIED

273 876

Volume I

Symposium on

PERSONNEL ARMOR

U.S. Naval Research Laboratory
October 4 - 5, 1961

CONTENTS

PREFACE

The second Personnel Armor Symposium under auspices of the Department of Defense was held at the U. S. Naval Research Laboratory on 4 and 5 October 1961. The program was arranged so that papers presented on the first day were unclassified. The proceedings have been reproduced in two volumes, one unclassified and the other classified Secret.

Plans for the symposium were made in informal meetings with representatives of the Air Force, Army, Marine Corps and the Navy. Among those individuals contributing to planning of the program including subject categories, securing speakers, etc., were Dr. George R. Thomas and Mr. M. I. Landsberg, Quartermaster Research and Engineering Command; Mr. Melvin C. Miller, Office Chief of Ordnance, Dept. of the Army; Mr. Charles N. Gardner, Office of the Quartermaster General, Dept. of the Army; COL R. J. Oddy, USMC, Office of Naval Research; LTCOL H. A. Hadd, Hdq. U. S. Marine Corps; Dr. Sanford P. Thompson of NRL; and MAJ T. G. Snipes, USMC Liaison Officer at NRL.

Dr. G. R. Irwin, Dr. H. M. Trent, LTCOL Robert H. Bennett, and Mr. M. I. Landsberg, Chairmen of the four sessions, each deserves commendation for the outstanding manner in which they stimulated and provided guidance of discussions following the technical presentations. In order to provide for uninhibited exchange of information and ideas the discussions were not recorded.

I wish to express appreciation to the authors for submitting their papers in a form suitable for reproduction and in general for promptness in supplying the manuscript.

W. J. FERGUSON
General Chairman

ii

ADDRESS OF WELCOME

Dr. Peter King
Associate Director
U. S. Naval Research Laboratory
Washington 25, D. C.

Good Morning, and Welcome Members of the Symposium -----

First I must bring you the regrets of CAPT Krapf, our Director, who had planned to welcome you this morning. Unfortunately for the Symposium, he was more or less summoned to the Bureau of Budget for one of the reviews which all of us must go through these days. When the Budget Bureau wants to discuss things there seems to be no way of avoiding the call. I can assure you that he would much rather be here, and I can assure you further that he would be more apt than I am in giving a welcome to all of you, although it would be no more sincere than mine. Many of you have in the past visited the Laboratory for other reasons, and we are happy to have you return.

The second annual meeting of the Department of Defense Personnel Armor Symposium is more than welcome to the Naval Research Laboratory. In reality there have been more than two meetings, but not on a formal basis as they are now organized. It is our good fortune to act as hosts for this second meeting. Not long ago I looked at the report of the First Armor Symposium, held a bit over a year ago at Natick, and once again was impressed with the kind of work done, the great effort put into personnel armor, and a bit of its effectiveness. Today, we will not hear from representatives of DOD, therefore, I hope you won't mind my taking a few minutes to speak generally about this subject.

My introduction to body or personnel armor came through Dr. Irwin, who is Chairman for the first session today. During World War II, George had me working with him on Doron. Since that time I have followed the field somewhat, but not in great detail. The original use of the material seemed to be as flak curtains and other armor to protect flyers. Its use as personnel armor, outside of helmets, seemed to have reached its climax during the Korean War, where, as stated at your meeting last year, both the Marine Corps and Army felt that it reduced casualties by 10%. Its use there left no doubt as to its tremendous importance, both physically and mentally to the

iii

1

individual fighting man, and thus to the entire Nation as well. Since the early days of plastic armor up to the present time, there have been no really startling improvements. The gain has been a matter of a few percent, where an order of magnitude is badly needed. The Advisory Group to help guide the development of personnel armor, wisely recommended that money should be put into materials, fibers for example, with strikingly improved strength. Although over the years the Army has been the major contributor of funds, it was the Marine Corps who came through with the money to let some contracts for the development of really high strength material. The fact that the Corps was willing to invest something of the order of 5% of its total budget in this field, I think, is the best testimony of the value it places on personnel armor. The Marine Corps' objective in employing personnel armor is to maintain the maximum number of men combat effective on the battle field. To this end they have maintained continuous, active interest in improving body armor. The Army is responsible, too, for retaining the maximum number of men effective on a battle field, and, thus, has an interest in body armor; also, all sorts of protective clothing, gas masks, and cold weather gear are part of the over-all picture, but today the Symposium is concerned with all aspects of armor. Any improvement made here will undoubtedly be valuable in some of the other kinds of clothing. There is here a rich field, but unless a really important improvement is made, a great deal of effort will have been wasted. Funds have been budgeted for fundamental work in materials. When the improved materials become available, the designer can reduce the weight necessary for protection and, thus, again increase the effectiveness of the man.

Today, with our increased emphasis on preparation for limited war, the subject which you are gathered to explore, seems more important than it did even a year ago. Anything which will help Army, Navy, Marine Corps, and Air Force to improve its position in limited war is certainly of national concern. The fact that you are here indicates that you, too, are concerned. Whether we are successful in having a really important improvement depends upon you.

Although recognizable advances have been made during the years covered by these sessions, it would be well on occasion to look to the future and think about those improvements which would be helpful toward increasing our military posture. Some of these are: (1) a significant improvement in the ballistic resistance of armor materials, (2) a more complete understanding of the effects of wounds on the ability of a foot soldier to perform defined, and perhaps limited, functions, (3) the establishment of more definitive criteria for the protection needed under various tactical situations such as brush warfare, atomic attack, and bacteriological warfare, and (4) the development of a more definitive policy on how and when personnel armor is to be employed.

Once again let me repeat, we are happy to be the hosts for the Symposium. We feel the subject matter has increased in importance in the past few months, and hope that this exchange of information will

lead to an accelerated program in this field.

INTRODUCTION OF DR. GEORGE IRWIN ------

The Chairman for your first session is Dr. George Irwin of our Laboratory, Superintendent of the Mechanics Division. Dr. Irwin has been interested in armor for many years. As a matter of fact, during World War II he went to Okinawa before the shooting was over to gather some data first hand on the effectiveness, both of our hand grenades and armor. George is a man who had spent a long time in ballistics, measuring velocities and small intervals of time. However, on his return from Okinawa I remember speaking with him, and he told me that he had finally found an interval of time too short to be measured. I couldn't imagine what it was, and had to ask him for the explanation. He said that it was the interval between the cry of 'halt' from a Marine and the shot that followed.

CHARACTERIZATION OF TEXTILE YARNS FOR USE
UNDER BALLISTIC IMPACT CONDITIONS

Jack C. Smith
Textiles Section
National Bureau of Standards
Washington 25, D. C.

Of the various types of flexible personnel armor that have been developed, one of the simplest consists of a series of layers of heavy cloth. This type of armor is surprisingly effective when the cloth is made from a suitable material, such as high-tenacity nylon. In the development of this armor, many kinds of materials, different kinds of weaves, different finishing treatments, different types of construction, and other variations have been tested. Thus it should now be possible in the design of personnel armor to incorporate improvements resulting from this vast empirical development program. From this point of view further improvement depends mostly upon the use of materials superior to those used at present.

However, it is also possible that improvements could result from a better understanding of the mechanism by which the armor material is able to absorb the energy of a shrapnel fragment traveling at ballistic velocities. The problem posed here is extremely complicated, but at least some of its simpler aspects are now understood. This paper deals with one of these aspects; namely, the behavior of a long textile yarn struck transversely by a high speed projectile. Theories required for understanding this behavior have been developed by Taylor, von Karman and others, and have been reviewed and extended in a series of papers by the author [1-4].

Analysis of the transverse impact problem has provided a better understanding of how strain energy is propagated along a filament, and has introduced the concepts of longitudinal and transverse critical velocities. The ideas discussed have wide applicability and can be profitably used to guide further research.

LONGITUDINAL IMPACT THEORY

Before discussing the problem of transverse impact, it will be necessary to consider the case of a long filament impacted in

tension at one end. Consider, therefore, a semi-infinite filament lying along the positive X axis with one end at the origin. It is assumed that the tension-strain curve applicable under the impact conditions being considered, is known for this filament. In addition it is assumed that this tension-strain curve is always concave downward. Let the end of the filament at the origin be impacted with velocity v in the negative direction. The impact causes a wave of variable strain to propagate longitudinally in the positive direction along the filament. This wave may be visualized as a train of infinitesimal wavelets, each wavelet traveling at a different velocity and adding an increment of strain to the wave. For example, in figure 1 the strain wave is represented schematically by a region of varying filament diameter.

The initial wavelet, or strain wave front is propagated with velocity C_0, given by the equation

$$C_0 = \sqrt{\frac{1}{M}\left(\frac{dT}{d\varepsilon}\right)}_{\varepsilon = 0} \tag{1}$$

where T is the tension or total force sustained by the filament and is given as a function of the strain ε by the tension-strain curve. M is the mass per unit length of the unstrained filament. The slope of the tension-strain curve in this case is evaluated at zero strain ($\varepsilon = 0$).

The velocity of each succeeding wavelet is proportional to the square root of the slope of the tension-strain curve evaluated at the strain value of the wavelet. In order that the wavelets do not overtake each other, the slope of the tension-strain curve must decrease as the strain increases. (The curve must be concave downward.) The final wavelet in the train propagates with velocity C_1 given by

$$C_1 = \sqrt{\frac{1}{M}\left(\frac{dT}{d\varepsilon}\right)}_{\varepsilon = \varepsilon_1} \tag{2}$$

The velocities at which the wavelets travel are expressed relative to a Lagrangian system of coordinates; i.e., a system fixed to the filament moving and extending with it. Filament material in the wake of the final wavelet is under constant strain ε_1.

In the wake of each wavelet, material flows backward toward the point of impact at a velocity that increases as each wavelet passes. The particle velocity W_1 at which filament material in the final wavelet flows is given by

$$W_1 = \int_0^{\varepsilon_1} \sqrt{\frac{1}{M}\left(\frac{dT}{d\varepsilon}\right)}\, d\varepsilon = \int_0^{\varepsilon_1} C(\varepsilon)\, d\varepsilon \tag{3}$$

This velocity is the same as the impact velocity if ε_1 does not exceed the breaking strain. In fact, the maximum strain in the

2

filament ε_1 achieved as a result of longitudinal impact of velocity W_1 is found by solving equation (3).

When the strain ε_1 is just equal to the breaking strain ε_b the corresponding impact velocity becomes the critical velocity W_c, or lowest velocity at which the filament breaks immediately upon impact. Thus this longitudinal critical velocity may be defined as

$$W_c = \int_o^{\varepsilon_b} \sqrt{\frac{1}{M}\left(\frac{dT}{d\varepsilon}\right)} \, d\varepsilon \tag{4}$$

From this definition it is possible to calculate the critical velocity if the tension-strain curve valid for critical velocity impact is known, and if this tension-strain curve is always concave downward, or if the curve is linear. If the tension-strain curve has a concave upward position, a modified form of equation (4) must be applied. This modification is discussed in a recent paper by the author [5].

TRANSVERSE IMPACT THEORY

Consider now the problem of transverse impact. As in the case of longitudinal impact, the filament is required to have a concave downward tension-strain curve valid under the impact conditions considered. When the filament is struck transversely by a projectile, two longitudinal strain waves are initiated which propagate in opposite directions away from the point of impact. In the region between the two wave fronts, material of the filament is set into motion towards the point of impact. This inward-flowing material forms itself into a transverse wave shaped like an inverted "V" with the impacting projectile at the vertex. The configuration of the filament at a time t after impact is shown in figure 2.

To understand what happens in the filament, let us look at the sequence of events as they would appear to a filament particle at a distance X from the point of impact as measured along the unstrained filament. Let the filament lie horizontally and be impacted at velocity V in the vertical direction. After impact, the particle does not experience any effects until the strain wave front reaches it at a time X/C_o later. At this time the filament in the region of the particle becomes strained and starts to move horizontally toward the point of impact. As time goes on, the strain at the particle and the inward flow velocity increase. The wavelet for the maximum strain reaches the particle at time X/C_1. At this time the strain has become ε_1 and the inward flow velocity W_1. Mathematical expressions for C_o, C_1, and W_1 are given by equations (1), (2), and (3).

After the strain wave has passed, the strain and velocity of horizontal flow of the particle remain constant until time X/U_1. This is the time of arrival of the transverse wave front; at this instant the particle stops moving horizontally and moves abruptly in the vertical direction at impact velocity V. The strain ε_1 at the

3

particle remains constant. The velocity U_1 of the transverse wave front relative to a Lagrangian coordinate system can be found from the formula

$$U_1 = \sqrt{\frac{T_1}{M(1 + \varepsilon_1)}} \qquad (5)$$

The tension T_1 to be used is found from the tension-strain curve.

If the mass per unit length M, and the tension-strain curve are known, the strain wave front velocity C_0 can be found from equation (1). However, the velocities C_1, W_1, and U_1, defined by equations (2), (3), and (4), can be expressed only as functions of the unknown strain ε_1. Another relationship is needed in order that the value of ε_1 may be found in terms of the known velocity V and the other known quantities. This relationship is [3,4]

$$V = \sqrt{(1 + \varepsilon_1)^2 \, U_1^2 - [(1 + \varepsilon_1) \, U_1 - W_1]^2} \qquad (6)$$

Equation (6) has several interesting uses. For instance, in one application, a longitudinal impact velocity W_1 can be found that will produce a strain distribution along the filament equivalent to that produced by a transverse impact at velocity V. Again, it should be noted that when the strain resulting from an impact is the breaking strain ε_b, W_1 becomes the longitudinal critical velocity W_c, and V becomes V_c the transverse critical velocity or lowest velocity at which the filament will break immediately upon transverse impact. This velocity is given by

$$V_c = \sqrt{(1 + \varepsilon_b)^2 \, U_b^2 - [(1 + \varepsilon_b) \, U_b - W_c]^2} \qquad (7)$$

where U_b is found by substituting values of the breaking strain ε_b and breaking tension T_b into equation (5).

POWER ABSORPTION IN A FILAMENT STRUCK TRANSVERSELY

When a filament is struck transversely by a flying projectile, energy of the projectile is converted in the filament to strain energy, kinetic energy of flow in the direction of the filament, and kinetic energy of transverse motion in the V-shaped wave. To calculate these different energy components, consider first the strain distribution along a semi-infinite filament t seconds after tensile impact at one end at velocity W_1. This strain distribution is depicted in figure 3. Here the strain ε is plotted for points X along the length of the filament. Distances along the filament are expressed relative to a Lagrangian coordinate system. In this figure it is seen that a wavelet increasing the strain by an increment $d\varepsilon$ travels a distance Ct, and causes the filament to increase in length by an amount $Ctd\varepsilon = tdW$, where dW is the increase in particle velocity. Because of a tensile force T acting along the filament the strain energy is increased by an amount $tTdW$. The total strain

energy in the filament is therefore equal to

$$t \int_0^{\varepsilon_1} T \frac{dW}{d\varepsilon} d\varepsilon.$$

By a similar argument it can be shown that the kinetic energy of longitudinal motion given to the filament is

$$t \int_0^{\varepsilon_1} MCW \frac{dW}{d\varepsilon} d\varepsilon = t \int_0^{\varepsilon_1} W \frac{dT}{d\varepsilon} d\varepsilon.$$

In the case of transverse impact there is no longitudinal flow of filament material in the region taken up by the transverse wave, so that the above expression must be corrected by subtracting the quantity $1/2 \ MU_1 tW_1^2$.

The kinetic energy of transverse motion in one side of the V-shaped wave is given by $1/2 \ MU_1 tV^2$.

If the above quantities are summed up, taking into account the strain and kinetic energies on both sides of the point of impact, and the result divided by t, the following expression is obtained for P, the initial rate at which energy is absorbed by the filament:

$$P = 2 \int_0^{\varepsilon_1} T \frac{dW}{d\varepsilon} d\varepsilon + 2 \int_0^{\varepsilon_1} W \frac{dT}{d\varepsilon} d\varepsilon - MU_1 W_1^2 + MU_1 V^2 \qquad (8)$$

Equation (8) can be simplified to the form

$$P = 2MU_1 V^2 \qquad (9)$$

by use of the relation

$$MU_1 tV^2 = 2t \int_0^{\varepsilon_1} T \frac{dW}{d\varepsilon} d\varepsilon + 2t \int_0^{\varepsilon_1} W \frac{dT}{d\varepsilon} d\varepsilon - MU_1 tW_1^2 \qquad (10)$$

This interesting relation, which states that the sum of the strain energy and longitudinal kinetic energy in the filament is equal to the kinetic energy of transverse motion, is easily proved as follows: From equation (6) it is seen that

$$MU_1 V^2 = MU_1 [2(1 + \varepsilon_1)U_1 W_1 - W_1^2] = 2M(1 + \varepsilon_1)U_1^2 W_1 - MU_1 W_1^2 \qquad (11)$$

Therefore it is only necessary to show that

$$2 \int_0^{\varepsilon_1} T \frac{dW}{d\varepsilon} d\varepsilon + 2 \int_0^{\varepsilon_1} W \frac{dT}{d\varepsilon} d\varepsilon = 2M(1 + \varepsilon_1) U_1^2 W_1 \qquad (12)$$

The left hand side of equation (12) reduces to the form

$$2 \int_{0}^{T_1 W_1} d(TW) = 2 T_1 W_1,$$ and the right hand side, upon using equation

(5), becomes $2M(1 + \varepsilon_1) \dfrac{T_1}{M(1 + \varepsilon_1)} W_1 = 2 T_1 W_1,$ so that equation (12)

and therefore equation (10) is proved.

THE SELECTION OF TEXTILE YARNS FOR PERSONNEL ARMOR

The function of personnel armor is to absorb the energy from an impinging projectile. The armor should be effective against projectiles of very high speed and should utilize the least weight of armor material possible. The effectiveness of armor composed of woven textile yarns will depend upon the construction as well as upon the yarn material used, but the analysis of construction effects is beyond the scope of this paper although its great importance is recognized. In the following discussion, therefore, the characteristics of yarn most suitable for absorbing transverse impact are determined. It is assumed that yarns exhibiting these characteristics will be most effective for use in personnel armor.

A yarn is most effective in stopping a projectile if it absorbs energy from transverse impact at a higher rate and at higher impact velocities than other yarns. The average rate of absorption is roughly proportional to the initial rate given by equation (9). Upon dividing both sides of this equation by M, it is seen that the initial rate of energy absorption per unit mass of yarn material is proportional to $U_1 V^2$. Thus it appears that a yarn effective in absorbing transverse impact must have a high transverse critical velocity V_c. The high value of U_1 which is also required means that the transverse wave front propagates rapidly, and the forward motion of the projectile is rapidly distributed over a long length of yarn on both sides of the point of impact.

If the value of U_1 given by equation (5) is substituted into equation (9), it is seen that the initial rate of energy absorption per unit mass is proportional to $V^2 \sqrt{T_1 / M(1 + \varepsilon_1)}$. It should be noted at this point that yarn fineness is customarily expressed in terms of linear density. For instance, a yarn or filament of 1 tex fineness weighs one gram per 1000 meters of length. Thus a quantity T_b/M, where T_b is the yarn tension at break, is proportional to the breaking tenacity expressed in units such as grams per tex. From the expression above it is apparent that a yarn effective in absorbing transverse impact energy must have a high breaking tenacity. The most effective yarn, then, is the one having the highest transverse critical velocity, and one which at the same time has the highest breaking tenacity.

An interesting question could be posed at this point. Suppose that a variety of yarns is available, each yarn with a different

6

stress-strain curve, but having the same breaking tenacity and the same breaking elongation. Which of these yarns has the greatest transverse critical velocity? It turns out to be the yarn with the stress-strain curve that is most nearly linear.

The proof of this statement is simplified by the following two observations. First of all it should be noted that in equation (7) for the transverse critical velocity, the value of U_b depends only on the breaking tenacity and breaking elongation and thus is the same for each of the curves in the family considered. The transverse critical velocity V_c for any one curve therefore depends only on the longitudinal critical velocity W_c, being large or small as W_c is large or small. Secondly, the stress-strain curves considered may be limited to those that are everywhere concave downward. This is because, in the calculation of longitudinal critical velocity, a concave-upward portion in a stress-strain curve is replaced by a straight line so that the resulting curve is everywhere concave downward [5].

It remains then to prove that longitudinal critical velocity computed from a linear stress-strain curve is greater than that computed from any other stress-strain curve having the same breaking elongation and breaking tenacity. This proof is given in Appendix A. An interesting corollary to this theorem states that, for a family of linear stress-strain curves having the same breaking tenacity, that curve with the greatest breaking elongation has the greatest longitudinal and transverse critical velocities. This follows because any curve with a breaking elongation less than the maximum may be continued at zero slope to the maximum elongation. The zero slope portion does not contribute to the critical velocity integral. Thus the curve becomes a member of a family of curves having the same breaking elongation and breaking tenacity. The longitudinal and transverse critical velocities for this curve are therefore less than the corresponding ones for the linear curve having the maximum breaking elongation.

In order to make the above statements clearer consider the curves depicted in figure 4. Here the stress-strain curves 1, 4, and 5 are part of a family of curves having the same breaking tenacity and breaking elongation. Curve 5 has the greatest longitudinal and transverse critical velocities. Curves 3 and 5 are linear curves having the same breaking tenacity. Curve 5 with the greater breaking elongation has the greater longitudinal and transverse critical velocities. The longitudinal and transverse critical velocities for curve 4 probably exceed those for curve 2 but this has not been proved.

It is likely that the longitudinal and transverse critical velocities for the curve 1 are closer in value to those of curve 3 than those of curve 5. A textile material having a stress-strain curve similar to curve 1 could probably be improved by use of a greater draw ratio during the manufacturing process. The resulting

7

yarn would have a greater breaking tenacity, a decreased breaking elongation, and its stress-strain curve would be more linear. Increased longitudinal and transverse critical velocities should result if the new drawing conditions are not too extreme.

The principles just developed are illustrated by the three textile yarns having the stress-strain curves given in figure 5. These stress-strain curves were obtained by a method involving high-speed photography of the yarns during transverse impact at velocities of approximately 40 m/sec. Details of the method have been published previously [6]. The transverse critical velocities for these yarns are of the order of 500 m/sec, an order of magnitude greater than the velocities employed in obtaining the stress-strain curves. Therefore critical velocities obtained from these curves must be regarded as approximations. They are, however, the best estimates available at present.

The stress-strain curve for the glass fiber yarn is linear and has a very steep slope. The breaking tenacity is high but the breaking elongation is very low. The rayon tire yarn has a curve that bends appreciably towards the strain axis. The breaking tenacity is low but the breaking elongation is very high. The curve for high-tenacity nylon is approximately linear, the slope is moderate, the breaking tenacity high, and the breaking elongation moderate. More complete data on these yarns may be found in Tables 1 and 2.

In figure 6 the tensile stresses corresponding to various transverse impact velocities are plotted for these yarns. It is apparent from the plots that the glass fiber yarn develops the highest stress for all impact velocities up to a transverse critical velocity of 433 m/sec. Rayon tire yarn develops less stress but has the higher transverse critical velocity of 574 m/sec. The high-tenacity nylon yarn does not develop much greater stress at the lower impact velocities, but it has a high transverse critical velocity of 685 m/sec. It is interesting to note from Table 2 that despite the difference in transverse critical velocities for the nylon and rayon yarns, the longitudinal critical velocities are about the same. According to equation (7) this difference in the transverse critical velocities depends upon a difference in U_b which in turn depends upon the different breaking tenacities of the two yarns.

The numbers placed at various points along the curves of figure 6 denote the maximum percent strains developed in the yarns at the corresponding impact velocities. In the case of the glass fiber it can be seen that the yarn does not deform very much during the energy absorption process. It is interesting to note that for impact velocities near 350 m/sec the glass fiber yarn develops a strain of 2%, nylon yarn a 5% strain, and rayon yarn a 10% strain.

In figure 7 the initial power absorptions (initial rate of energy absorption) corresponding to different impact velocities are

plotted for the glass fiber, nylon and rayon yarns. It is seen from this plot that the nylon yarn with its approximately linear stress-strain curve, high breaking tenacity, and high transverse critical velocity is most effective at absorbing energy from a projectile, especially at the higher impact velocities. At the lower velocities the glass fiber yarn is most effective because of its steep linear stress-strain curve.

In order to provide a better idea of the capabilities of representative textile yarns, data on yarns in addition to those discussed are presented in Tables 1 and 2. More complete data on these yarns may be obtained in previous publications [5,7]. The yarns may be identified by the code letter given in parentheses beside each name.

It is interesting to compare the data in Table 2 for polyester yarn with that for glass fiber. These two yarns have approximately the same breaking tenacity and stress-strain curves that are closely linear. However, the polyester yarn has a greater breaking elongation and consequently greater longitudinal and transverse critical velocities, in agreement with the corollary discussed previously.

Of the two vinal yarns, the one of moderate tenacity has the greater longitudinal and transverse critical velocities. This illustrates how the properties of a yarn material may be optimized by the proper manufacturing process.

The high-tenacity vinal yarn is evidently superior to the glass fiber yarn in initial power absorption at low impact velocities, because its initial modulus is greater. Also the transverse and longitudinal critical velocities for the high tenacity vinal yarn are the greater.

The moderate tenacity vinal yarn has almost the same transverse critical velocity as the high tenacity nylon. It is slightly superior to nylon in initial power absorption at low impact velocities but loses this advantage at the higher velocities. It, however, might well provide a satisfactory substitute for nylon as a personnel armor material. A modified acrylic fiber might also be used as a nylon substitute.

SUMMARY

The selection of superior fibrous materials for use in personnel armor can be guided by results derived from theories on transverse impact of textile yarns at ballistic velocities. These theories show how the kinetic energy of an impacting projectile is converted into strain and kinetic energy in the yarn and diffused away from the point of impact by wave propagation. The initial rate of energy absorption by the yarn can be computed for transverse impact velocities up to the transverse critical velocity, if the

stress-strain curve for the yarn valid under the impact conditions is known. At the transverse critical velocity the yarn attains its breaking strain immediately upon impact and breaks at the point of impact without absorbing any appreciable energy.

The value of the transverse critical velocity can be computed from the stress-strain curve of the yarn. To some extent the magnitude of the transverse critical velocity depends upon the shape of the stress-strain curve. For instance, the transverse critical velocity is greater for a linear stress-strain curve than for any other curve having the same breaking elongation and breaking tenacity. Also, in the case of linear stress-strain curves having the same breaking tenacity, the curve with the greatest breaking elongation has the greatest transverse critical velocity. These two principles may be of value in determining how a yarn material can be modified in the manufacturing process to be most effective for use in personnel armor.

For transverse velocities less than the transverse critical velocity, the initial rate of energy absorption by a yarn is proportional to the square of the impact velocity and to the square root of the stress developed at that impact velocity. Thus it appears that the yarn most effective for use in personnel armor should have the highest breaking tenacity possible consistent with a high transverse critical velocity. The stress-strain curve for such a yarn will be approximately linear.

REFERENCES

1. G. I. Taylor, The plastic wave in a wire extended by an impact load. British Ministry of Home Security Report R.C. 329 (1942).

2. T. von Karman and P. Duwez, The propagation of plastic deformation in solids. J. Appl. Phys. 21, 987 (1950).

3. J. C. Smith, F. L. McCrackin, and H. F. Schiefer, Stress-strain relationships in yarns subjected to rapid impac' loading: 5. Wave propagation in long textile yarns impacted transversely. J. Research NBS 60, 517 (1958), Textile Research J. 28, 288 (1958).

4. J. C. Smith, F. L. McCrackin, and H. F. Schiefer, Characterization of the high-speed impact behavior of textile yarns. Journal of the Textile Institute 50, T55 (1959).

5. J. C. Smith, J. M. Blandford, and K. M. Towne, Stress-strain relationships in yarns subjected to rapid impact loading: 8. Shock waves, limiting breaking velocities and critical velocities. To be published in Textile Research J. 1961-62.

6. J. C. Smith, F. L. McCrackin, H. F. Schiefer, W. K. Stone, and K. M. Towne, Stress-strain relationships in yarns subjected to rapid impact loading: 4. Transverse impact tests. J. Research NBS 57, 83 (1956), Textile Research J. 26, 821 (1956).

7. J. C. Smith, P. J. Shouse, J. M. Blandford, and K. M. Towne, Stress-strain relationships in yarns subjected to rapid impact loading: 7. Stress-strain curves and breaking-energy data for textile yarns. Textile Research J. 31, 721 (1961).

Table 1*

Description of Yarns and Test Conditions for
Data Given in Table 2

(A) Acetate, bright, 16.7 tex, 16 filament, stretch ratio 1.09
Transverse impact, 42 m/sec, 7300 %/sec rate of straining.

(E) Polyester, bright, 6.7 tex, 34 filament, 3.61X draw ratio
Transverse impact, 42 m/sec, 4100 %/sec rate of straining.

(F) Glass fiber, D 450-4/3, 141 tex, continuous filament, 4.4 S twist
Transverse impact, 39 m/sec, 1800 %/sec rate of straining.

(H) Vinal, 54.3 tex, 600 filament
Transverse impact, 38 m/sec, 3000 %/sec rate of straining.

(I) Vinal, 83 tex, 600 filament
Transverse impact, 40 m/sec, 5000 %/sec rate of straining.

(J) Nylon, high tenacity, bright, 93.3 tex, 140 filament, 1/2 Z twist
Transverse impact, 41 m/sec, 4800 %/sec rate of straining.

(K) Acrylic, semi dull, 16.7 tex, 80 filament, 8X draw ratio
Transverse impact, 41 m/sec, 5100 %/sec rate of straining.

(P) Rayon tire yarn (experimental), 199 tex, 980 filament, 4.2Z twist
Transverse impact, 41 m/sec, 6500 %/sec rate of straining.

(S) Braided silk fishing line, 24 lb test, approximately 330 tex
Transverse impact, 39 m/sec, 5300 %/sec rate of straining.

---

*More complete data for the yarns in this table are published elsewhere [5,7], and may be identified by means of the code letter given in parentheses.

Table 2

High Velocity Impact Data for Some Textile Yarns

Yarns	Initial Tensile Modulus g/tex	Breaking Elongation %	Breaking Tenacity g/tex	Longitudinal Critical Velocity m/sec	Transverse Critical Velocity m/sec
(A) Acetate	350	30.7	14.6	165	340
(E) Polyester	1000	8.0	60.5	221	558
(F) Glass fiber	2470	2.6	63.1	127	433
(H) Vinal, high tenacity	2760	5.3	82.0	202	573
(I) Vinal, moderate tenacity	1130	14.3	63.9	219	677
(J) Nylon, high tenacity	360	11.1	81.4	297	685
(K) Acrylic	1020	14.6	60.6	287	625
(P) Rayon tire yarn	550	22.9	42.1	297	574
(S) Braided silk fishing line	490	17.9	42.3	256	549

More complete data including stress-strain curves may be found in other publications [5,7]. The yarns may be identified by the code letter given in parentheses.

APPENDIX

Proof That the Longitudinal Critical Velocity Computed
From a Linear Stress-Strain Curve is Greater Than That
Computed From any Other Concave Downward Stress-Strain
Curve Having the Same Breaking Elongation and Breaking
Tenacity.

In figure 8, let ORQ be the linear stress-strain curve, and
OPQ be any other concave downward stress-strain curve having the same
breaking elongation ε_b and breaking tenacity T_b. Let the curve OPQ
be approximated by a number of infinitesimal straight line segments
having slopes m_{01}, m_{12}, m_{23}, ... m_{kl} ..... etc. where $l = k + 1$.
Let the values of strain at each junction of the line segments be
designated by ε_1, ε_2, ... ε_k, ε_l, ... and the infinitesimal
strain increments be designated by $\Delta\varepsilon_{01}$, $\Delta\varepsilon_{12}$, $\Delta\varepsilon_{23}$, ... $\Delta\varepsilon_{kl}$,
..... etc. Let the slope of the linear stress-strain curve be m_0,
and let the secants drawn between the junctions of the infinitesimal
segments and the point Q have the slopes m_1, m_2, m_3, ... m_k,
m_l ..... etc.

By definition the longitudinal critical velocity for the
linear curve ORQ is

$$W_0 = M^{-1/2} \, m_0^{1/2} \, \varepsilon_b \tag{1A}$$

Let W_{kl} and W_k represent the quantities

$$W_{kl} = M^{-1/2} \, m_{kl}^{1/2} \, \Delta\varepsilon_{kl} \tag{2A}$$

$$W_k = M^{-1/2} \, m_k^{1/2}(\varepsilon_b - \varepsilon_k) \tag{3A}$$

It is obvious from figure 8 that the following relationship holds:

$$m_{kl}\Delta\varepsilon_{kl} + m_l(\varepsilon_b - \varepsilon_l) = m_k(\varepsilon_b - \varepsilon_k) \tag{4A}$$

Also note that

$$\varepsilon_b - \varepsilon_l = \varepsilon_b - \varepsilon_k - \Delta\varepsilon_{kl} = (\varepsilon_b - \varepsilon_k)\left[1 - \frac{\Delta\varepsilon_{kl}}{\varepsilon_b - \varepsilon_k}\right] \tag{5A}$$

Consider the quantity

$$M^{1/2}(W_{kl} + W_l) = m_{kl}^{1/2}\Delta\varepsilon_{kl} + m_l^{1/2}(\varepsilon_b - \varepsilon_l)$$

By substitution using equations 3A, 4A, and 5A this quantity becomes

13

$$M^{1/2}(W_{k\ell} + W_\ell) = m_{k\ell}{}^{1/2}\Delta\varepsilon_{k\ell}$$

$$+ m_k{}^{1/2}\left[1 - \frac{m_{k\ell}}{m_k}\frac{\Delta\varepsilon_{k\ell}}{\varepsilon_b - \varepsilon_k}\right]^{1/2}\left[1 - \frac{\Delta\varepsilon_{k\ell}}{\varepsilon_b - \varepsilon_k}\right]^{-1/2}(\varepsilon_b - \varepsilon_k)\left[1 - \frac{\Delta\varepsilon_{k\ell}}{\varepsilon_b - \varepsilon_k}\right]$$

After an expansion in which only linear terms are retained, this quantity becomes

$$M^{1/2}(W_{k\ell} + W_\ell) = m_{k\ell}{}^{1/2}\Delta\varepsilon_{k\ell}$$

$$+ m_k{}^{1/2}(\varepsilon_b - \varepsilon_k)\left[1 - \frac{1}{2}\left(\frac{m_{k\ell}}{m_k} + 1\right)\frac{\Delta\varepsilon_{k\ell}}{\varepsilon_b - \varepsilon_k}\right]$$

$$= m_{k\ell}{}^{1/2}\Delta\varepsilon_{k\ell} + M^{1/2}W_k - \frac{1}{2}m_k{}^{1/2}\left(\frac{m_{k\ell}}{m_k} + 1\right)\Delta\varepsilon_{k\ell}$$

So that

$$M^{1/2}(W_k - W_{k\ell} - W_\ell) = \left[\frac{1}{2}\left(\frac{m_{k\ell}}{m_k} + 1\right)m_k{}^{1/2} - m_{k\ell}{}^{1/2}\right]\Delta\varepsilon_{k\ell} \qquad (6A)$$

It is obvious from figure 8 that $m_{k\ell} > m_k$ so that $m_{k\ell}$ in equation (6A) can be replaced by pm_k, where p is a number greater than unity. The right hand side of equation (6A) thus becomes $\left[\frac{1}{2}(p + 1) - p^{1/2}\right]m_k{}^{1/2}\Delta\varepsilon_{k\ell}$ which is always positive. Therefore

$$W_k - W_\ell - W_{k\ell} > 0 \qquad (7A)$$

If n is the number of infinitesimal segments into which the curve OPQ is divided, then from equation (7A)

$$\sum_{k=0}^{n}(W_k - W_\ell) > \sum_{k=0}^{n}W_{k\ell} \qquad (8A)$$

Note, however, that

$$W_o = \sum_{k=0}^{n}(W_k - W_\ell) \qquad (9A)$$

So that equation (8A) becomes

$$W_o > \sum_{k=0}^{n}W_{k\ell} \qquad (10A)$$

14

As the number of segments becomes infinite and the length of each segment approaches zero, equation (10A) still holds so that

$$W_o > \lim_{n \to \infty} \sum_{k=0}^{n} W_{k\ell} \tag{11A}$$

By definition, $\lim_{n \to \infty} \sum_{k=0}^{n} W_{k\ell}$ is the longitudinal critical velocity

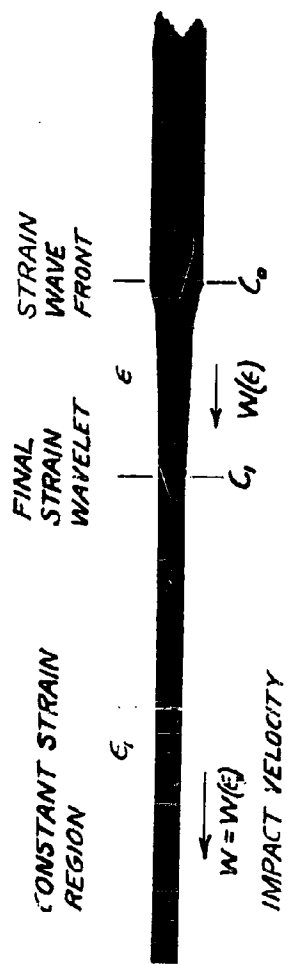for the curve OPQ, so the theorem has been proved.
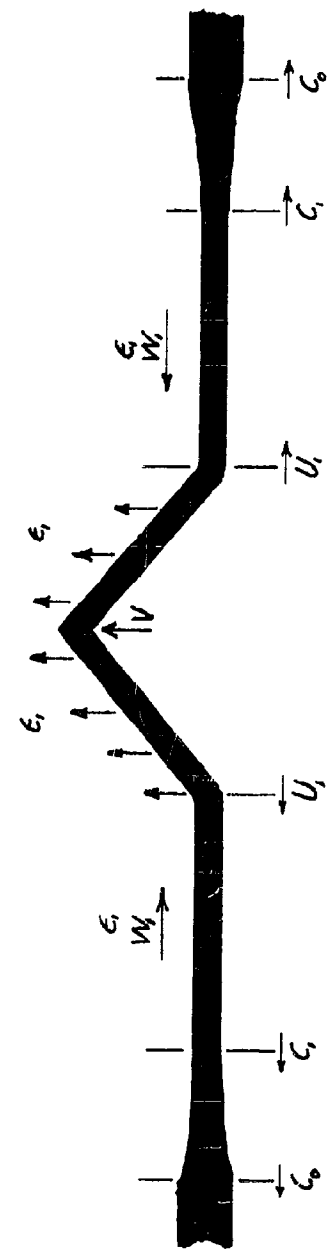
Smith

FIG. 1 LONGITUDINAL IMPACT
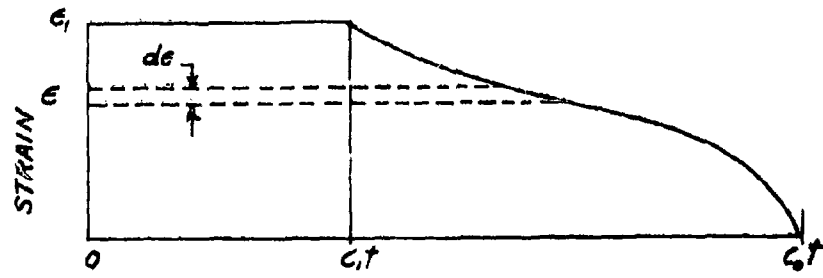

FIG. 2 TRANSVERSE IMPACT

16

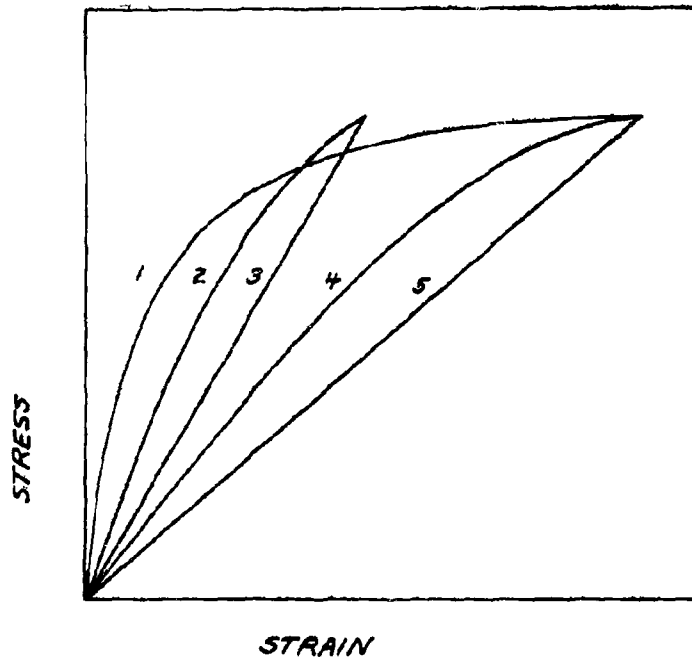FIG.3 STRAIN DISTRIBUTION ALONG FILAMENT
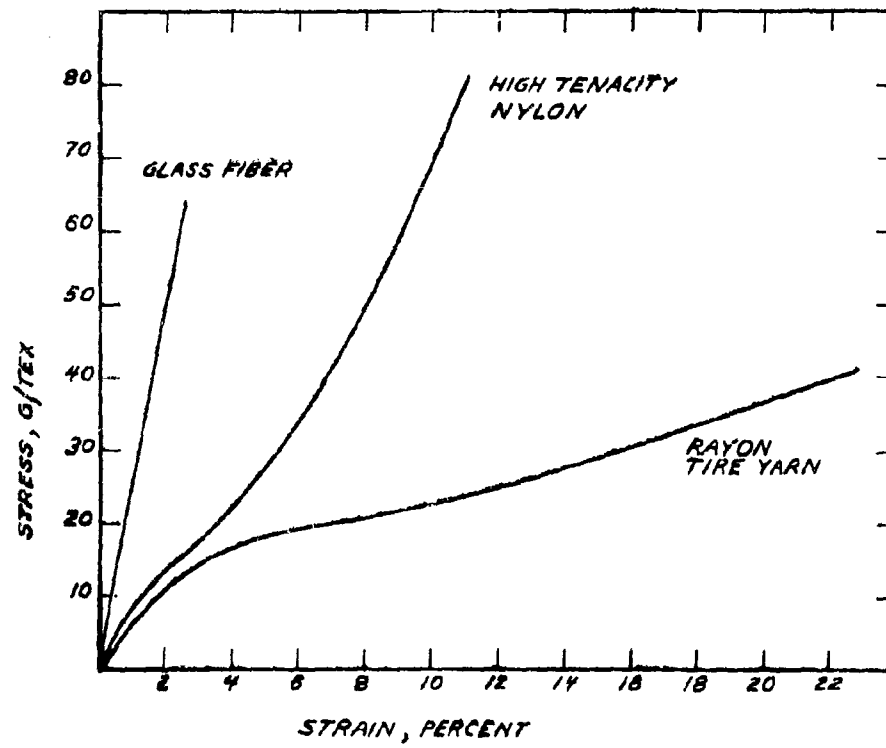

STRAIN

FIG.4. STRESS-STRAIN CURVES

FIG. 5
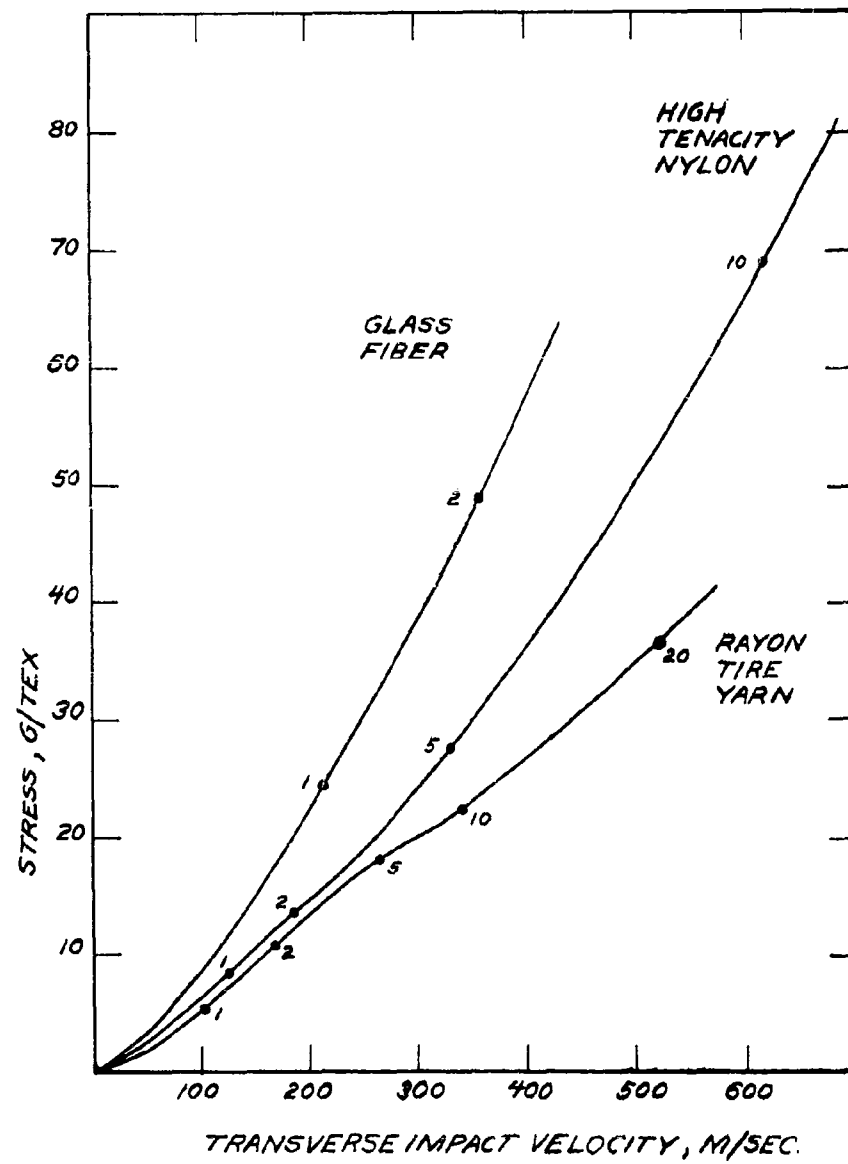
FIG. 6

19
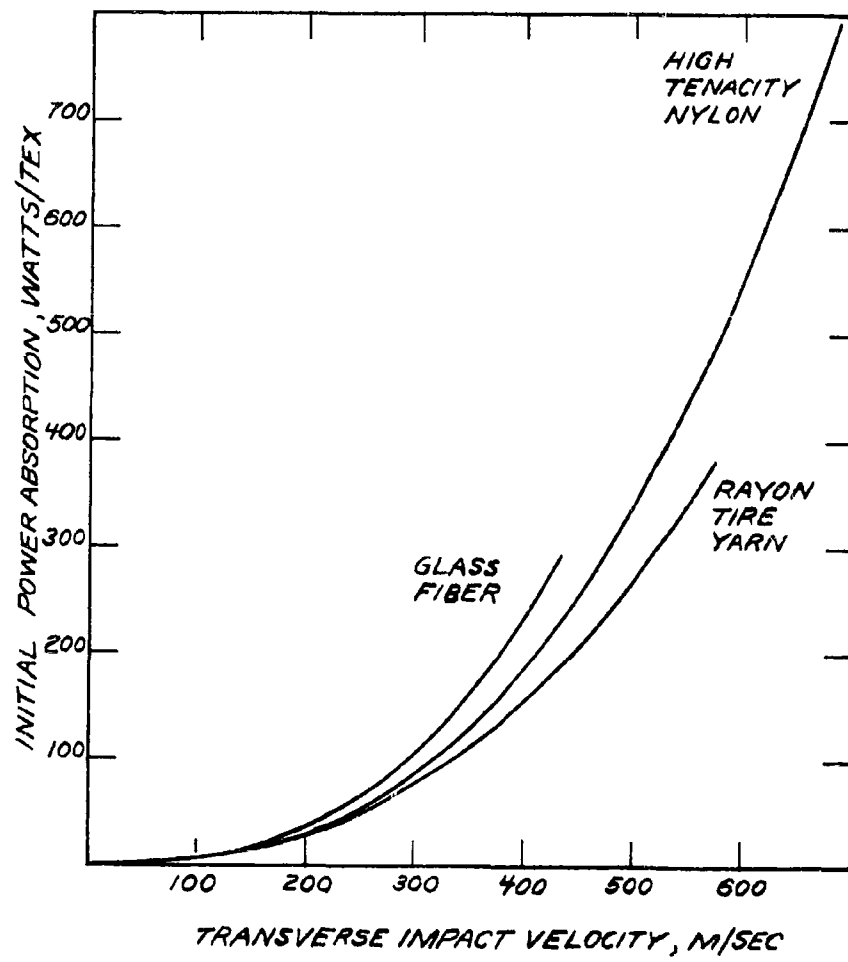
FIG. 7

20
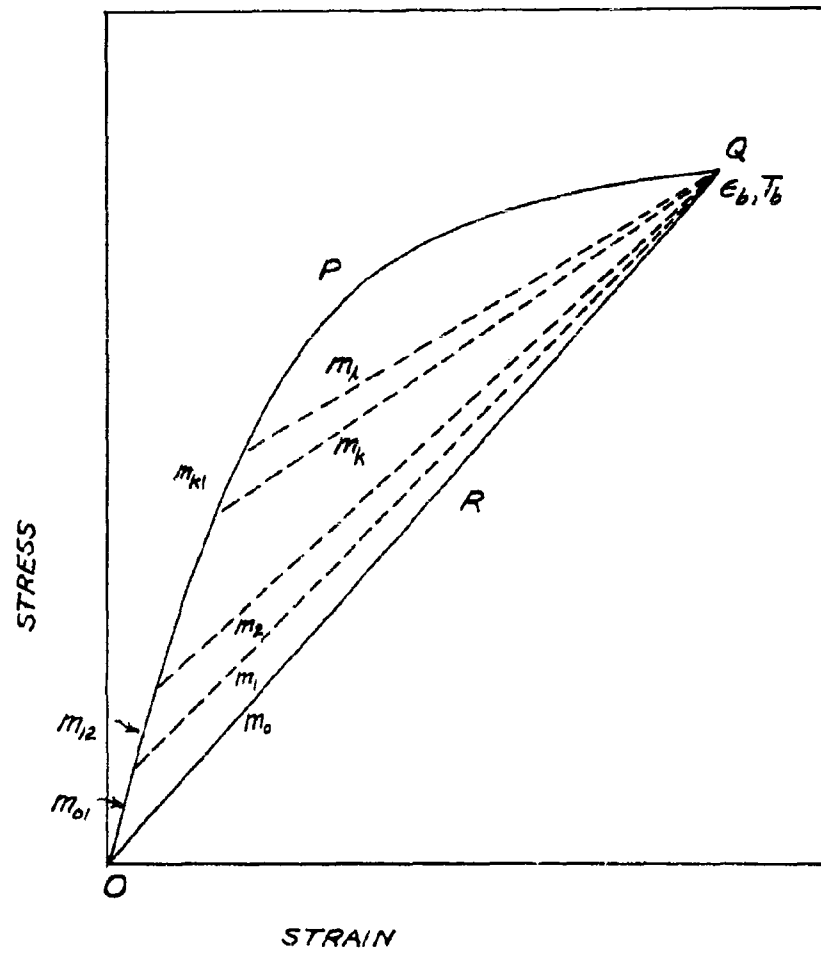
FIG. 8

DYNAMIC BEHAVIOR OF TEXTILE FIBERS AND
STRUCTURES AS RELATED TO PERSONNEL ARMOR

Henry M. Morgan[*]
Fabric Research Laboratories, Inc.
Dedham, Massachusetts

[*]Now with KLH Research and Development Corp.

Abstract

Fibers made from linear polymers have been shown to be
important materials for personnel armor. The useful physical
properties of fibers, i.e., strength, elongation, modulus, derive
from their molecular structure. In turn, the useful properties of
yarns and fabrics derive from the manner in which the fibers are put
together. All these properties are also dependent upon the conditions
of measurement and use. Textile fibers and structures studied at
dynamic and "impact" conditions will be discussed with reference to
their use as personnel armor.

Dr. Morgan's manuscript has not been submitted.

A THEORETICAL STUDY OF PENETRATION AND RESIDUAL
PROJECTILE VELOCITIES

L.E. Fugelso
American Machine & Foundry Co.
Niles, Illinois

1.0 INTRODUCTION

The design of light personnel armor is greatly aided by the knowledge of how and when a plate fractures under impact stress. Adequate qualitative and quantitative information for prediction of threshold impact velocities for failure, dependence of punchout and spall masses and velocities on material parameters, residual bullet velocities and energy absorption within the plate are necessary to guide the practical engineer on his quest for improved armor.

The description of the penetration of a plate by a projectile is an intimate intermingling of several theoretical descriptions. Several basic physical mechanisms, each of which may be quite complicated and involved, occur simultaneously or successively in the course of the deformation.

This paper presents the successive application of some of the physical theories to obtain a theoretical prediction of the residual velocity of the projectile and the threshold impact velocity for penetration. A unified theoretical approach to this problem, rather than an empirical or semi-empirical approach is given. A most obvious advantage of this approach is that if reasonable correlation to experimental data is obtained, the effect of the variation of individual material parameters may be quickly evaluated.

The basic sequence of physical events upon impact are first, a stress wave which is composed of elastic and non-elastic parts, including plastic flow, is propagated into the plates and, second, fracture patterns are produced in reaction to this transient stress. Simultaneously, a stress wave is propagated backwards into the projectile.

A detailed study of the propagation of the non-elastic stress wave under impact loads was made utilizing the theory of dislocation

movement under stress.[2,4]

Plastic flow takes time to occur. If the stress wave is held for a very short period, the total relaxation of stress due to the flow and the added displacements are negligible. If the load duration is a microsecond, an error about 3% in the displacement is introduced.

For the impact velocity of interest the second order terms in the elastic stress-strain curve are small. An error of about 8% at 4500'/sec impact for the case of an aluminum bullet striking an aluminum plate is introduced by neglecting them.[3] However, the neglect of these terms allows a detailed picture of the orientation of stresses in the plate to be readily calculated. This increase in physical insight more than makes up for the quantitative error introduced. Thus, a linear elastic model for the propagation of the stress wave is chosen.

One of three major patterns of fracture occur when a projectile impacts a plate. The first pattern of fracture is the spall which is caused by the reflection of a tensile stress wave from the back surface. The second type of fracture is failure in radial tension. This pattern occurs when the stress wave impulse is long compared with the thickness of the plate.

The third type of fracture, which is the only fracture considered in this paper, is breakup of material directly under the projectile, which is caused by the direct stress wave. A myriad of tiny fissures are formed in this region, reducing the material there to a powder and scooping out a large cavity.

A model for fracture in compression has been derived from the theory of dislocation movement under stress.[3] The fracture process is assumed to consist of three steps: initiation, growth and propagation. The time dependence of the micromechanism, i.e., the movement of dislocations through the medium, is taken as the rate determining step for high loading rates.

The two models that will be applied are:
1) Linear elastic stress wave propagation
2) Fracture in compression

The details of either step are still somewhat complicated, even with the sweeping simplifications already introduced. The basic results for each individual component will be discussed and then the two physical processes will be combined to evaluate several parameters of interest.

A short synopsis of the basic results is presented in the next two sections. Only the results of more elaborate calculations are reported here. For details the reader is referenced to ref. (3)

24

2.0 ELASTIC STRESS WAVE

When a projectile strikes a plate, a series of stress waves are propagated in both the plate and the projectile. If cylindrical symmetry of the plate and projectile is assumed, i.e., normal incidence, the equations of motion are both the projectile and plate. (1)

$$\frac{\partial \sigma_r}{\partial r} + \frac{\partial \tau_{rz}}{\partial z} + \frac{\sigma_r - \sigma_\theta}{r} = \rho \frac{\partial^2 u_r}{\partial t^2}$$

$$\frac{\partial \tau_{rz}}{\partial r} + \frac{\partial \sigma_z}{\partial z} + \frac{\tau_{rz}}{r} = \rho \frac{\partial^2 u_z}{\partial t^2}$$

λ, μ Lame's Constants

ρ density

$$\sigma_r = \lambda \Delta + 2\mu \frac{\partial u_r}{\partial r}$$

$$\sigma_z = \lambda \Delta + 2\mu \frac{\partial u_z}{\partial z}$$

$$\sigma_\theta = \lambda \Delta + 2\mu \frac{u_r}{r}$$

$$\tau_{rz} = \mu \left| \frac{\partial u_r}{\partial z} + \frac{\partial u_z}{\partial r} \right|$$

$$\Delta = \frac{\partial u_r}{\partial r} + \frac{u_r}{r} + \frac{\partial u_z}{\partial z}$$

Formal integral solutions for the stresses and displacements in the plate are (1)

$$u_r = \frac{1}{2\pi i} \int_{Br} e^{s\tau} ds \int_o^\infty \frac{\xi^2 \hat{p}(\xi,s)}{2\mu \, G(\xi,s)} \times$$

$$[(\xi^2 + \tfrac{1}{2} \beta^2 s^2) e^{-mz} - mne^{-nz}] J_1 (\xi r) d\xi$$

25

$$u_z = \frac{1}{2\pi i} \int_{Br} e^{s\tau} ds \int_0^\infty \frac{\xi \hat{m} p(\xi,s)}{2\mu G(\xi,s)} \times$$

$$[(\xi^2 + \frac{1}{2}\beta^2 s^2) e^{-mz} - \xi^2 e^{-nz}] J_0(r\xi) d\xi$$

$$\sigma_z = \frac{1}{2\pi i} \int_{Br} e^{s\tau} ds \int_0^\infty \frac{\xi \hat{p}(\xi,s)}{G(\xi,s)} \times$$

$$[(\xi^2 + \frac{1}{2}\beta^2 s^2)^2 e^{-mz} - \xi^2 mn\, e^{-nz}] J_0(r\xi) d\xi$$

$$\tau_{rz} = \frac{1}{2\pi i} \int_{Br} e^{s\tau} ds \int_0^\infty \frac{m\xi^2 \hat{p}(\xi,s)}{G(\xi,s)} \times$$

$$[2(\xi^2 + \frac{1}{2}\beta^2 s^2) e^{-mz} - (n^2 + \xi^2) e^{-nz}] J_1(r\xi) d\xi$$

$$\sigma_r + \sigma_\theta = \frac{1}{2\pi i} \int_{Br} e^{s\tau} ds \int_0^\infty \frac{\xi^2 \hat{p}(\xi,s)}{G(\xi,s)} \times$$

$$[\xi^2 - s^2 (\beta^2 - 2)] (\xi^2 + \frac{1}{2}\beta^2 s^2) e^{-mz} - \xi^4 mn\, e^{-nz}\ J_0$$

$$(r\xi)d\xi$$

$$\sigma_r = \frac{1}{2\pi i} \int_{Br} e^{s\tau} ds \frac{1}{r} \int_0^\infty \frac{\xi^2 \hat{p}(\xi,s)}{G(\xi,s)} \times$$

$$[mn\, e^{-nz} - (\xi^2 + \frac{1}{2}\beta^2 s^2) e^{-mz}] J_1(\xi r) d\xi$$

$$+ \int_0^\infty \frac{\xi \hat{p}(\xi,s)}{G(\xi,s)} \times [(m^2 - \frac{1}{2}\beta^2 s^2)(\xi^2 + \frac{1}{2}\beta^2 s^2) e^{-mz}$$

$$- \xi^2 mn\, e^{-nz}] J_0(r\xi) d\xi$$

$$G(\xi,s) = (\xi^2 + \frac{1}{2}\beta^2 s^2)^2 - mn\xi^2$$

26

$$m^2 = s^2 + \xi^2$$
$$n^2 = \beta^2 s^2 + \xi^2 \qquad \beta^2 = \frac{\lambda + 2\mu}{\mu}$$

$$\hat{p}(\xi, s) = \int_0^\infty e^{-s\tau} d\tau \int_0^\infty r\, p(r, \tau)\, J_0(r\xi)\, dr$$

This is the transform of the pressure on the surface $z=0$. Similar equations are available for the bullet.

The determination of the pressure for the impact problem is complicated. The complete expression for the applied pressure on the surface of the plate is [3]

$$p(r, t) = \left\{ \frac{\gamma_1\, P_o}{(a^2 - r^2)^{1/2}} + \gamma_2 P_o \right\} \left| 1(t) - 1(t + t_0) \right|$$

$$t \le t_0 = \frac{2l}{c_1}$$

$$= \left\{ \frac{\gamma_1\, (P_o - \Sigma\alpha^n)}{(a^2 - r^2)^{1/2}} + \gamma_1\, (P_o - \Sigma\alpha^n) \right\} \times$$

$$\left| 1(t) - 1(t + nto) \right| \qquad \frac{2l}{c_1} n \le t \le \frac{2l}{c_1}(n+1)$$

with
$$P_o = \frac{\rho_1 c_1 + \rho_0 c_0}{\rho_1 c_1\ \rho_0 c_0} \quad v_1$$

ρ_1, c_1 density and compressional velocity of the bullet

ρ_0, c_0 density and compressional velocity of the plate

$$\alpha = \frac{2\,\rho_0\, c_0}{\rho_1 c_1 + \rho_0 c_0}$$

l =   length of bullet

$\gamma_1\ \gamma_2$ constants to be determined

27

For simplicity we shall assume that the pressure may be represented by

$$P(r,t) = \frac{\gamma_1 \; P_0}{(a^2-r^2)^{1/2}} \; [1\,(t) - 1\,(t+t_0)\,] \quad t \le t_0 = \frac{2l}{c_1}$$

$$= \gamma_1 \frac{(P_0 - \sum\limits_{n=1}^{n} \alpha^n)}{(a^2-r^2)^{1/2}} \; [1\,(nt) - 1\,(t+nt_0)\,] \quad nt_0 \le t \le (n+1)t_0$$

This pressure on the plate represents the following process. When the bullet strikes the plate, a stress wave is sent back in the bullet.

This compressive wave is reflected in tension from the end of the bullet and propagates forward until it strikes the front end of the bullet. The plate meanwhile sees only the initial pressure during this period. When the tensile wave strikes the front side of the bullet, the entire bullet is now traveling at a uniform lower velocity. Now this process repeats itself. A second compressive wave is sent back into the bullet and the plate sees a lower applied stress for the next interval of reflection and compression, ad infinitum.

Solution of the equations for the plate indicates that three stress waves are sent propagating into the plate, a P-wave (compressive), an S-wave (shear) and a PS-wave (diffracted shear wave). Analytical and numerical solutions of these equations for the stresses and displacements have been obtained (3) (Figures 1-4 are examples).

A quantity of great importance in the applications is the average vertical stress in the plate in the region immediately below the bullet. The average stress in the region between the dilatational wave and the shear wave has been graphically determined. Three regions for approximate expressions occur. Denoting by h the thickness of the plate and by a the radius of the bullet, the expressions are

$$\sigma_z = \frac{\rho_1 c_1 \, \rho_0 c_0}{\rho_1 c_1 + \rho_0 c_0} \; v_1 \qquad 0 \le \frac{h}{a} < 0.6$$

$$= 0.77 \frac{\rho_1 c_1 \, \rho_0 c_0}{\rho_1 c_1 + \rho_0 c_0} \; \left(\frac{h}{a}\right)^{-1/2} \qquad 0.6 \le \frac{h}{a} \le 1.5$$

$$= 0.95 \frac{\rho_1 c_1 \, \rho_0 c_0}{\rho_1 c_1 + \rho_0 c_0} \; \left(\frac{h}{a}\right)^{-1} \qquad 1.5 \le \frac{h}{a} \le 3.0$$
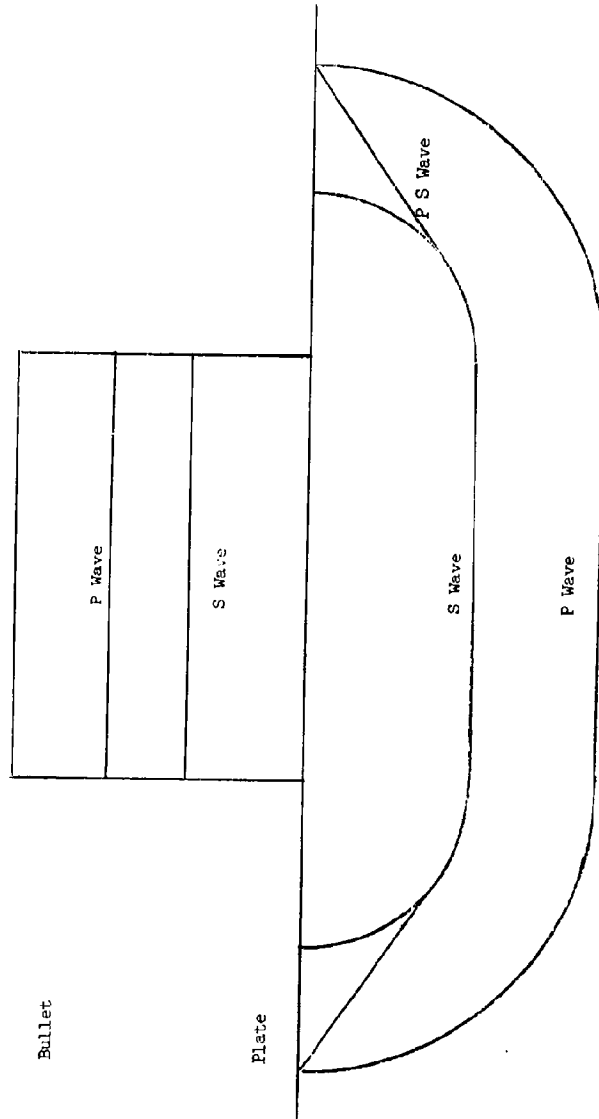
Figure 1 - Wave fronts in bullet and plate

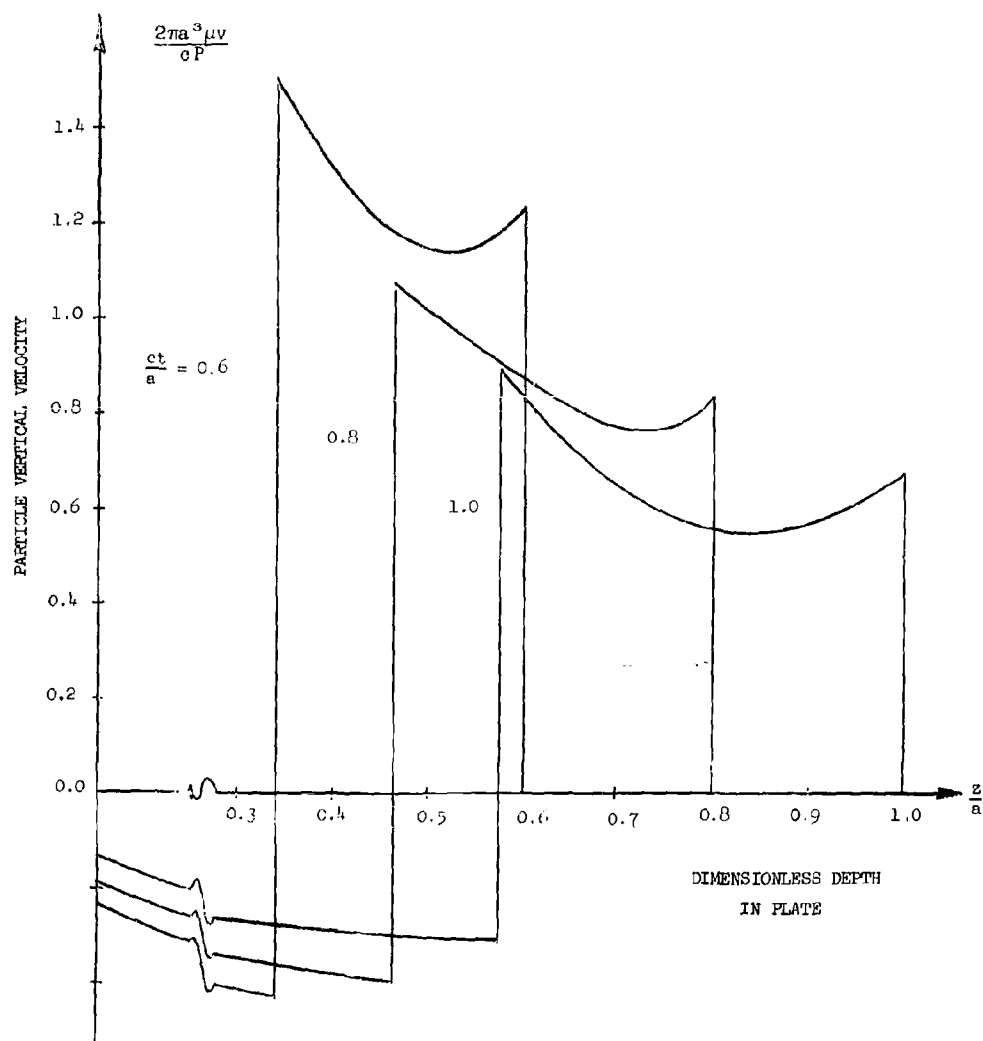The figure contains the following labels: Bullet, Plate, P Wave, S Wave, S Wave, P S Wave, P Wave
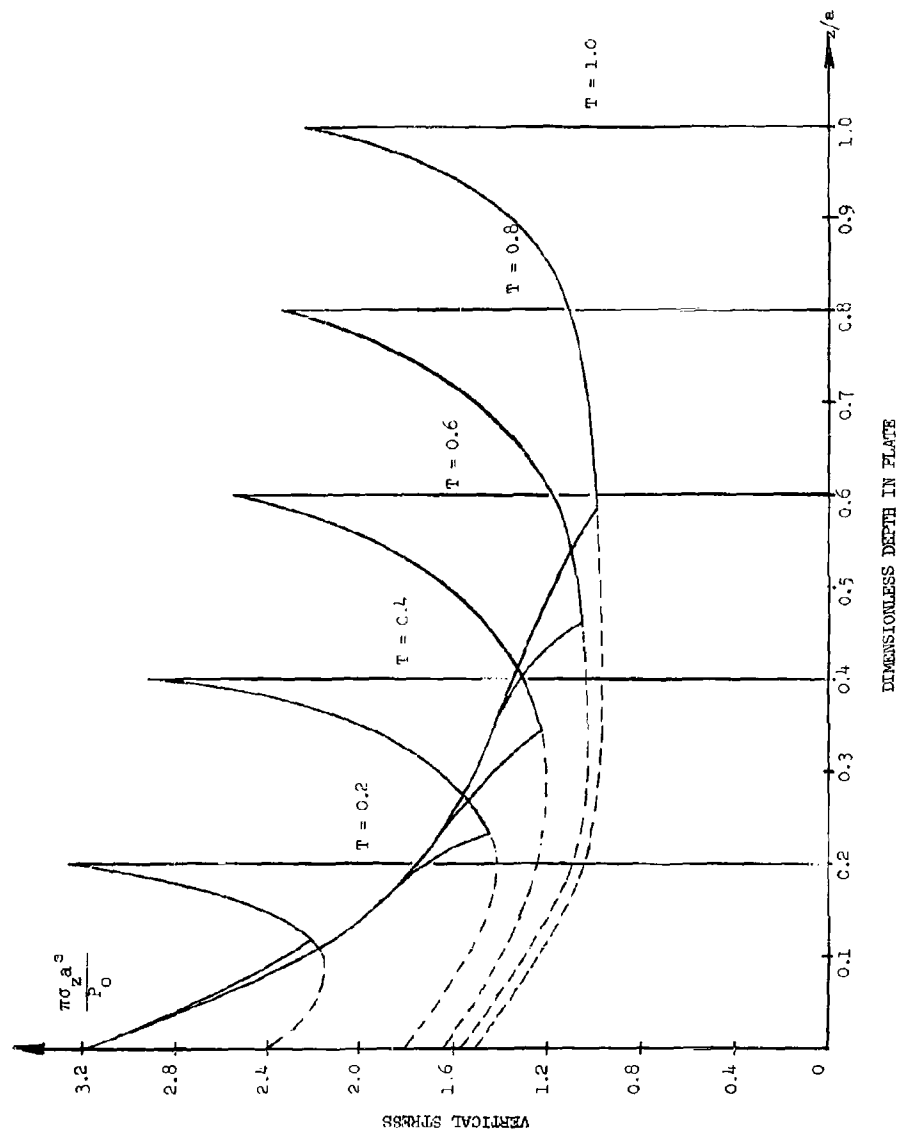
Figure 2 - Verticle particle velocity vs depth

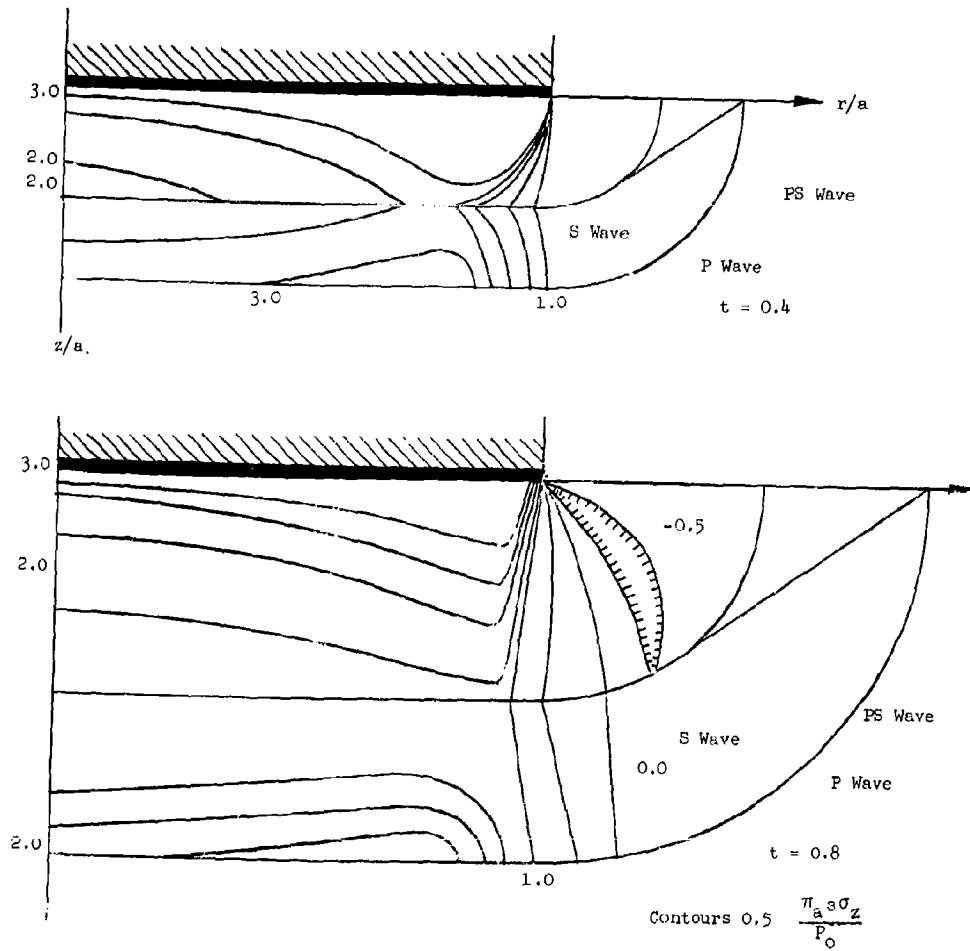Figure 3 - Vertical stress vs depth (r = 0)

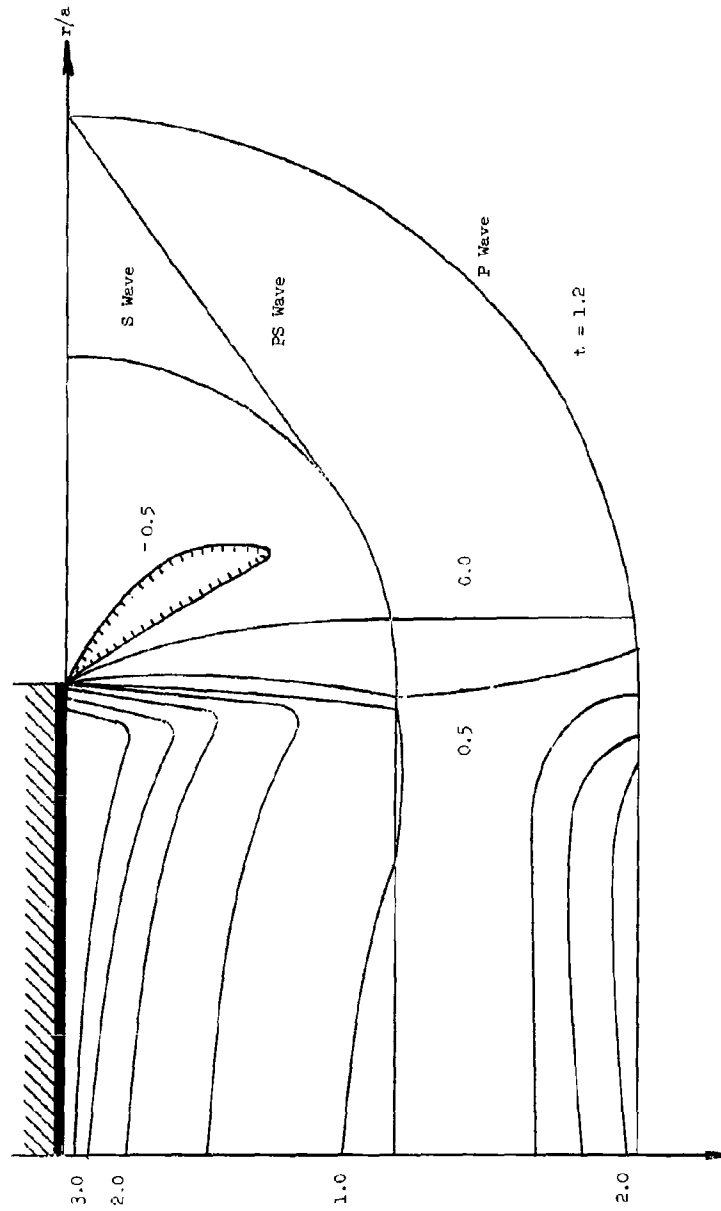Figure 4a - Vertical stress in the plate

Figure 4b – Vertical stress in the plate

The first region corresponds to that region in the plate where the vertical wave is virtually a plane wave. In the second region, the geometrical dispersion of the stress wave has moderate influence. Geometrical dispersion becomes predominate in the third region.

3.0 FRACTURE CRITERIA

Fracture occurs under transient stress when a state of stress is maintained for a specific length of time. The time to fracture is dependent on the octohedral shear stress and the mean stress. If the mean stress is compressive as will be the case for the outgoing stress waves in the plate, the rate determining mechanism is the movement of dislocation. By considering a simplified model of dislocation motion under stress (3) (4), an exponential dependence of the time to fracture is found

$$\ln \frac{t}{t_o} = \frac{\Delta E_o - \gamma \tau}{kT} + \frac{\tau_o}{\tau - \tau_o} \qquad\qquad \gamma \tau < E_o$$

$$\ln \frac{t}{t_o} = \frac{\tau_o}{\tau - \tau_e} \qquad\qquad \gamma \tau > E_o$$

where τ is maximum shear stress

t is the time to fracture

t_o is a material constant

E_o is the activation energy for a dislocation to move

k is Boltzmann's constant

T is the absolute temperature

τ_o, γ, τ_e are material constants

For this application the stress durations are of the order of magnitude of 10^{-6} sec, so that only times to fracture shorter than 10^{-6} sec. need be considered. This occurs where high octohedral shear stresses are formed. If the pattern of stresses in the plate are known, the expression may be converted to an expression in the vertical stress

$$\ln \frac{t}{t_o} = \frac{\Delta E_o - \gamma' \sigma_z}{kT} = \frac{\sigma_o'}{\sigma_z - \sigma_e'}$$

4.0 CRITICAL VELOCITIES FOR PENETRATION AND RESIDUAL BULLET VELOCITIES

The critical impact velocity for penetration and the residual velocities after penetration of the bullet and of the plug will be calculated. After the impact, a sequence of stress waves are sent forth into the plate. The magnitude of these waves is determined by the velocity of impact and the materials of the plate and projectile. Thereafter, the propagation of the stress waves in the plate determines the subsequent behavior, i.e. the plate tears itself apart.

Numerical solutions of the integrals in Section 2.0 for the stresses in the plate offer an insight into the break-up of the plate under impact stress. There are three waves that are propagated into the plate

1. A compressional wave
2. A shear wave
3. A diffracted PS wave

The state of stress between the P wave front and the S wave is transient, but the state of stress behind the shear front is very nearly the static stress state. Recall the behavior of the stresses in the region directly under the bullet as given in Section 2.0. Fig3 shows the variation of the vertical stress with plate depth directly under the bullet center. Figures 4a and 4b show contours of the vertical stress with position for various times. Compared with the static solution (Figure 5) the state of stress beneath the bullet and behind the shear wave front is essentially the static solution.

Using this criteria, the octahedral shear stress behind the shear wave (5) may be rapidly calculated. (Figure 6). Apply now the derived criteria for fracture to occur. This critical octahedral shear stress for fracture is shown as a function of position for several applied stresses (Figures 7-10).

The material in this region between the shear front and the critical shear stress is presumed to be completely fractured, thereby reduced to powder. This fracture pattern will reduce the size of the punch out. For higher impact velocities the whole region behind the shear wave front is fractured.

If the outer rim of this critical octahedral shear stress is examined, the increase of the volume of material pulverized, or equivalently weight loss of the plate, may be calculated graphically. This solution is shown graphically for two plate thicknesses in Fig. 11. The use of this graph is self evident.

The locus of the octahedral shear stress between the compression wave front and the shear wave front that satisfies the fracture criteria is directly under the rim of the bullet. The stress pattern in this region will determine whether or not the plug will separate and therefore, whether penetration will occur.
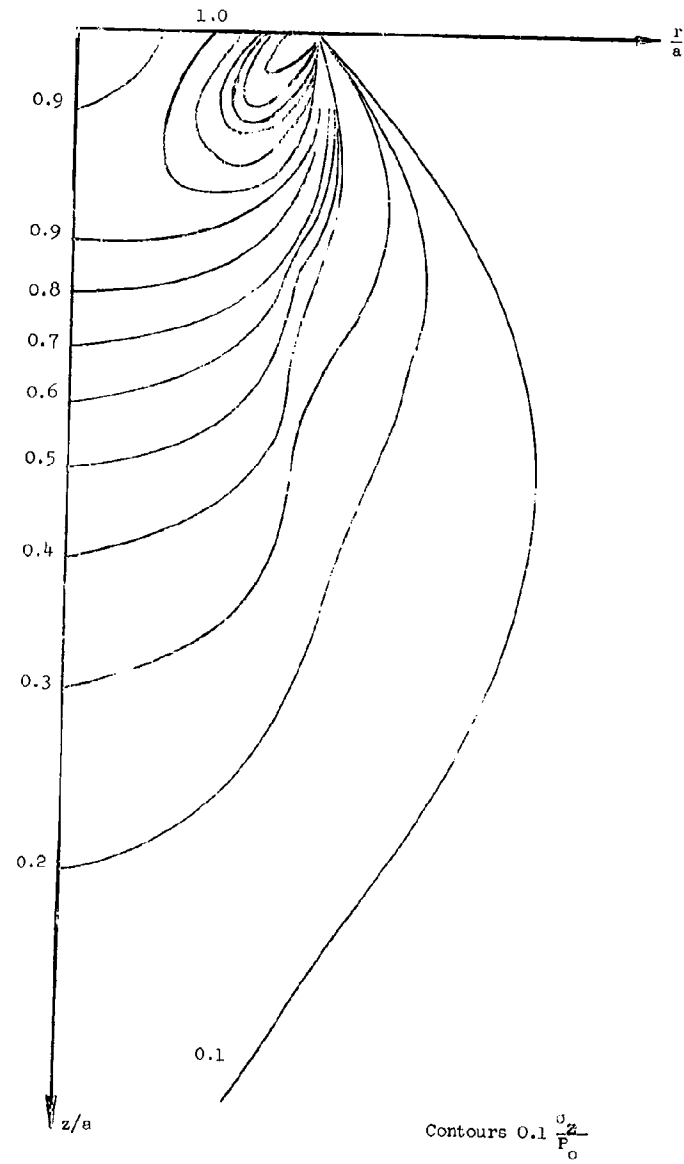
Figure 5 - Static vertical stress in plate
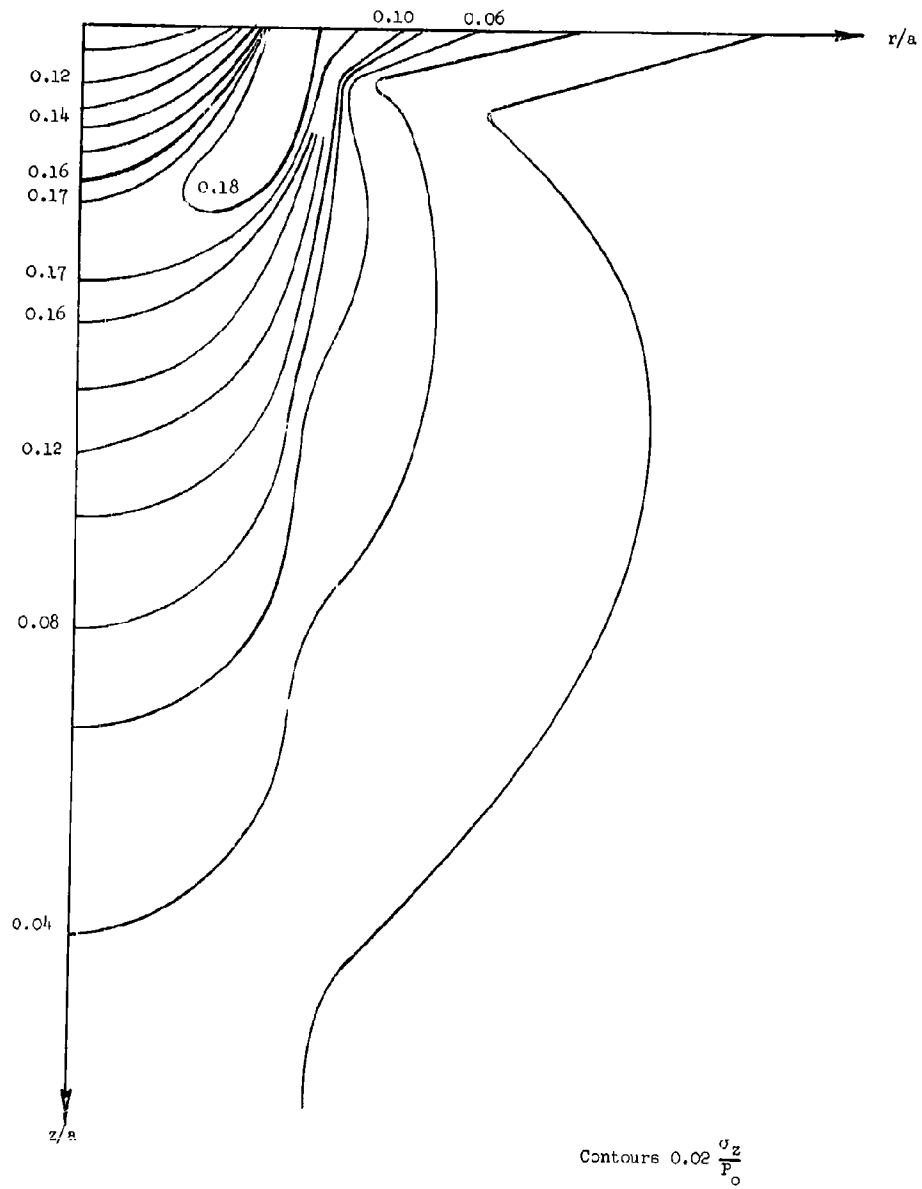
Contours $0.02 \frac{\sigma_z}{P_o}$
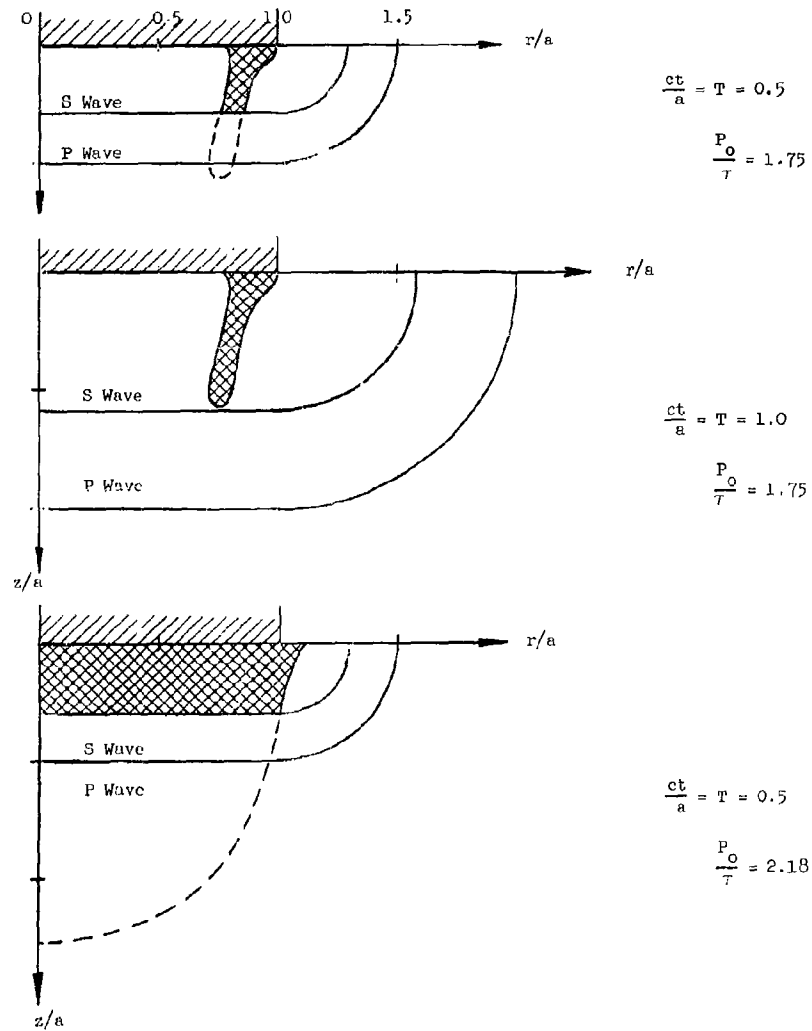
Figure 6 - Octahedral shear stress

38

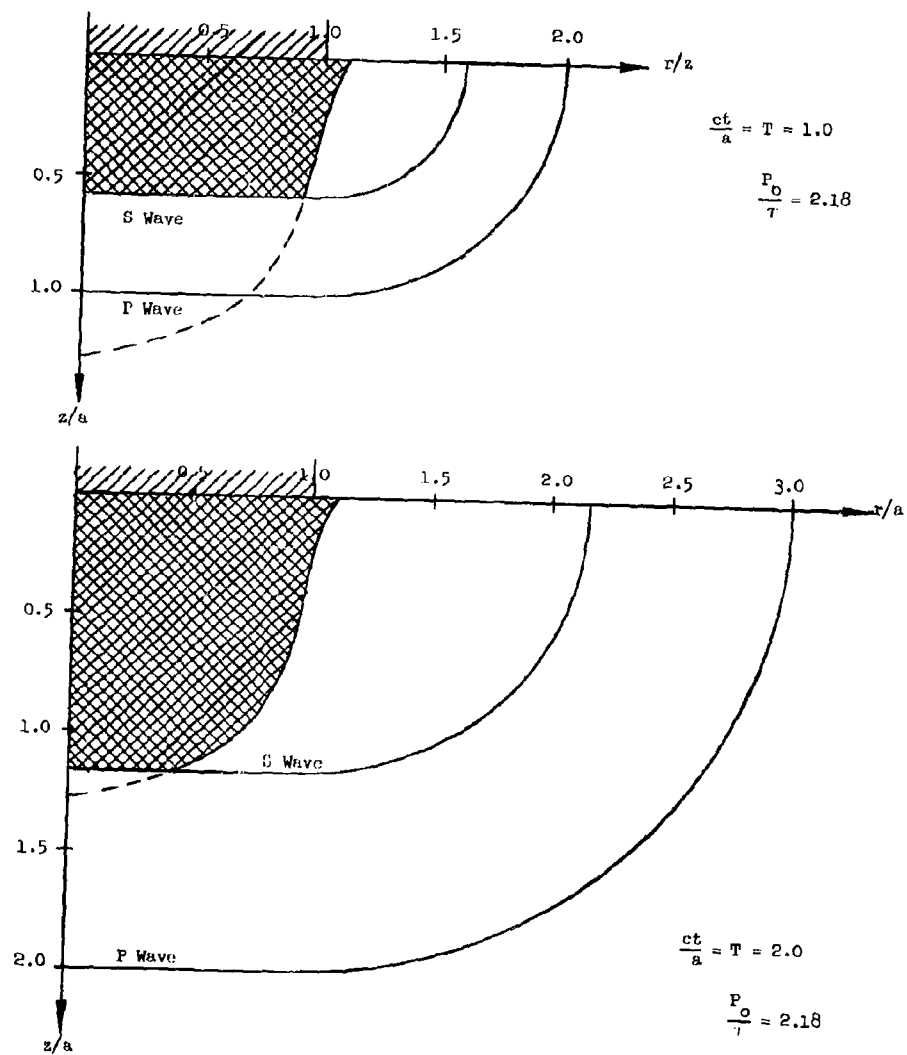Figure 7 - Pulverized regions in plate at various times

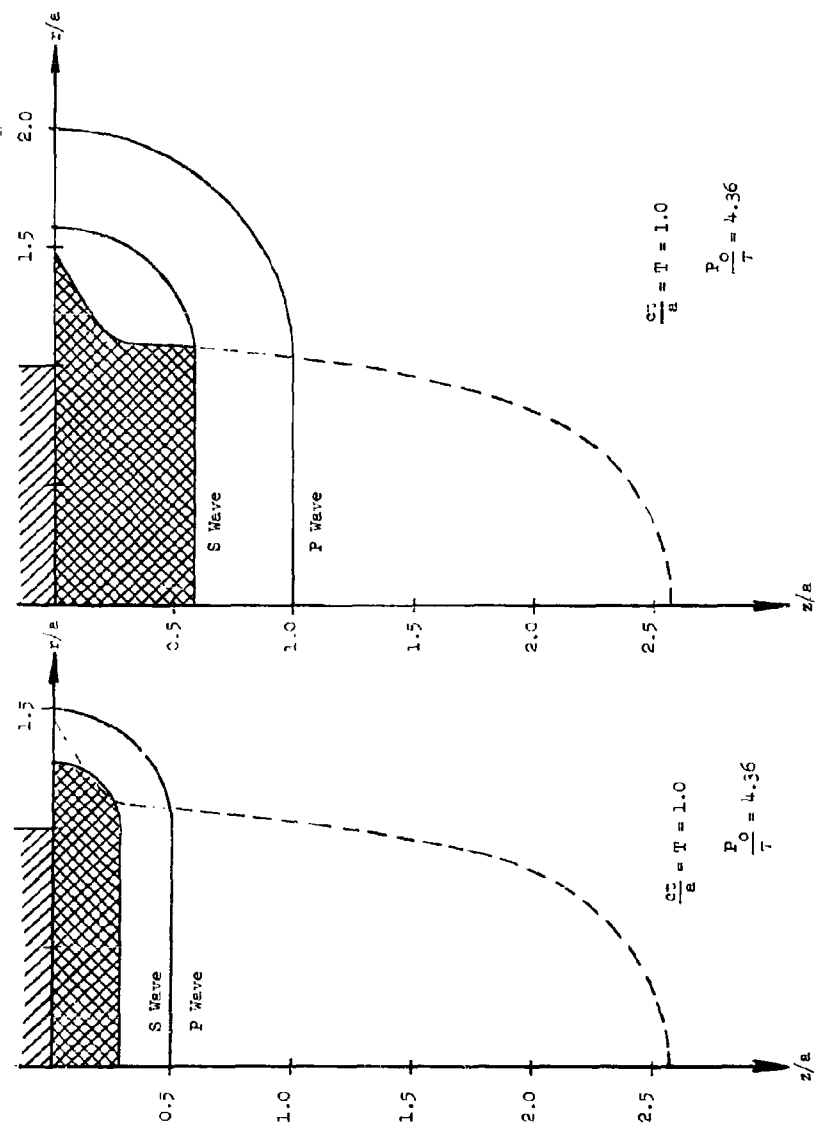Figure 8 - Pulverized regions in plate at various times

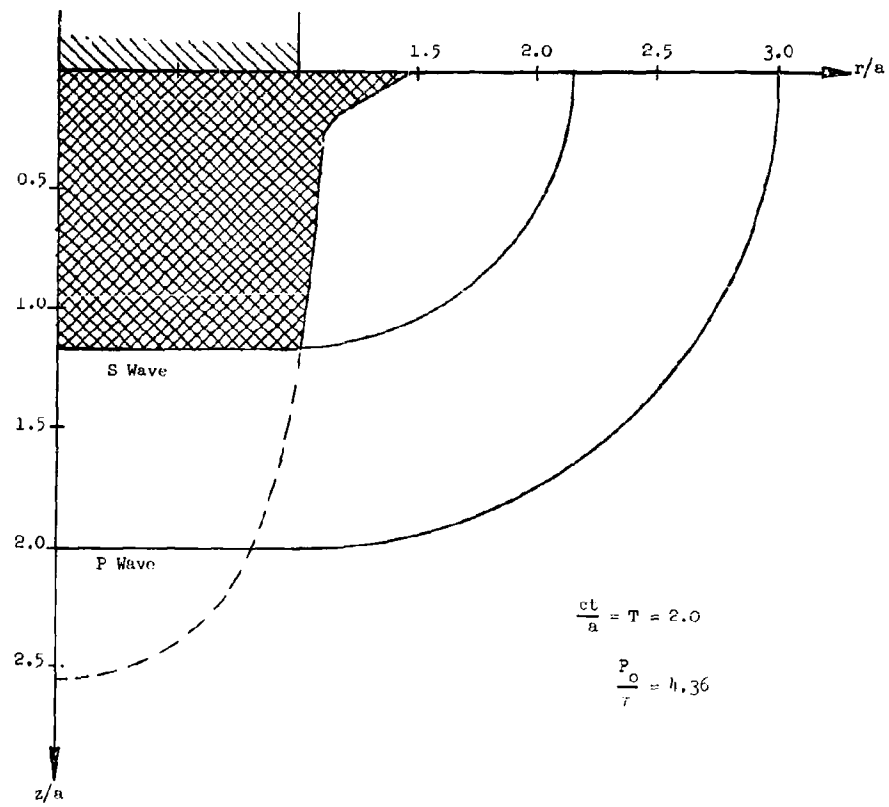Figure 9 – Pulverized regions in the plate
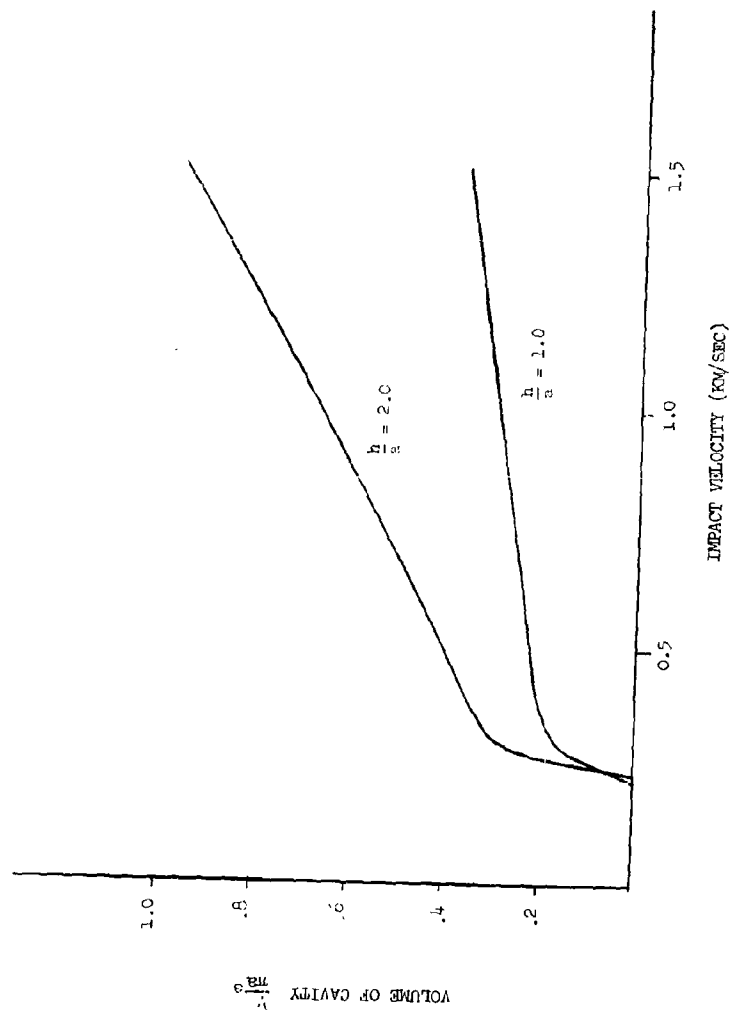
Figure 10 - Pulverized regions in the plate

Figure 11 – Volume of fracture capacity or volume loss to plate
by fracture as a function of impact velocity

This will give the v_{50} point or the critical impact velocity for penetration. The calculation of the v_{50} point may become quite involved. To simplify the procedure, the plate thickness to bullet radius ratio will be assumed to be less than 0.6. Then the stress wave that is propagated is virtually constant across the thickness of the plate. The peak at the compressive wave front is

$$\frac{\rho_0 c_0 \rho_1 c_1}{\rho_0 c_0 + \rho_1 c_1} \qquad v_i$$

Now the time duration of the lowest possible stress level is calculated. This will be compared with the time to fracture. The lowest possible stress that has a time to fracture less than or equal to this applied load time will determine the critical velocity for penetration.

The region behind the shear front is presumed to be completely fractured. The total pulverized region is that region behind the shear front at the time the P-wave strikes the back of the plate. The longest sustained stress pulse then has a duration.

$$t^* = (1.577)\,\frac{h}{c_1}$$

A crack is formed directly under the lip at the shear front and propagates vertically at 1/5 of the sound speed. When this crack reaches the back surface the plug will separate.

The stress level that is maintained for this longest time interval is obtained from the graphical solution for the vertical stress and is

$$\sigma_z\ min = 0.436\ \sigma_z\ (\text{wave front})$$

$$= 0.436\ \frac{\rho_0 c_0 \rho_1 c_1}{\rho_0 c_0 + \rho_1 c_1}\ v_i$$

Inserting this value for σ_z and t^* into the equation for time to fracture and using

$$t_0 = 10^{-10}\ \text{sec.}$$

and σ_0 = static compressive yield strength, the lowest possible value of v_i for fracture under the lip of the bullet is determined.

The threshold velocity for penetration is then

$$v_1^T = \frac{\sigma_o}{0.436} \frac{(\rho_o c_o + \rho_1 c_1)}{\rho_o c_o \rho_1 c_1} \frac{\ln \frac{t_1}{t_o}}{\ln \frac{t^*}{t_o}}$$

where t_1 is the time to fracture of the static yield stress (t_1 is taken to be 10 sec.)

Similarly for $0.6 \leq \frac{h}{a} \leq 1.5$ the threshold velocity may be calculated. It is

$$v_1^T = \frac{\sigma_o}{0.32/} \frac{(\rho_1 c_1 + \rho_o c_o)}{\rho_1 c_1 \; \rho_o c_o} \frac{\ln \frac{t^*}{t_o}}{\ln \frac{t_1}{t_o}} (\frac{h}{a})^{1/2}$$

Solutions for the critical velocity versus plate thickness for several combinations of plate and projectile materials are shown in Figure   . The expressions for the variation of average stress given on the following page are used for calculating the higher plate thickness ratios. The increase of critical velocity in the low range is slow. In the thicker plates this increase becomes much **more** rapid. Interpretation and use of this graph is self evident.

The residual projectile and plug velocities after penetration will now be calculated.

Assume now that the plate fractures under the rim of the bullet immediately on arrival of the compressive wave. This assumption demands that the impact velocity be sufficiently greater than the threshold penetration velocity and thus leads to the linear approximation for residual velocities at high impact velocities. The region of the plate that forms the punch-out is that between the P-wave and S-wave and directly under the bullet.

At this instant, the stress on the cylindrical sides of the punch-out is relieved and a converging stress wave is generated. The nature of the stress wave is such that after propagation of this converging wave, coupled with the reflected tensile wave from the back surface, the average vertical velocity in the punch-out is independent of radial position and very nearly equal to twice the Beltrami product $\sigma_z = \rho c v$ for the average vertical stress at r=0.

Thus

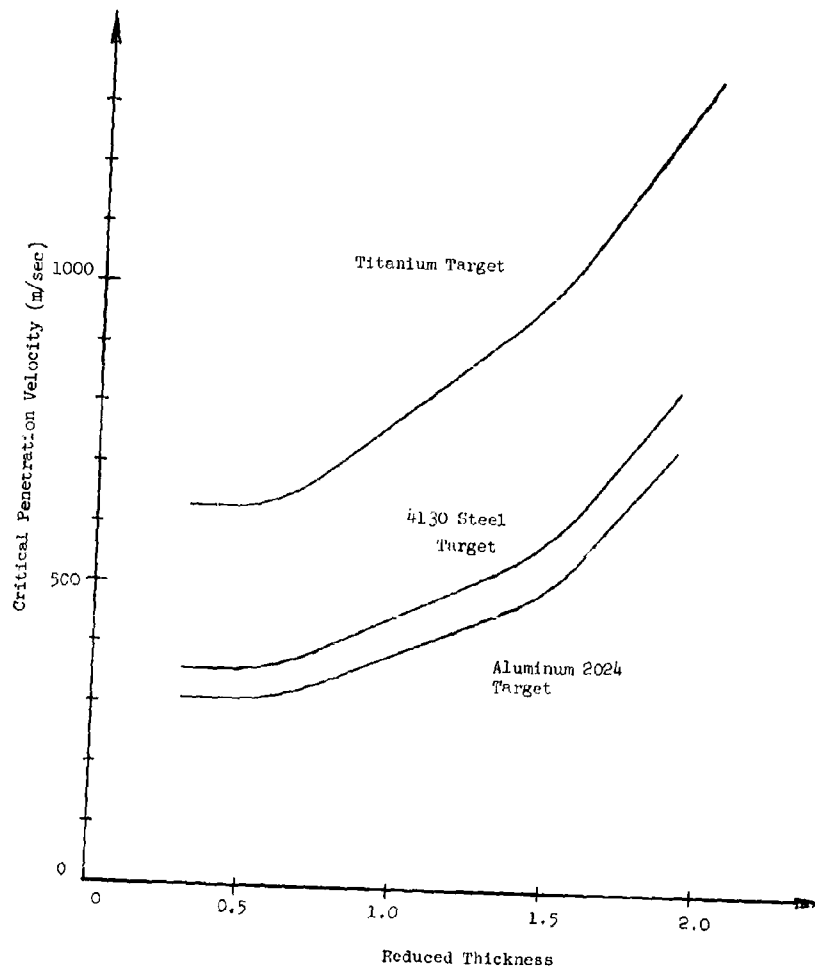$$v_p = \frac{\sigma_z(\text{avg}) \; r=0}{\rho_1 c_1}$$

45

Figure 12 - Variation of critical impact velocity for
penetration as a function of plate thickness
(steel bullet)

This value has been numerically computed for several plate thicknesses.

Approximate numerical forms of this average stress are

$$\bar{\sigma}_z \approx A \qquad\qquad 0 \le \frac{h}{a} < 0.6$$

$$\bar{\sigma}_z \approx 0.77A \left(\frac{h}{a}\right)^{-1/2} \qquad 0.6 \le \frac{h}{a} \le 1.5$$

$$\bar{\sigma}_z \approx 0.95A \left(\frac{h}{a}\right)^{-1} \qquad 1.5 \le \frac{h}{a} \le 3.0$$

where

$$A = \frac{\rho_o c_o \, \rho_1 c_1}{\rho_1 c_1 + \rho_o c_o} \; v_1$$

The reduction in bullet velocity may be computed by considering the stress waves generated in the bullet and is given by the formula

$$\frac{v_1}{v_i} = 1 - \sum_{i=1}^{n} \alpha^i - \alpha^{i+1} \quad \frac{c_o t}{2L} \qquad n = 0, 1, 2 \ldots$$

$$\alpha = \frac{2\rho_o c_o}{\rho_1 c_1 + \rho_o c_o} \qquad \frac{2L}{c_1} n \le t \le \frac{2L}{c_1} (n+1)$$

The time that is used in computing these values is the time it takes the P-wave to reach the back of the plate, since the fracture there is assumed to occur very rapidly with respect to the pulse duration. Thus

$$t = \frac{h}{c_1}$$

The residual velocities are plotted in Figures 13-18 for various combinations of bullet and target materials. To determine the residual velocities of the plug and projectile, calculate the ratios $\frac{h}{a}$, $\frac{L}{a}$ for the particular problem. Locate $\frac{h}{a}$ on the abcissa for the particular combination of plate and projectile materials. Look at the curve parameterized by $\frac{L}{a}$ to determine the residual bullet velocity. The residual plug velocity is given by the value of the

47

Figure 13 – Residual velocities of plug and bullet versus
plate thickness and bullet length

Figure 14 – Residual velocities of plug and bullet versus plate thickness and bullet length

Figure 15 - Residual velocities of plug and bullet versus
plate thickness and bullet length

Aluminum Bullet

$\rho_0 = 2.71$ gm/cc

$c_0 = 5104$ m/sec

Steel Target

$\rho_1 = 7.83$ gm/cc

$c_1 = 5000$ m/sec

Reduced Plate Thickness

v_p/v_i, v_1/v_i

Residual Velocity Ratios

v_1/v_i $L/a = 2.0$

v_p/v_i

v_1/v_i $L/a = 1.0$

v_1/v_i $L/a = 0.4$

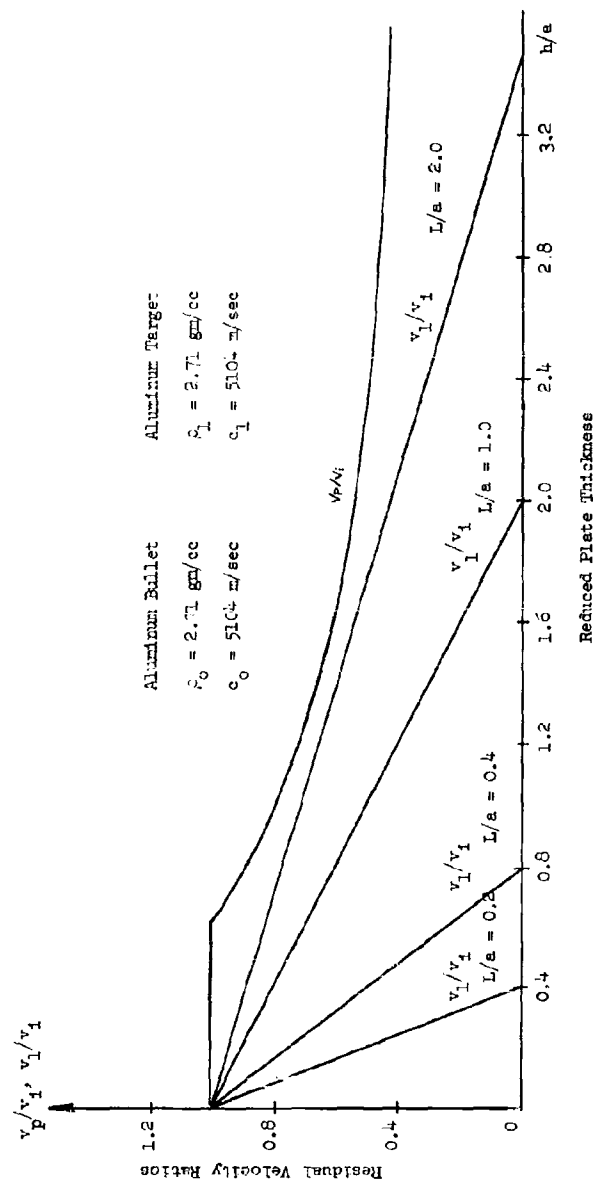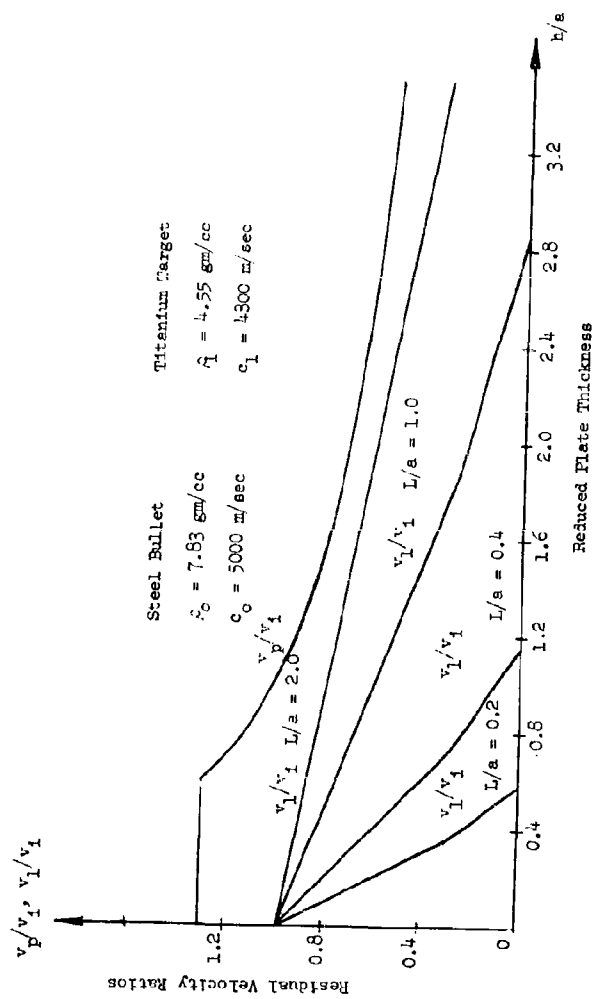v_1/v_i $L/a=0.2$

v_1/v_i

h/a

Figure 16 - Residual velocities of plug and bullet versus
plate thickness and bullet length

51

Figure 17 – Residual velocities of plug and bullet versus plate thickness and bullet length
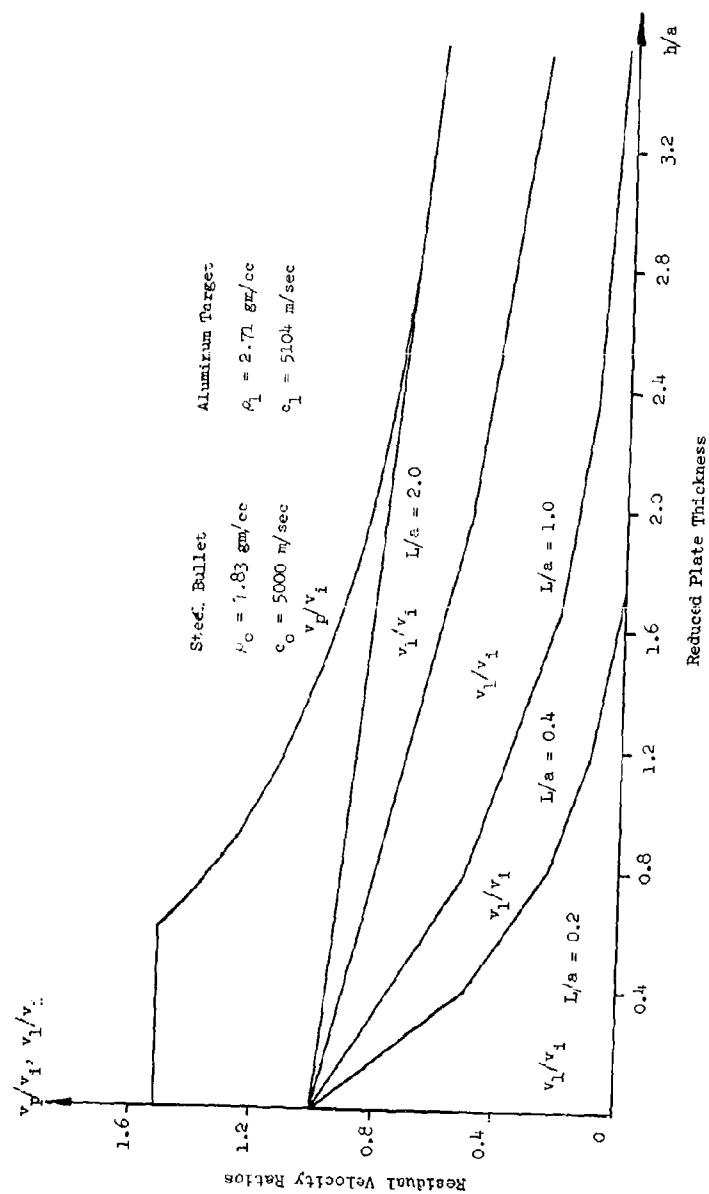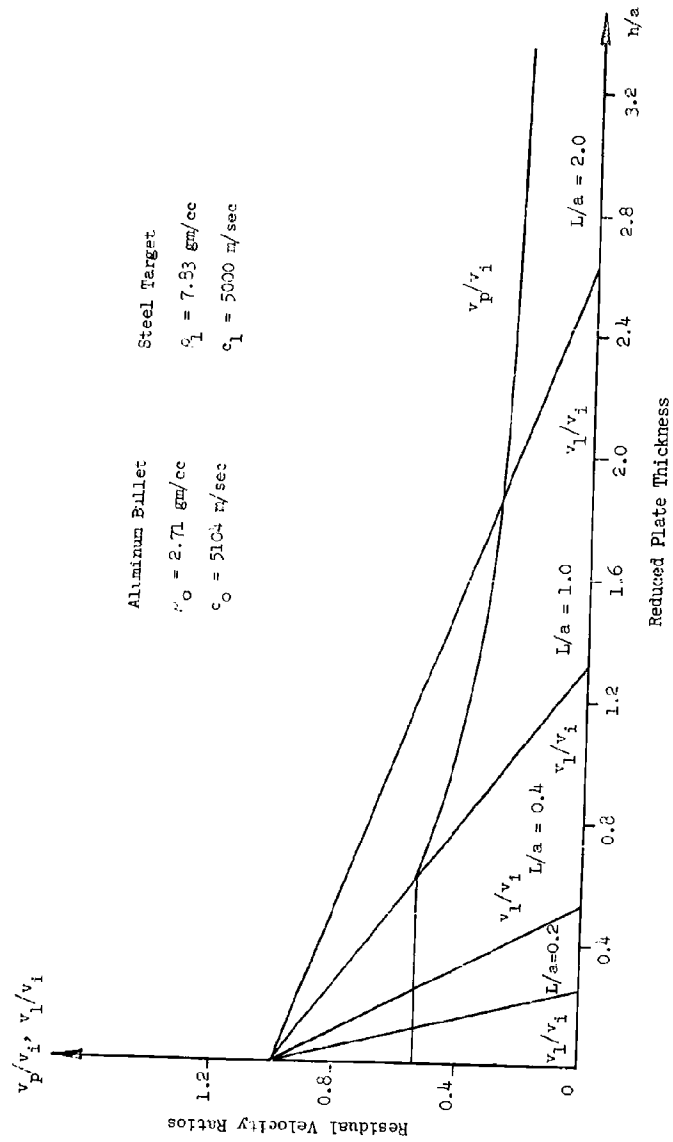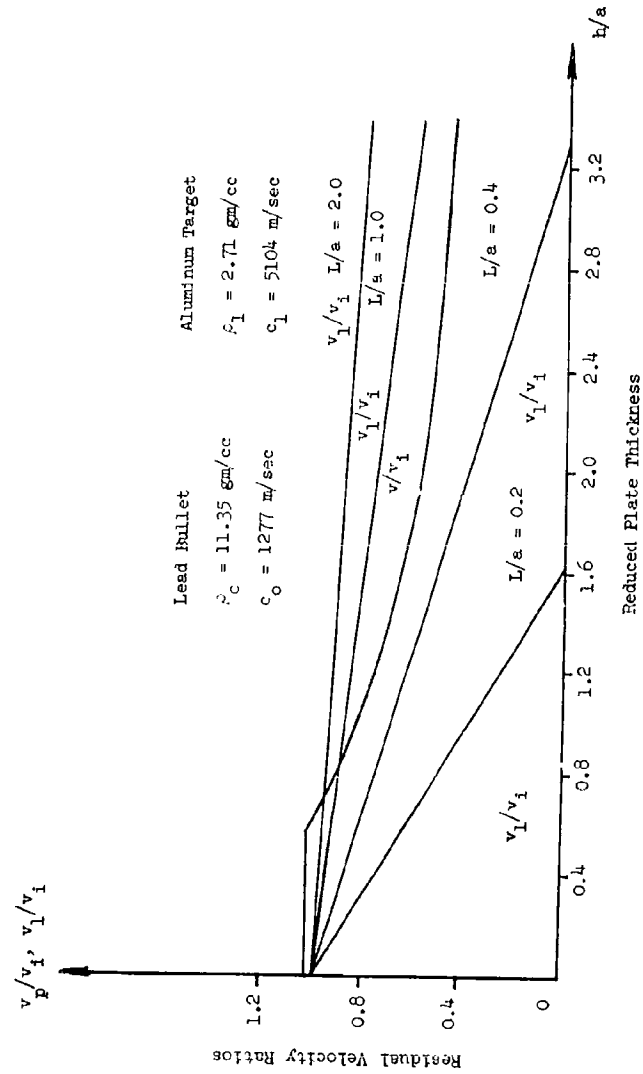
$\frac{v_p}{v_i}$ curve at that $\frac{h}{a}$. If the $\frac{v_p}{v_i}$ value is greater than $\frac{v_i}{v_i}$, this in-dicates that the bullet is coming through faster than the plug that it is pushing. In this case, the velocities of both the plug and projectile are the same and are given by an average value

$$\frac{v_i}{v_i}^* = \frac{v_p}{v_i}^* = \frac{h(\frac{v_p}{v_i}) + L(\frac{v_i}{v_i})}{h + L}$$

Thirty specific examples are explicitly evaluated for the reduction of bullet velocities and punch-out velocities for specific geomet-ries and material combinations (Figure 18 and Table I).

An example for the entire velocity range and the threshold velocities is given. The example is carried out for a particular case of engineering interest. The bullet is steel, diameter o.50 cm. and length 0.50 cm.

Three target materials, aluminum 2024 alloy, titanium and steel are chosen so that the mass per unit surface area is constant. The respective thicknesses ar Al 0.288 cm, Ti 0.172 cm, steel 0,10 cm.

This problem is chosen to correspond to a common design pro-blem in personnel armor plates, namely, comparative evaluation of ballistic resistance of different materials with the same total weight.

The reduction in projectile velocity is made as before, using, however, the time that the crack reaches the back side in the equation for velocity reduction. This is

$$t_c = \frac{h}{c_1} + 5\ (.429)\ \frac{h}{c_1} = 3.15\ \frac{h}{c_1}$$

These results are shown in Table II . The residual bullet velocities are shown in Figure 19. For this particular example, the titanium alloy plate offers the best resistance to penetration. At higher velocities, the reduction of bullet velocity is very near-ly the same, each plate differing from the others by a very small percentage.
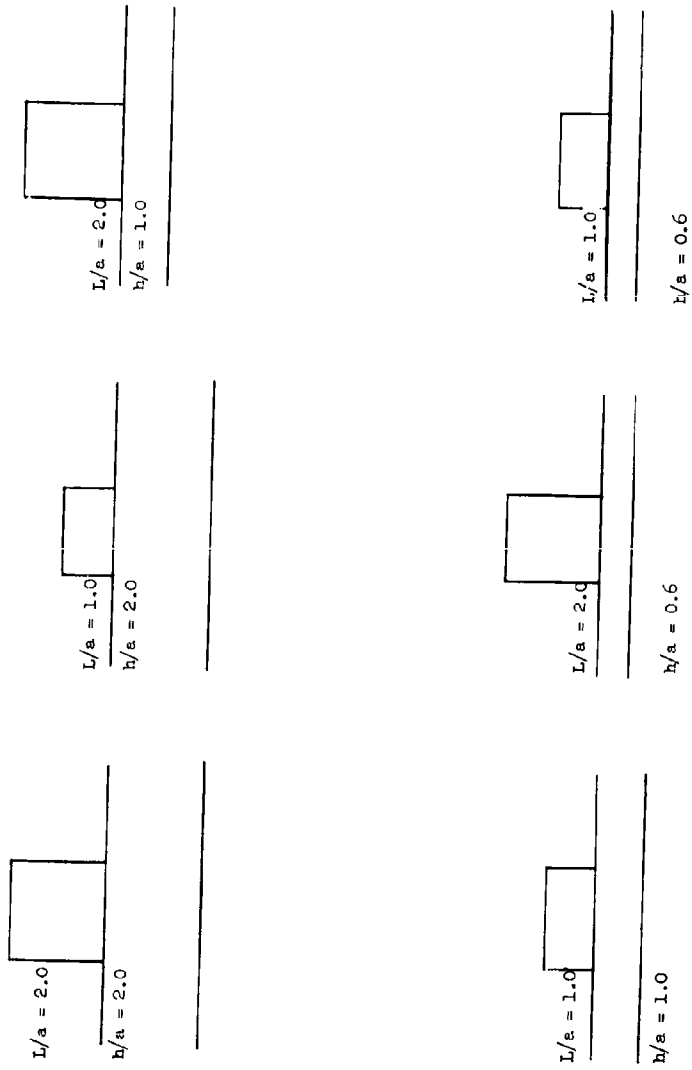
Figure 18 – Geometries for six cases of penetration

TABLE I   RESIDUAL VELOCITIES OF PLUG AND BULLET

		Projectile - Target				
		Al-Al	Al-Fe	Fe-Al	Pb-Al	Fe-Ti
Case I	$L/a = 2$ v_l/v_i	0.50	0.25	0.79	0.75	0.62
	$h/a = 2$ v_p/v_i	0.56	0.29	0.83	0.75	0.72
Case II	$L/a = 1$ v_l/v_i	0.00	0.00	0.50	0.65	0.26
	$h/a = 2$ v_p/v_i	0.56	0.29	0.83	0.65	0.72
Case III	$L/a = 2$ v_l/v_i	0.75	0.55	0.89	0.94	0.79
	$h/a = 1$ v_p/v_i	0.80	0.55	1.18	0.80	0.98
Case IV	$L/a = 2$ v_l/v_i	0.50	0.25	0.75	0.86	0.58
	$h/a = 1$ v_p/v_i	0.80	0.42	1.18	0.86	0.98
Case V	$L/a = 2$ v_l/v_i	0.85	0.71	0.94	0.96	0.88
	$h/a = 0.6$ v_p/v_i	1.03	0.71	1.51	1.03	1.33
Case VI	$L/a = 1$ v_l/v_i	0.70	0.54	0.85	0.93	0.77
	$h/a = 0.6$ v_p/v_i	1.03	0.54	1.51	1.03	1.33

TABLE II   PARAMETER FOR EQUAL MASS PER UNIT AREA EXAMPLE

STEEL PROJECTILE a = 0.25 cm, L = 0.50 cm

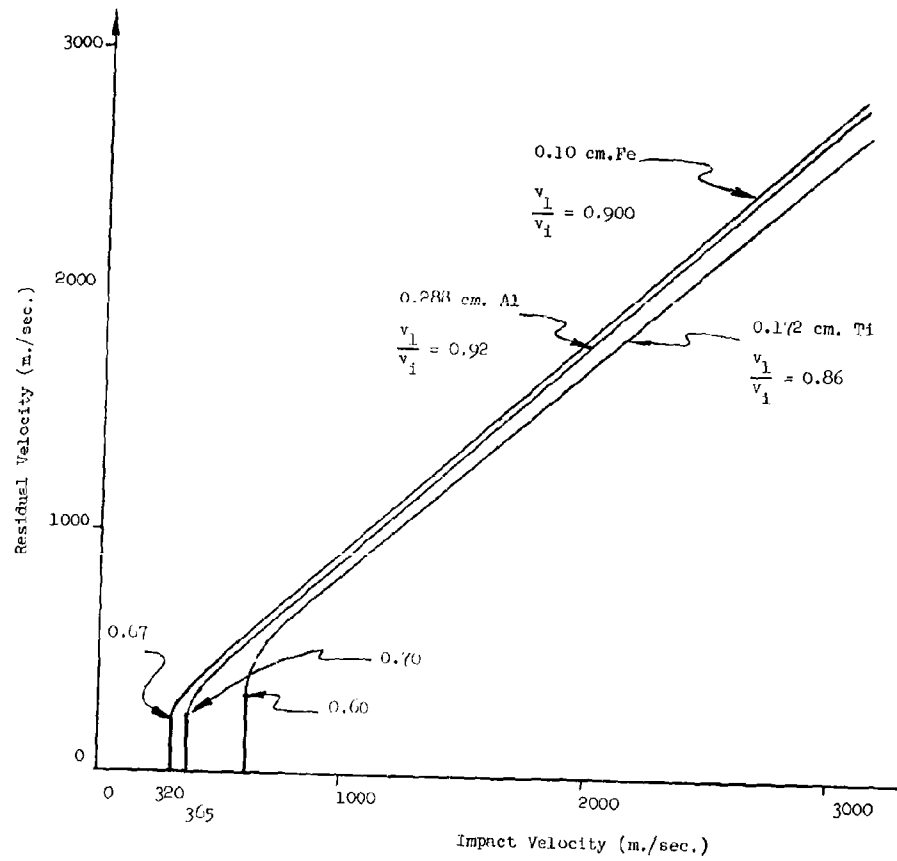|	h/a	L/a	$\frac{v_1}{v_1}$	σ_o $\frac{dynes}{cm^2}$	v_1^T m/Sec	$\frac{v_1}{v_1}$ at v_1^T
Case I						
Steel Target	0.40	2.0	0.90	6.67×10^9	364	0.70
h = 0.10 cm						
Case II						
Titanium Target	0.688	2.0	0.86	8.0×10^9	568	0.60
h = 0.172 cm						
Case III						
Aluminum Target	1.15	2.0	0.92	3.0×10^9	321	0.67
h = 0.288 cm						

Figure 19 - Residual bullet velocity versus impact velocity

5.0 CONCLUSIONS

In the design of light personnel armor to resist or retard penetration by projectiles, the knowledge of the fracture and subsequent behavior is a necessity. This information is aided by the theoretical studies of the deformation.

The linear elastic solution is sufficient to describe, to within reasonable accuracy, the deformation in a plate due to projectile impact under the restrictions;

      1) The impact velocity is less than 4000'/sec.
      2) The time duration of the load is less than 50μ sec.

The contributions of finite strain and plastic deformation in this regime are not zero, to be sure, but reasonable quantitative information is obtained without considering these effects. At higher velocities, or with longer impact durations, or with alteration of material properties, particularly with regard to inelastic deformation, these effects must be included.

Two elementary physical theories have been applied to the problem of penetration of thin plates by impacting projectiles. These two mechanisms were the linear elastic stress wave and fracture associated with the direct stress wave. Despite the obvious limitations imposed on the quantitative data by choosing these two approximations, reasonable agreement with experimental data is obtained.

The threshold impact velocity for penetration is a function of several parameters, among them the static yield stress, the acoustic impedence of the plate and the thickness of the plate.

The mass of the plug ejected in the penetration process will decrease in two steps corresponding to two different fracture occurences. The first reduction in plug size is caused by the pulverization of material behind the shear wave front of the direct stress wave. The second reduction is caused by spall from the stress waves generated at the side of the plug.

The residual velocities for the projectile and plug for any combination of materials thickness and are easily calculated.

The dependence of the residual bullet velocity on the plate thickness to bullet length has been shown.

Several specific problems occurring in the application of this basic analytical work were carried out. Two major conclusions that may be reached concerning impact are as follows.

I. To increase the threshold velocity for fracture, the combination of several factors must be maximized. We recall the expressions for the threshold velocity for thin plates

58

$$V_1^T = \frac{\sigma_0 \, (\rho_1 c_1 + \rho_0 c_0)}{0.436 \, \rho_1 c_1 \rho_0 c_0} \cdot \frac{\ln \frac{t^*}{t_0}}{\ln \frac{t_1}{t_0}} \qquad \frac{h}{a} \leq 0.6$$

$$V_1^T = \frac{\sigma_0}{0.327} \cdot \frac{(\rho_1 c_1 + \rho_0 c_0)}{\rho_1 c_1 \rho_0 c_0} \cdot \frac{\ln \frac{t^*}{t_0}}{\ln \frac{t_1}{t_0}} \; (\frac{h}{a})^{1/2} \quad 0.6 \leq \frac{h}{a}$$

$$\leq 1.5$$

Thus the acoustic impedence $\dfrac{\rho_0 c_0 \rho_1 c_1}{\rho_0 c_0 + \rho_1 c_1}$ between plate material and expected projectile material must be lowered at the same time the static yield strength in compression is raised. The term in the times to fracture is roughly constant for most metals.

The other variable to be maximized is the thickness of the plate.

II. To increase retardation of the projectile velocity when penetration occurs, the acoustic impedence must be maximized.

1) Cinelli, G. and Fugelso, L.E., "Theoretical Study of Ground Motion Produced by Nuclear Blast" AFSWC-TR-60-8, Final Report (1960)

2) Fugelso, L.E., "A Theoretical Study of Dynamic Plastic Deformation Under Impact Loads" Proc. 5th Hypervelocity Sympossium (1961) (To be published)

3) Fugelso, L.E., and Arentz, A.A. Jr., "Mechanics of Penetration" Final Tech. Report Contract DA-19-129-QM-1542 (1961)

4) Fugelso, L.E., "A Study of Dynamic Plastic Deformation Under Impact Loading by the Theory of Dislocations", Contract AF 29 (601)-2533 Final Tech. Report (1961)

5) Sneddon, I.N., "Boussinesq's Problem for a Flat End Cylinder", Proc. Cambridge Soc. (1946)

METHOD FOR OBTAINING YIELD STRESSES AT HIGH STRAIN RATES

J. W. Corcoran
Beckman & Whitley, Inc.
San Carlos, California

Introduction

Strain rates observed in armor penetration experiments characteristically have values of the order of 10^3 to 10^4/sec. While it has been noted that the properties of materials are altered from their static test values[1], very little experimental data is available under these circumstances. The reason is obvious. Standard testing machines can be modified to give rates of 10^2/sec (Manjoine[2]) but for greater rates than this new test methods based on impulses rather than steadily applied forces are necessary.

Test Theory

An experimental arrangement to achieve this is shown in Fig. 1. A cylindrical charge is placed on the axis of a hollow cylindrical test specimen and the intervening space filled with water. When the charge is detonated a conical shock wave moves out radially thru the water and imparts an impulse to the test material. After the shock reaches the free surface a rarefaction (negative pressure) wave immediately propagates back thru the specimen and water. This negative pressure causes cavitation of the water at the inner surface of the specimen effectively isolating it from the water and it moves outward under its own inertial forces. This sequence of waves may be observed in Fig. 2, a series of high speed photographs taken thru a longitudinal section of such a specimen.

As the specimen moves radially outward it develops a tensile hoop stress within itself which acts to decelerate it. The kinetic energy is thereafter absorbed by elastic and plastic deformation of the cylinder. From the law of conservation of energy the velocity is given by the formula:

$$\frac{1}{2}\rho(V_o^2 - V^2) = \int_0^{\epsilon_1} E\epsilon \, d\epsilon + \int_\epsilon^\epsilon S_u d\epsilon \qquad (1)$$

where ρ is the density of the material
V_o is the initial velocity
V is the instantaneous velocity
E is the elastic modulus
ϵ is the strain
S_u is the plastic yield stress

This form of equation assumes the idealized stress strain curve of Fig. 3(a). It should be understood that this experiment is not limited to this hypothesis but rather that it may be tested by appropriate plots of the test data.

For the elastic region this equation can be put in the form:

$$\left(\frac{V}{V_o}\right)^2 = 1 - \frac{E\epsilon^2}{\rho V_o^2} \qquad (2)$$

which indicates the modulus of elasticity can be obtained from the slope of the curve shown in Fig. 3(b).

Typically the plastic region is of much greater significance as the bulk of the energy is dissipated in it and for this zone the equation is:

$$\left(\frac{V}{V_o}\right)^2 = 1 - \frac{S_u\epsilon_1}{\rho V_o^2} - \frac{2S_u\epsilon}{\rho V_o^2} \qquad (3)$$

where ϵ_1 is the limit of elastic strain. In this case the data should be plotted as in Fig. 3(c), and the plastic yield stress can be obtained from the slope as indicated.

Test Results

A typical high speed camera record of the expansion of such a cylinder taken with a Beckman & Whitley Model 189 Camera is shown in Fig. 4. The camera is focused on the edge of the cylinder, in this case 5" in diameter, and the field is backlighted to show the cylinder and the distance

61

gage wires which were placed 0.125 inch apart. The framing rate was 480,000 frames/sec hence the individual pictures were taken 2.08 sec apart.

A typical data plot is given in Fig. 5. The material was 2024 T4 Aluminum and a plastic yield stress of 32,600 psi was obtained at a strain rate of **2900**/sec.

It may be easily shown that the strain rate is given by:

$$\frac{d\epsilon}{dt} = \frac{V}{r} \qquad (4)$$

hence variation of the initial velocity and the diameter of the specimen permits its adjustment. An estimate of the initial velocity of a thin metal shell can be obtained from the formula[3].

$$\frac{V}{D} = 0.38 \frac{\rho_w}{\rho_e} \left[(\frac{r_2}{r_1})^2 - 1 \right]^{0.4} \qquad (5)$$

where D is the detonation velocity of the explosive,
ρ_w is the density of water
ρ_e is the density of the explosive
r_1 is the radius of the explosive
r_2 is the radius of the cylinder

By suitable adjustments of the charge geometry, then, a range of strain rates between 200/sec and 12,000/sec are attainable. Data obtained for a series of shots taken at various strain rates are shown in Fig. 6.

Conclusion

The test technique described offers a simple experiment which produces an unidirectional tensile stress at strain rates comparable to those observed in armor penetration.

Cylinder end effects are eliminated because failure is caused to occur in sections in the center of the tube.

Data obtained on standard aluminum indicates that the plastic yield stress at high strain rates is approximately twice the static value in general agreement with the estimates from other investigators.

Bibliography

1. Bodner, S. R. and Symonds, P. S. "Plastic Deformations in Impact and Impulsive Loads of Beams" Plasticity, Pergamon Press, pp. 488-500, 1960

2. Manjoine, M. J. "Influence of Rate of Strain and Temperature on Yield Stresses in Mild Steel" J.App.Mech. Vol. 11, pp. 211, 1944

3. Holland, T. E., Final Report, George Washington University Research Laboratory, AD 306050, 1959

Table of Figures

EXPLOSIVE
CHARGE

SPECIMEN

WATER

Figure 1 - Charge Configuration For Producing High Strain Rates
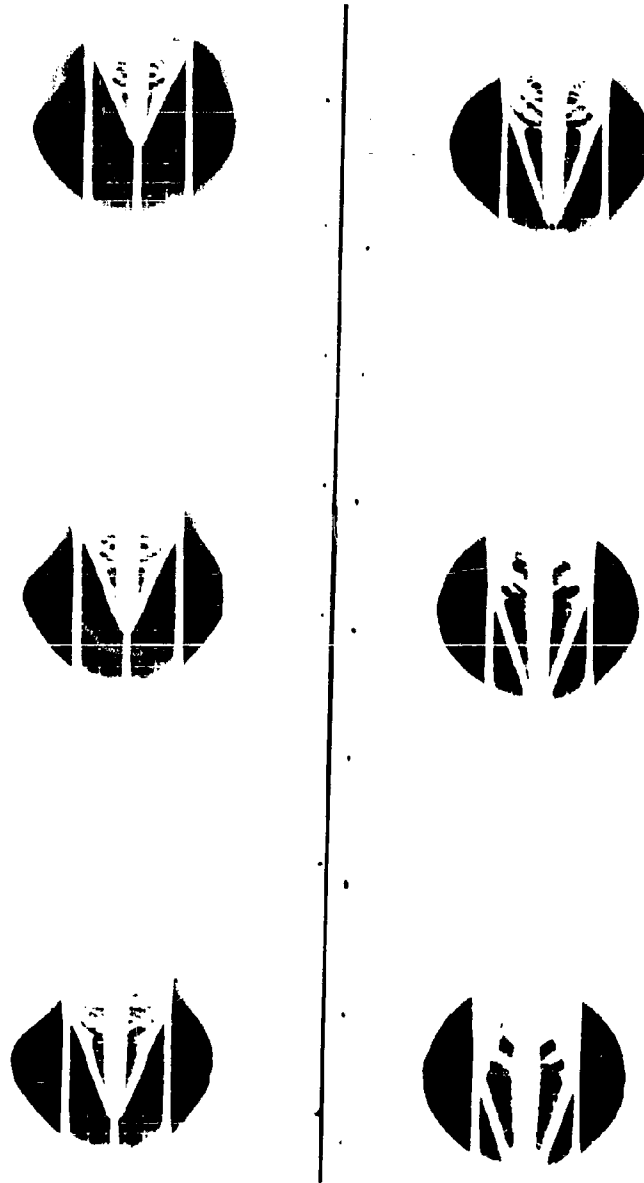
Figure 2 - Framing camera picture of shock and rarefaction waves in a longitudinal section of Figure 1.
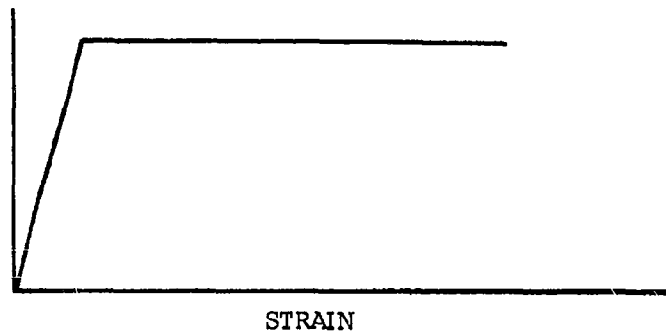
FIGURE 3(a)   IDEALIZED STRESS-STRAIN CURVE
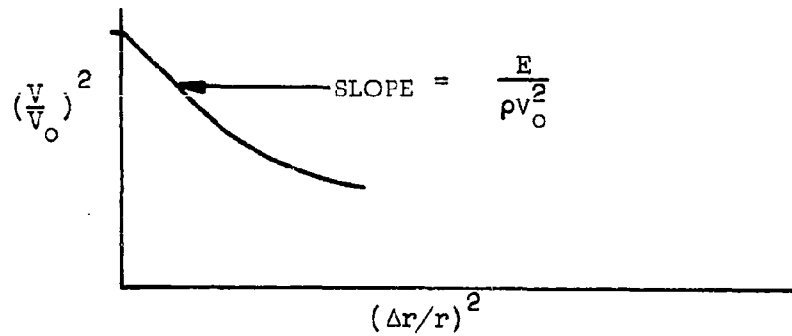
FIGURE 3(b)   PLOT FOR DETERMINING ELASTIC MODULUS
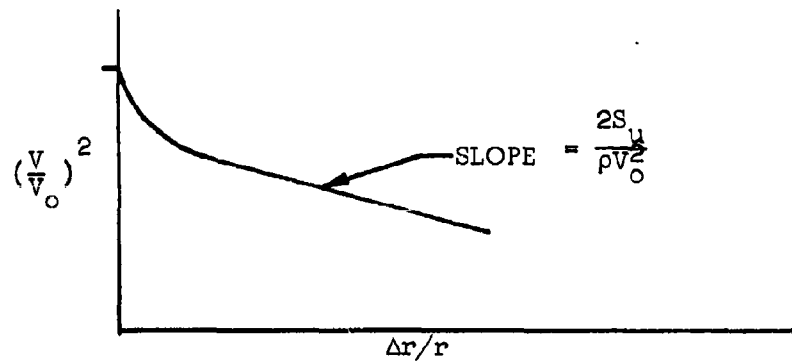
FIGURE 3(c)   PLOT FOR DETERMINING PLASTIC YIELD STRESS
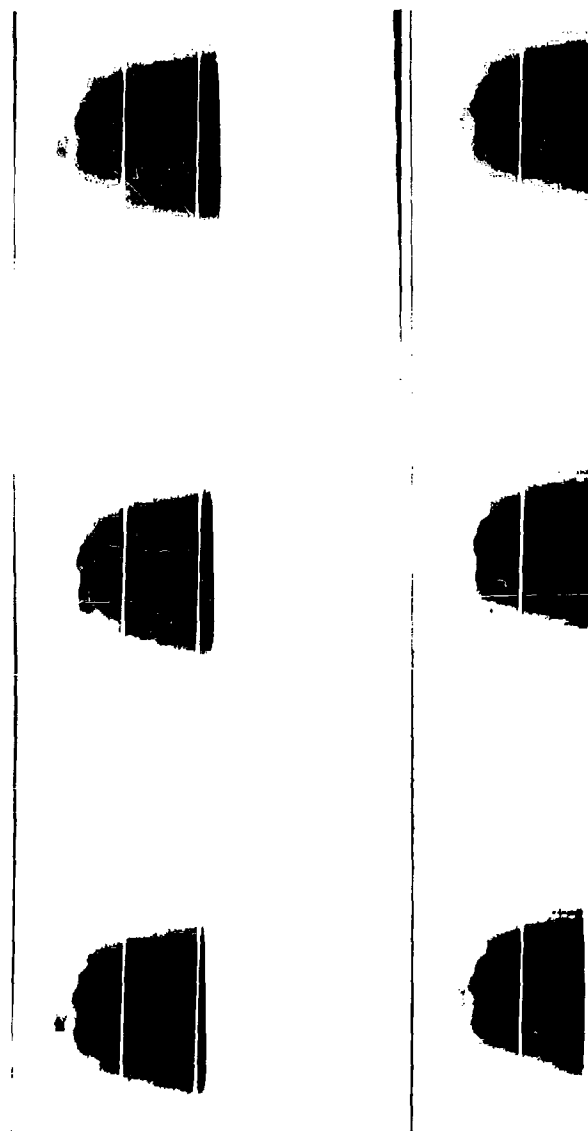
Figure 4 - Sequence of picture taken with a
Beckman & Whitley Model 189 Framing Camera.
Framing rate is 480,000 frames/sec. Note pro-
gressive motion of right side of frame, the edge
of the aluminum cylinder across the first gage
wire.

LIGHT SOURCE

TEST SPECIMEN

BACK
LIGHTING
LENS

GRID
WIRES
SPACED 1/8"

MODEL 189
FRAMING CAMERA

Figure 5

SHOT No. 112
V^2 vs. x

DECELERATION-0.00318 $\dfrac{mm}{usec^2}$

INDICATED STRESS-32,600psi

STRAIN RATE-2900 ^{1}/sec

Figure 6

70

YIELD STRESS vs. STRIAN RATE

TEST
SPECIMEN

IDEALISED STRESS–STRAIN DIAGRAM
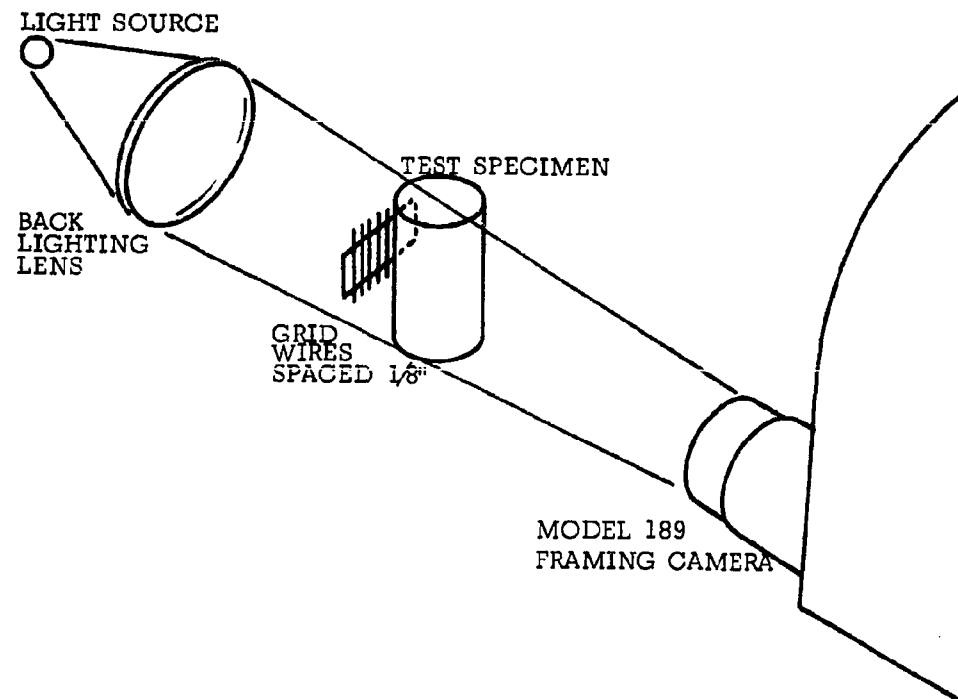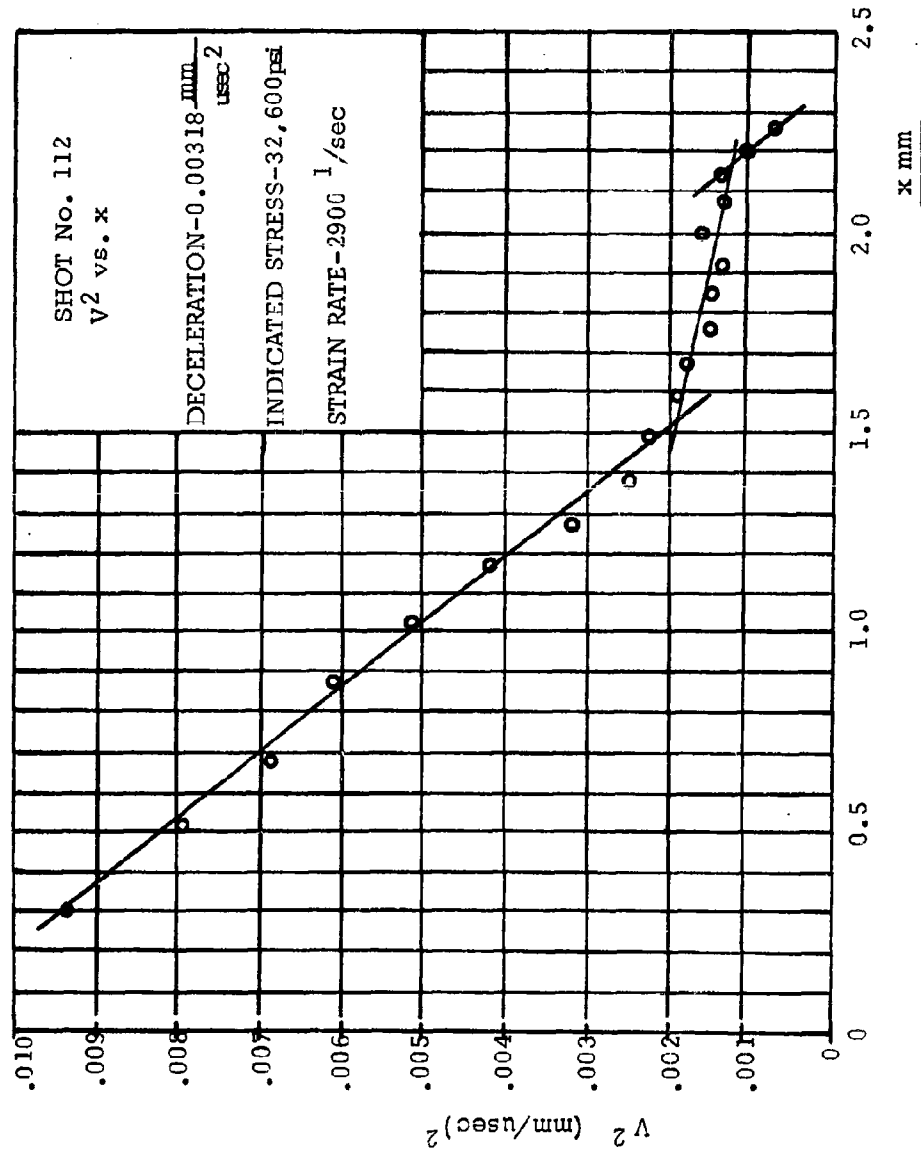
Figure 7
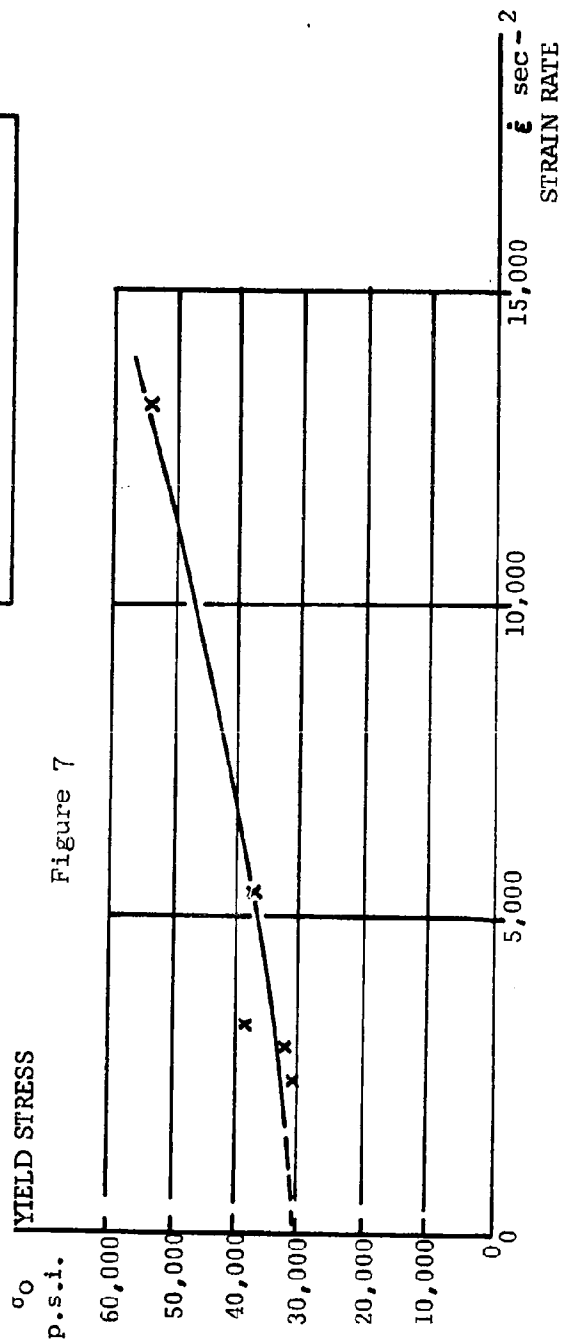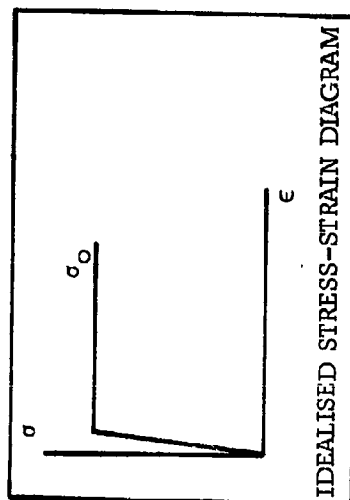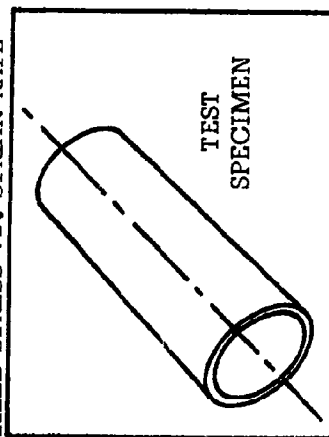
THE DYNAMIC PROPERTIES OF HIGH TENACITY YARNS AND
THEIR RELATIONSHIP TO BALLISTIC RESISTANCE

R. C. Laible
QM R&E Command
Natick, Mass.

Two possible inter-related advantages result from the study of the mechanical properties of textile materials. The first is that we may predict the usefulness of the material under study for personnel armor applications. The second is that the information gained about several different synthetics should allow us to predict the ideal properties that the material should possess. With this information in the fiber manufacturer's hands, we would be insured improved materials.

At last year's symposium, the stress-strain properties of Vinal, a highly oriented polyvinyl alcohol type fiber, were discussed.(1) The high strength and high work to rupture characteristics were pointed out with special emphasis on the relative constancy of work to rupture with increasing strain rate. The details of this stress-strain work will appear in the September issue of the Journal of Polymer Science and will not be repeated here.(2) Fabrication of the Vinal yarn into fabric and subsequent ballistic testing showed a 5-10% improvement over the standard nylon body armor. The vinal could also be bonded for use as a helmet liner. The future of Vinal in the ballistic program will now depend upon its domestic availability.

The next new material investigated was isotactic polypropylene.(3) Prior to Natta's developments in the field of stereospecific polymerization, polypropylene was a low melting solid unsuitable for forming fibers of any kind. In contrast, isotactic polypropylene lends itself to the formation of fibers with excellent mechanical properties and would therefore appear to be a likely candidate for personnel armor applications.

Experimental Methods

Polypropylene yarn with a crystallinity of 65% and an orientation of about 90% was subjected to stress-strain testing

at many different strain rates encompassing five decades of testing time. The methods used included the Instron for static tests, several pneumatic and pneumatic-hydraulic systems for intermediate speeds, the rotating disk method for impact testing, the falling weight and ballistic methods.

Results and Discussion

The stress-strain curves for polypropylene at several different strain rates are shown in Fig. 1. More detailed information concerning the ultimate properties (breaking strength, breaking
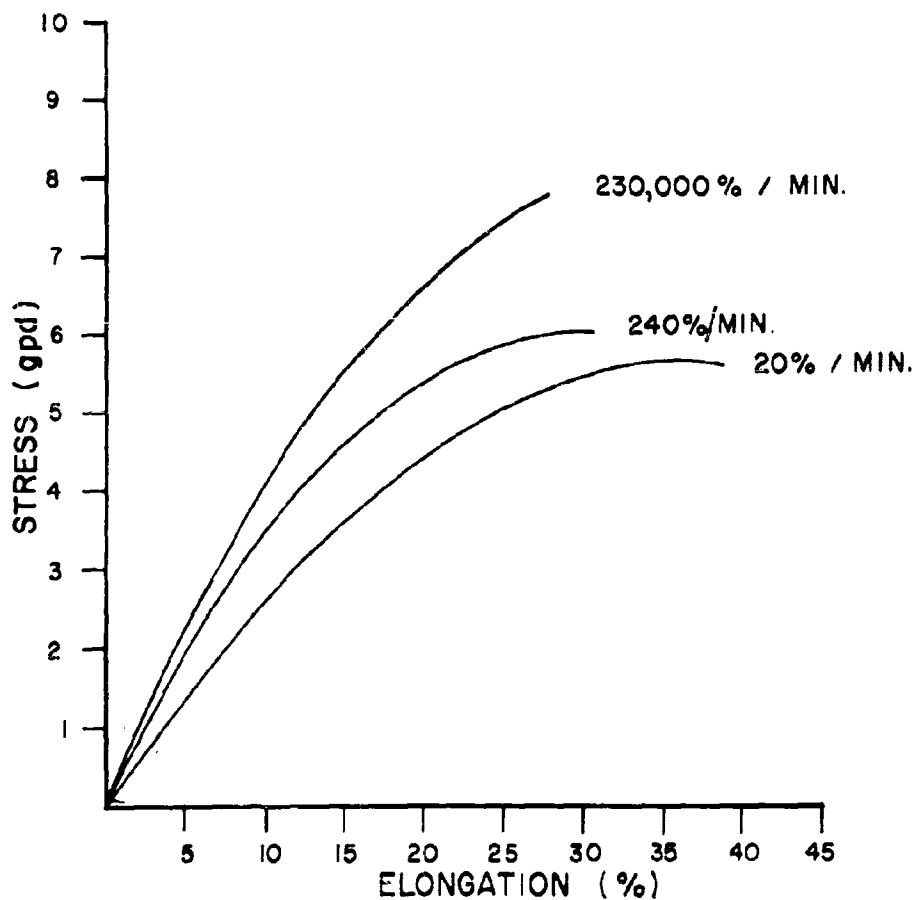
Fig. 1 Stress-Strain Behavior of Isotactic Polypropylene
At Different Strain Rates

elongation and work to rupture at wide variety of strain rates) is shown in Table I. Note that as the speed of testing increases, tenacity increases but rupture extension decreases. The work to rupture values are very high throughout the strain rate spectrum but tail off somewhat at very high speeds.

TABLE I

MECHANICAL PROPERTIES AT VARIOUS STRAIN RATES

Laboratory	Speed of Testing (inches/minute)	Speed of Testing (% per minute)	Rupture Load (gpd)	Rupture Extension (%)	Work to Rupture (joules/gm)
QM	1	20	5.7	38.0	126
QM	12	240	6.0	32.2	118
P-T	300	10,000	6.1	32.1	119
FRL	2,400	96,000	6.7	29.8	113
P-T	3,300	110,000	7.0	30.7	120
QM	12,000	200,000	6.9	28.0	111
FRL	5,760	230,000	7.1	27.0	105
MIT	21,600	270,000	7.0	28.0	107
FRL	9,400	370,000	8.0	27.7	113
NBS	-	400,000	-	-	69
FRL	12,500	500,000	8.4	28.4	115
FRL	432,000 to 650,000	>1,500,000	5.5	13.5	34
FRL	940,000	>2,000,000	9.6	12.0	40

Actually, failure phenomena are so complicated that scientists interested in the mechanical behavior of polymers usually restrict themselves to very low strains. In this work we have compromised on strain levels of 2, 6, 12 and 16% elongation. The stress values for the various strain levels and strain rates were used to form simulated stress relaxation experiments as shown in Fig. 2. Stress in dynes/cm^2 has been plotted against log time over a spectrum of 5 decades. Note the shape of these curves with two areas of high time dependency separated by a plateau characteristic of little or no relaxation at intermediate speeds.

This behavior can be represented by a rather simple mechanical model composed of two Maxwell units in parallel. This model is shown in Fig. 3 with values of modulus, viscosity and retardation time given for 6% extension. The models for extensions lower and higher than 6% are similar with similar retardation times (10^{-2}, 10^{+2}) but different moduli and viscosity constant values.

Theoretical modulus - lot time curves can be constructed based upon this model by the use of the expression.

$$6_{\epsilon} \;=\; S/_{\epsilon} \;=\; G_1\, e^{-t/\tau_1} \;+\; G_2\, e^{-t/\tau_2}$$

where G_t is total modulus, S= stress, ϵ = elongation, and τ_1, τ_2 are the relaxation times for the model and t is the time of testing under consideration. This has been done for 2, 6, 12 and 16% extension using the following values for the model (Table II).
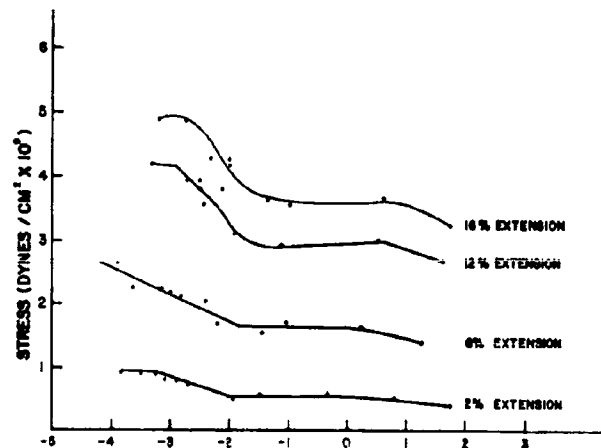
Fig. 2   Stress Log Time Plots in the Form of Stress
Relaxation Curves
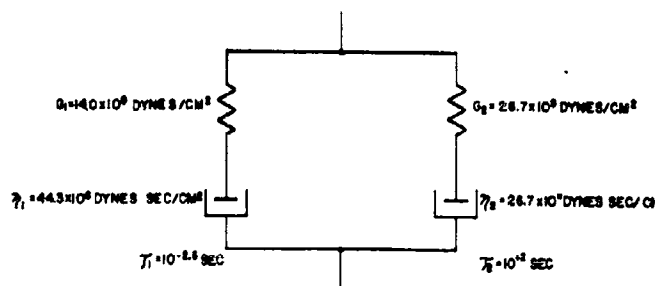
Fig. 3   Mechanical Model Representing Isotactic
Polypropylene at 6% Extension

75

TABLE II

PARAMETERS FOR THE MECHANICAL MODEL AT DIFFERENT EXTENSIONS

Extension (%)	c_1 (dynes/cm²)	η_1 (dyne sec/cm²)	τ_1 (sec)	c_2 (dynes/cm²)	η_2 (dyne sec/cm²)	τ_2 (sec)
2	21.1×10^9	6.69×10^7	$10^{-2.5}$	26.0×10^9	26.0×10^{11}	10^{+2}
6	14.0	4.43	$10^{-2.5}$	26.7	26.7	10^{+2}
12	10.2	10.2	10^{-2}	24.2	24.2	10^{+2}
16	8.1	8.1	10^{-2}	21.8	21.8	10^{+2}

In Figure 4 the smooth modulus - log time curve was obtained from calculations using the expression above and the constants for 6% extension. The dots are the experimental points obtained from the stress-strain data expressed as modulus as a function of testing time. Similar comparisons for 2, 12 and 16% extension show good agreement at each extension (considering the simplicity of the model) for the high speed testing range of greatest interest (Figs. 5, 6, 7).
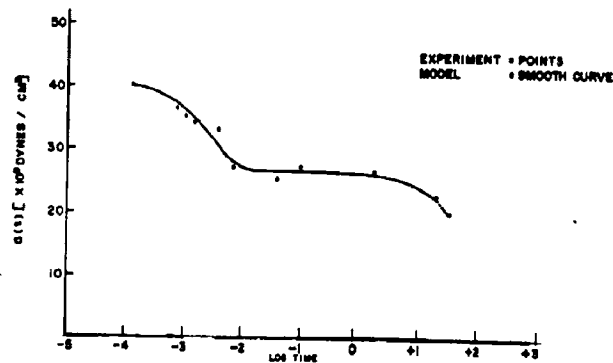
Fig. 4   Comparison of Experimental Data with Mechanical Model (6% Extension)
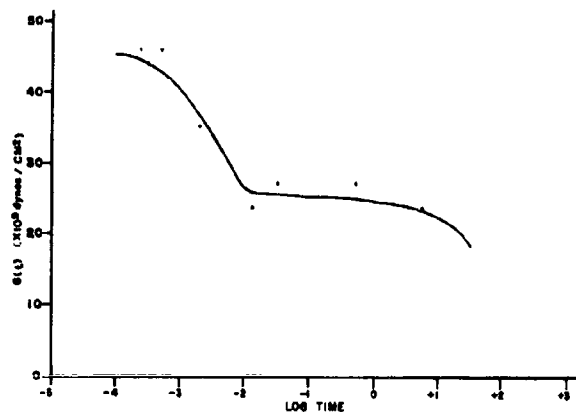
Fig. 5 Comparison of Experimental Points with Curve for Mechanical Model (2% Extension)
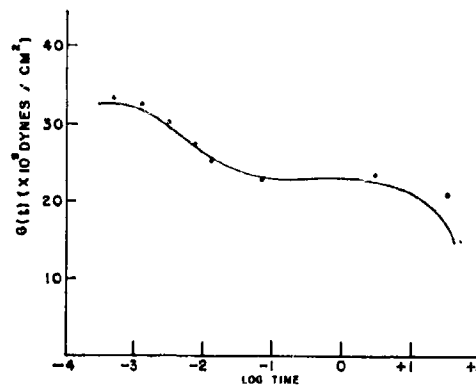
Fig. 6 Comparison with Theoretical Curve from Proposed Model with Experimental Data (12% Extension)

77
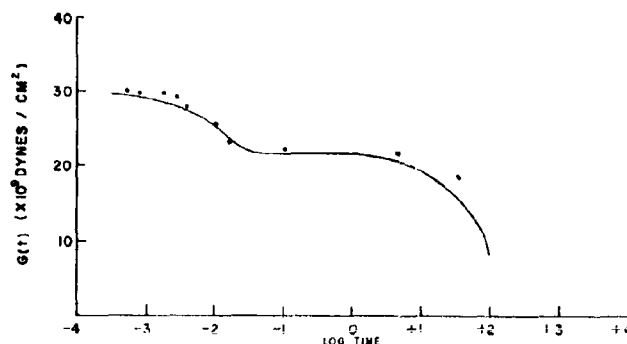
Fig. 7 Comparison of Theoretical Curve from Proposed
Model with Experimental Data (16% Extension)

However, close inspection of the curves shows that the long
time relaxation phenomenon is better represented by a more compli-
cated system. This is even more dramatically pointed out when we
try to suggest a similar model to represent data obtained by Hall on
isotactic polypropylene (Fig. 8) (4). The so-called box distribution
would appear to be a more likely candidate for the long time data.

It is apparent that the stress-strain behavior of polypro-
pylene is interesting from a theoretical point of view and promising
from the standpoint of applications. The ultimate properties of
tenacity, elongation and work to rupture compare favorably with any
known textile fiber available today. Based upon these properties or
upon the single criterion of work to rupture, one would predict that
isotactic polypropylene would be a better candidate for materials
requiring high impact resistance than nylon, Dacron, Fortisan 36 or
any other synthetic fibers available today. Isotactic polypropylene
has been prepared in fabric forms utilizing both plain weave and
basket weave structures as well as different cover factors. Finish-
ing has been varied from lubricant added to Syton treatment with
intermediates of different scouring methods because of our previous
experience with nylon. The ballistic results obtained for all these
fabrics using the 17 grain fragment simulator fell below those
attainable with a well prepared basket weave fabric. These results
could lead to several alternate conclusions:

(1) There is something wrong with the stress-strain
data presented.
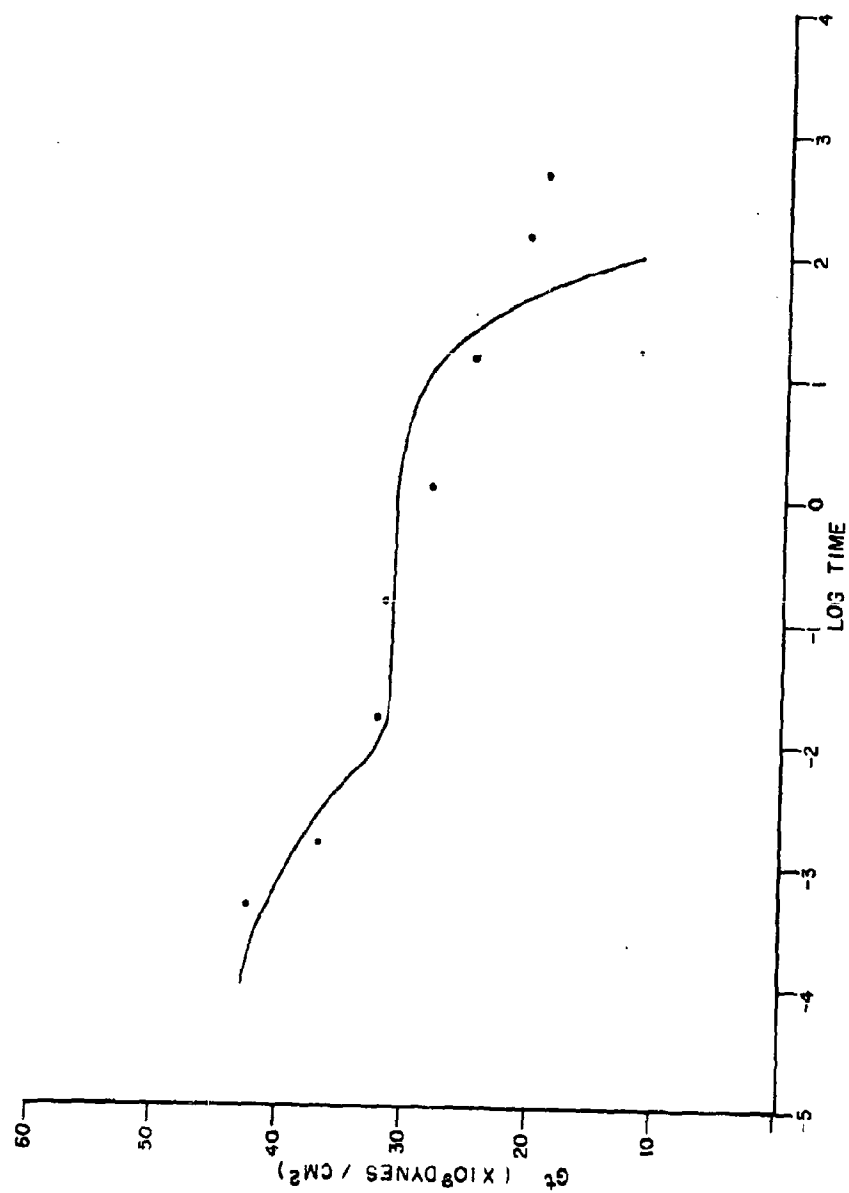
Fig. 8 Attempt to Represent Hall's Data by a Simple Mechanical Model (15% Extension)

(2) Research into the mechanical properties of materials will not answer the ballistic problem because good mechanical properties do not necessarily lead to good ballistic properties.

(3) The properties of isotactic polypropylene yarn are good but we have not yet learned to make use of them in a suitable fabric system.

There could be some truth to the first conclusion because it is difficult to measure the properties accurately at the very high ballistic speeds. The second conclusion would be of paramount importance as it would show the need for an entirely different approach. However, perhaps we can test this conclusion by reference to work on nylon 700, an 840 denier nylon yarn with improved mechanical properties. Under a very small QM program with West Point Manufacturing Company, four fabric types were prepared from the yarn including plain, 2x2 twill, 2x2 basket and 2x1 basket weaves. All of the fabrics show resistance to ballistic penetration superior to the present nylon standard as shown in the following table.

TABLE III

BALLISTIC RESULTS FOR NYLON 700

Fabric Type	Weight	Count	V_{50}
2 x 2 Twill	11.97 oz/yd^2	50 x 43	1344 ft/sec
2 x 2 Basket	12.77	56 x 30	1306
2 x 1 Basket	11.08	56 x 30	1265
Plain	10.67	50 x 31	1323

The standard nylon fabric exhibits a ballistic V_{50} value of 1225 - 1260 ft/sec therefore we have options of lower weight or increased ballistic limit from the use of this material. As a bonus the 840 denier yarns are $.50 a pound cheaper therefore the substitution represents a substantial potential savings. This recent work with nylon 700 is introduced as an example where the improved yarn properties of nylon do lead to improved ballistic properties.

Past work in personnel armor was then reviewed in an attempt to find some other solution for the disappointing behavior of isotactic polypropylene. You may remember that in the period 1950-53, Dr. George Susich of the QM R&E Command was studying fired nylon panels as part of a study to determine the energy distribution of a missile after impact with the standard nylon fabric vest. The results of this excellent research study were presented at several Personnel Armor Symposiums and the unclassified results published in the Textile Research Journal. In the course of this investigation, the actual number of yarns

broken in each layer was determined. (5) A similar investigation was conducted for this present study but polypropylene and Vinal fabrics as well as nylon were included.

The results obtained are shown in Table IV.

TABLE IV

YARN BREAKAGE AS INFLUENCED BY FABRIC TYPE

Fabric	Speed of Missile	Warp Yarns Broken	Filling Yarns Broken	Total
Nylon	1232 ft/sec	50	55	105
Vinal	1226	48	59	106
Polypropylene	1223	38	20	58
Polypropylene	1222	47	29	76

Based upon this information, even if the isotactic polypropylene exhibited a work to rupture per yarn 20% higher than nylon, the total energy consumed by yarn breakage would still be 30% less than for nylon due to the fewer number of yarns broken. Inspection of a polypropylene panel shos that yarn slippage and partial pullout are much more pronounced than for Vinal, nylon and Fortisan panels previously tested. Control of yarn slippage and pullout by resin treatments and changes in fabric structure should result in reduced slippage and realization of the full potential of isotactic polypropylene. Polypropylene also could be used in felt form where the low fiber to fiber friction seems to be less of a problem.

Summary

The stress-strain properties of an isotactic polypropylene yarn have been studied over a wide variety of strain rates and a mechanical model suggested to portray the viscoelastic characteristics. From the ultimate properties found, isotactic polypropylene should be an excellent candidate for personnel armor. To date, it has failed to live up to expectations. Two explanations are given for this failure as follows:

(1) The work to rupture tends to decrease at ballistic speeds.

(2) Excess slippage results in fewer yarns being broken in a polypropylene fabric than for nylon or vinal.

The most important conclusion from this work is that we must gain an understanding of the penetration of materials whether these materials be metal, fibers, plastic sheets or felts. The advantage to be gained from the use of higher tenacity yarns is evident from the excellent ballistic resistance exhibited by fabrics prepared from nylon 700. However, although we want high tenacity yarns, there is no point in spending too much money to produce a 9 gpd or 12 gpd polypropylene yarn until we have solved the basic problem of the mechanism of penetration of the 6-7 gpd polypropylene. This is the approach we have been following and by the next symposium we hope to have modified the polypropylene fabric so that its full potential is realized.

References

1. Laible, R. C. "New High Tenacity Fibers for Personnel Armor"
   Department of Defense Armor Symposium, Natick, Mass., 7-9
   June 1960, pp. 131 - 6 (5).

2. Laible, R. C. and Morgan, H. M. "The Viscoelastic Behavior of
   Oriented Polyvinyl Alcohol Fibers at Large Strains" J of
   Polymer Science 54, 159, 53-63, 1961

3. Morgan, H. M. and Laible, R. C. "A Mechanical Model to
   Represent the Viscoelastic Properties of Polypropylene"
   Textile Research J. , November 1961, (in print).

4. Hall, I. H. "Time Dependent Tensile Strength of Solids"
   Nature 189, 131 (1961).

5. Susich, G. Unpublished work 1958.

BUOYANT INSULATING BODY ARMORS FROM STAPLE FIBERS

M. C. Jaskowski
Mellon   Institute
Pittsburgh 13, Pa.

Abstract

Staple fibers show great promise as effective personnel body
armor. In contrast to the multifilaments used in the nylon armor
cloth, these armors contain cut fibers of relatively low tenacity,
1.5-3 grams per denier. In order to convert the staple fibers into
usable forms, they are carded into a batt, essentially a laminated
web structure, which is then compressed to desirable thicknesses.

The ballistic test employed is a modification of the proposed
military standard acceptance method which utilized the .22 T-37 (17
grain) fragment simulator. Initially, the 0.020 inch thick aluminum
witness plate served as a means of determining the limiting veloci-
ties of the test samples; but this was replaced by a device capable
of accurately measuring the velocities of the projectiles which
pass through the armor samples. With this technique, the protective
efficiency of an armor can be found at any striking velocity above the
limiting velocity. By plotting initial or striking velocity vs. per-
centage loss of velocity due to the sample (i.e. percentage of
original energy of the projectile absorbed by the sample), a curve may
be drawn from which one may readily obtain the value representing the
velocity at which complete arrestment of the projectile is attained.

The ballistic performances of carded fibrous batts have
been found to be dependent upon fiber type, fiber length, fiber
diameter, surface characteristics of the fiber and the areal densities
of the mats. By the addition of an efficient water-repellent, a batt
composed of fine fibers may be transformed into a thermal insulating
body armor possessing an outstanding degree of buoyancy.

Introduction

In 1954 the Bureau of Ships became interested in incorporating ballistic protection into the bulk-type life preservers. The standard buoyant filler, fiber glass, offered little if any, protection against shrapnel. The problem was to replace the glass with a material capable of maintaining the same level of buoyancy but with a high degree of resistance to shrapnel penetration. Organic staple fibers presented the greatest possibilities. The author investigated the application of various staples to life preservers while the actual ballistic tests were conducted at the Naval Research Laboratories and the Dahlgren Naval Proving Grounds.

Subsequent to this work, the Bureau of Supplies and Accounts through the U S. Naval Supply Research and Development Facility became cognizant of the possibility of preparing an unique jacket liner with excellent thermal insulation, sufficient buoyant properties to keep the wearer afloat for a reasonable period and an adequate measure of ballistic protection. The performance of this liner would be limited, however, by those conditions accompanying practical applications such as drape, weight, size, etc. The initial requirements suggested a liner 3/8" - 1/2" thick and with an areal density of 10 - 20 oz/yd^2.

In contrast to the armors using high tenacity filaments such as nylon or fiber glass, (8 - 10 grams/denier), we will discuss those that are composed of staple fibers of low tenacity (1.5 - 3.0 gms/denier). At this time, a comparison between the mechanisms apparently employed by the two systems to withstand projectile penetration would be pertinent. In the case of the Doron or nylon armor cloths, the energy of the striking projectile is expended mainly in two ways: one, by breaking or shearing the filaments and, two, by de-laminating the layers. In the staple-fiber batts, retardation of the projectile is due essentially to the dissipation of energy through the movement of fibers against fibers as they are pushed aside by the projectile. When the spinning pellet first engages the fibrous sample, it is immediately wrapped with fibers. This increases its size, resulting in greater hindrance to its passage.

During the presentation of the data accumulated, it should be remembered that the scope of the ballistic investigation was dictated by the buoyant and insulation requirements of the program; such as fiber diameter and the use of a water-repellent.

85

Preparation of Test Samples

For the preparation of the test liners, the staple fibers were carded to form batts. These are essentially laminated structures, representing multi-layers of fibrous webs. The batts, unless otherwise indicated, were placed between cotton print cloth covers and then between two rigid metal sheets which could be separated at any predetermined distance. The thickness of the sample was thus kept constant over its entire area. Holes in the metal, relatively large in comparison with the diameter of the projectile, permitted passage of the projectile.

Testing Procedure

The ballistic test method employed was similar to the proposed military standard acceptance method utilizing the .22 caliber T-37 (17 grain) fragment simulator. Originally, the prescribed aluminum witness plate served to indicate the ballistic effectiveness of the samples. Eventually, this was replaced with two accurately spaced detectors capable of determining the velocities of those projectiles which pass through the samples. Thus the initial and residual velocities can easily be obtained as well as the amount of energy absorbed by the test specimens.

Nomenclature

Our definition of the term "limiting velocity" which will be used repeatedly is that range of velocities between partial penetration and no penetration. Of course this applies only in those cases where the aluminum witness plate was used. On the other hand, when the initial and residual velocities were found, and a curve obtained by plotting initial velocity versus the percentage velocity loss due to the sample, the limiting velocity is that point resulting from the extrapolation of the curve to 100% velocity loss.

Experimental Results

Generally at velocities slightly below the limiting velocities of these carded staple batts, conical fiber wads are found

protruding from the back cover cloth. This phenomenon has caused concern. We have found that this effect may be minimized and, at times, eliminated with the use of nylor armor cloth as the back cover. Several representative examples are: Two batts of 1.0 denier per filament hydrophobed Orlon (3.0" cut) at 10 oz/yd^2 each and covered with the cotton print cloth were compressed to a thickness of 0.25". This combination was found to have a limiting velocity of approximately 873 ft/sec, and exhibited the conical wads. By replacing the back covers of each batt with single layers of the nylor armor cloth, the limiting velocity was raised to approximately 976 ft/sec. Of greater significance was the fact that up to an initial velocity of 952 ft/sec, the fragment simulators were retained in the sample without the appearance of the conical wads.

Another significant example was found when a 40 oz/yd^2 batt of hydrophobed 1.0 denier per filament Orlon (3.0" cut) was placed between a front cover of the cotton print cloth and a back cover of four layers of nylon armor cloth. Up to a velocity of 1109 ft/sec, no projectile penetrated the nylon cloth preventing any wad protuberance.

Throughout our investigations, we have observed a striking relationship between the length of the staple fiber and the limiting velocity of the carded fiber batt. The first table demonstrates this effect. The data had been obtained by the Naval Research Laboratory using the yawed-dart technique.

Table 1

Fiber Length vs. Limiting Velocity
Yaw-Dart Method

1.0 dpf Orlon + 4% Decetex-104 Finish
3.5" Thickness--180 oz/sq. yd.

Fiber Length (inches)	Limiting Velocity (ft/sec)
1.5	1140 + 10
2.0	1175 + 50
2.5	1230 ∓ 20
3.0	1365 + 35
4.5	1320 + 40
5.5	1310
7.0	1270

As evident, a maximum limiting velocity is found for a fiber length of 3.0 inches. Similar relationships have been found for several other synthetics.
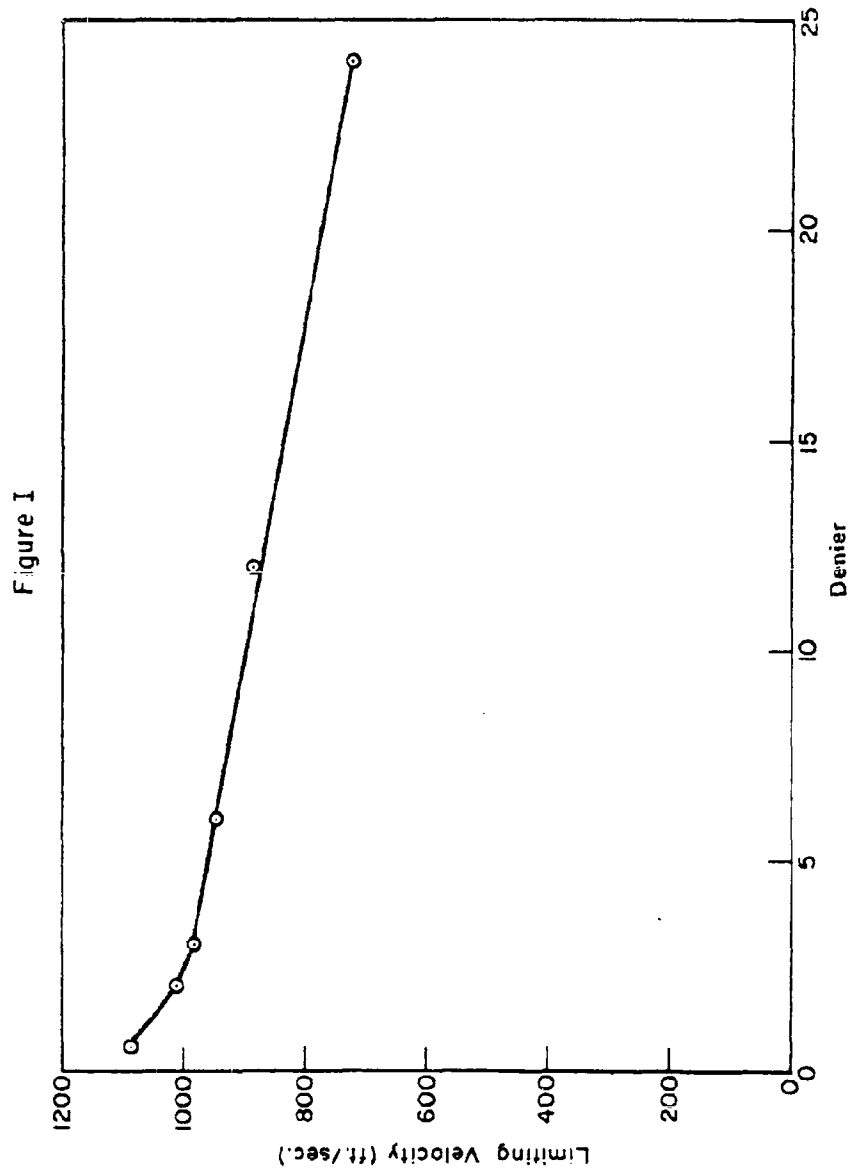
The effect of fiber diameter upon ballistic performance was observed. Since buoyancy and thermal insulation of staple fiber batts are indirectly proportional to fiber diameter, it was necessary to determine whether ballistic protection was similarly affected. Fortunately, we have found this to be true. Figure I exemplifies the relationship. The physical characteristics of the Dynel staple fibers were identical in all respects, e.g., length, crimp, finish, with only a variation in their diameters. With reference to Figure II, a comparison between 0.5 denier and 1.0 denier Acrilan fibers again demonstrates superior ballistic performance by the "finer" fiber.

As you will observe throughout the presentation of the experimental data, a majority of the staple batts were prepared at an areal density of 42 oz/yd^2. Although our interest lies in fibrous liners with areal densities up to 20 oz/yd^2, the heavier samples served to differentiate between the various fibers and finishes Generally, the limiting velocities of the 42 oz batts were in the range 900 ft/sec to 1200 ft/sec.

The relationship between areal density and limiting velocity at a constant thickness was obtained for 1.0 denier per filament Orlon (3.0" cut) and 1.5 denier per filament Dacron (3.0" cut). These fibers were chosen because of their superior buoyant characteristics. A comparison of the resultant curves (Figure III), shows that the Orlon batts are slightly superior. The extrapolation of the Orlon curve promises extremely large limiting velocities at areal densities greater than 45 oz/yd^2.

Figure IV is the first representation of what we have termed "protective efficiency" of two fibrous batts. The percentage loss of initial velocity due to the sample batt is plotted against initial velocity. Thus at velocities greater than the limiting velocity, the effectiveness of the liners in slowing down the projectiles can be known. The limiting velocity can also be found by extrapolating the curve to 100% velocity loss.

Of the staples examined to-date, it appears that 1.0 dpf Orlon (3.0" cut) exhibits the highest ballistic performance. Originally, only hydrophobed Orlon fibers were tested, the presence of a water-repellent being required for buoyancy. However, the effect of this finish and others upon ballistics became of interest academically. A comparison between the Decetex-104 silicon finish, the original anti-static agent applied by the manufacturer and hydrophobed aerogel is presented in Figure V. A visual examination of these three samples have shown that the Decetex best reduces the fiber-to-fiber friction while the aerogel increases the friction tremendously. The curves may, therefore, be interpreted as showing that any increase in the fiber-to-fiber friction above that for the Decetex sample, lowers the ability of the batts to withstand fragment penetration. We have observed this effect with other fibers, that decreasing the mobility of the fibers below a certain value decreases the ballistic efficiency.

Figure I

EFFECT OF FIBER DIAMETER UPON BALLISTIC PERFORMANCE

Dynel Staple Fiber (2" - 3" cut)
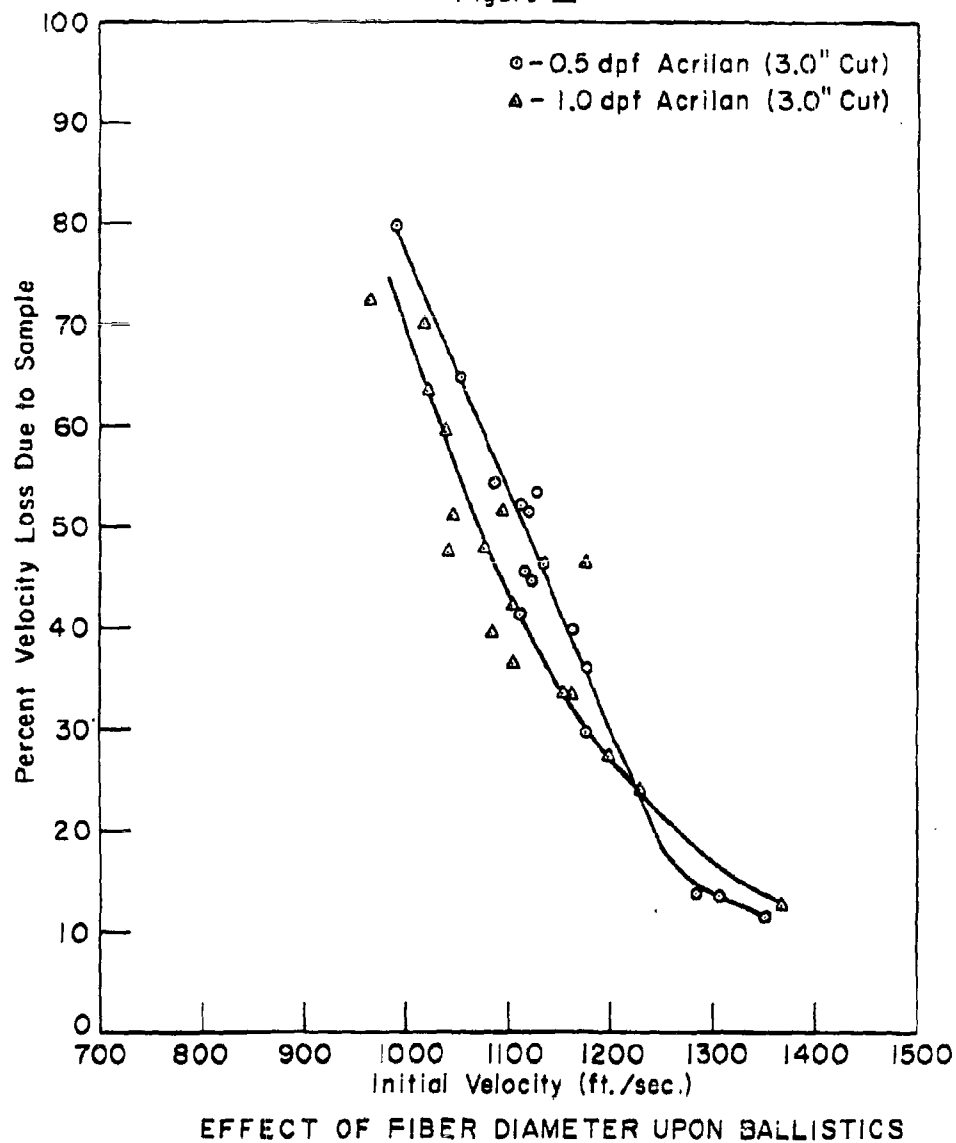
Figure II

EFFECT OF FIBER DIAMETER UPON BALLISTICS
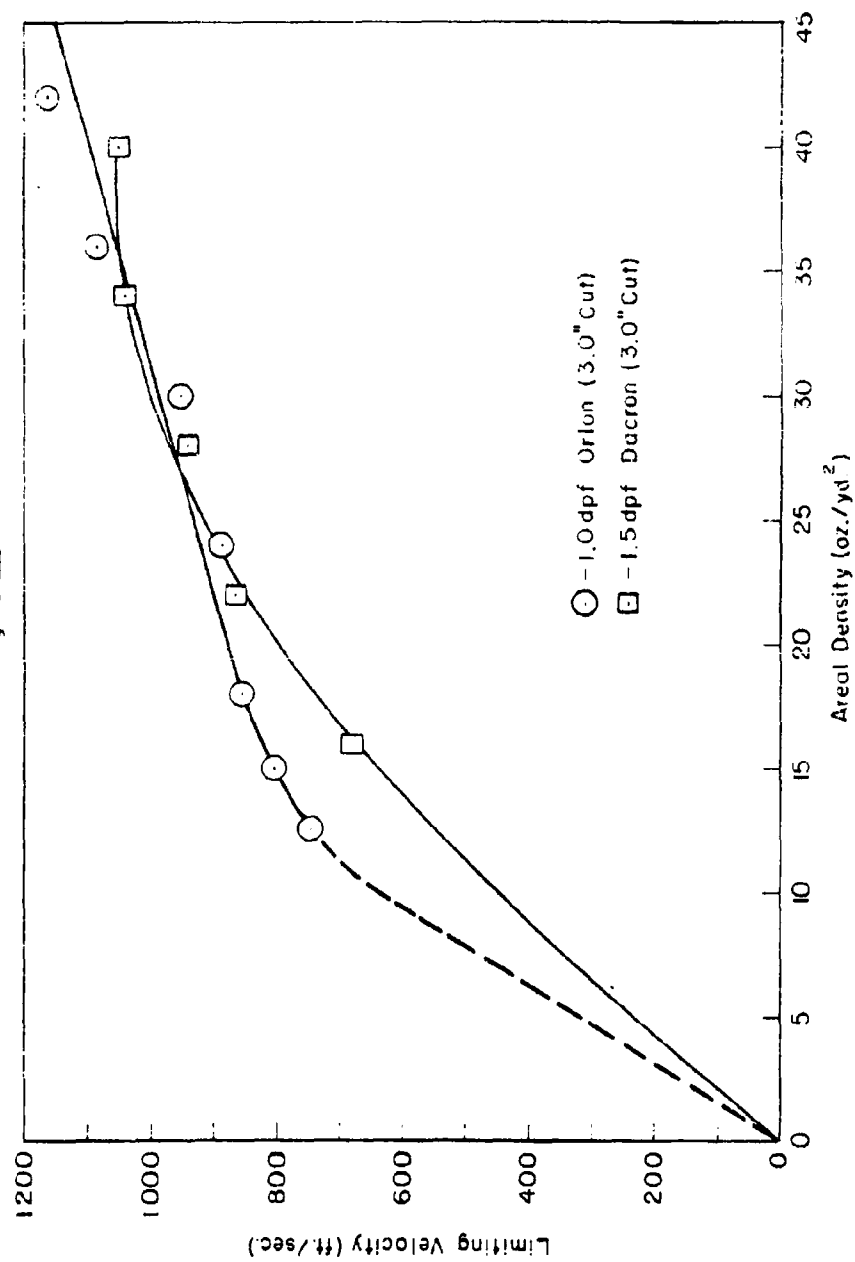
Figure III

HYDROPHOBED STABLE FIBER BATTS AT SAMPLE THICKNESS = 0.5"

○ — 1.0 dpf Orlon (3.0" Cut)
☐ — 1.5 dpf Dacron (3.0" Cut)

Areal Density (oz./yd²)

Limiting Velocity (ft/sec.)

Figure IV

HYDROPHOBED 1.0 dpf ORLON BATTS (3.0" CUT)

Figure V

EFFECT OF SURFACE FINISH ON 1.0 dpf
ORLON BATTS (3.0" CUT) 42 oz/yd^2

There are three commercially-available staple fibers with small diameters which form highly-buoyant batts. These are 1.0 dpf Orlon (3.0" cut) 1.0 dpf Acrilan (3.0" cut) and 1.5 dpf Dacron Type 5400 (3.0" cut). A comparison between the ballistic efficiencies of these was made and can be seen in Figure VI.

For numerous reasons, manufacturers occasionally alter, chemically or physically, their commercial staple fibers. This, we know, can affect the ballistics of carded batts prepared from them. As an example, we have found that hydrophobed batts of 1.5 dpf Dacron Type 5400 (3.0" cut) are considerably superior ballistically to those containing hydrophobed 1.5 dpf Dacron Type 64 (2.5" cut). The difference in the staple length does not appear to account for the great difference in the ballistic efficiencies. Figure VII contains the representative curves.

The present phase of our investigation encompasses the preparation and testing of fiber blends and composites. Preliminary work has been done using mixtures of 1.5 dpf Dacron and 0.5 dpf Acrilan. By referring to Figure VIII, one may perceive that the 50/50 blend and composite are essentially equal ballistically and have the effect of totally up-grading the Dacron as well as increasing the limiting velocity of the 0.5 dpf Acrilan.

The last two figures show the "protective efficiencies" of the Doron armor and the 12 layer nylon armor cloth. In Figure IX considerable variation exists among the points obtained. It appears logical to assume that these are due to inconsistent delamination, which, in turn, may be attributed to irregularities encountered in manufacture. The same inconsistencies exist in the results of the ballistic tests upon the nylon armor. Here again, the delamination of the spot-sealed layers appears to have a great effect.

An interesting and significant interpretation of the "protective-efficiency" data for the 1.0 dpf Orlon batt at an areal density of 42 oz/yd^2 and either the Doron or nylon armor, points to the preparation of a composite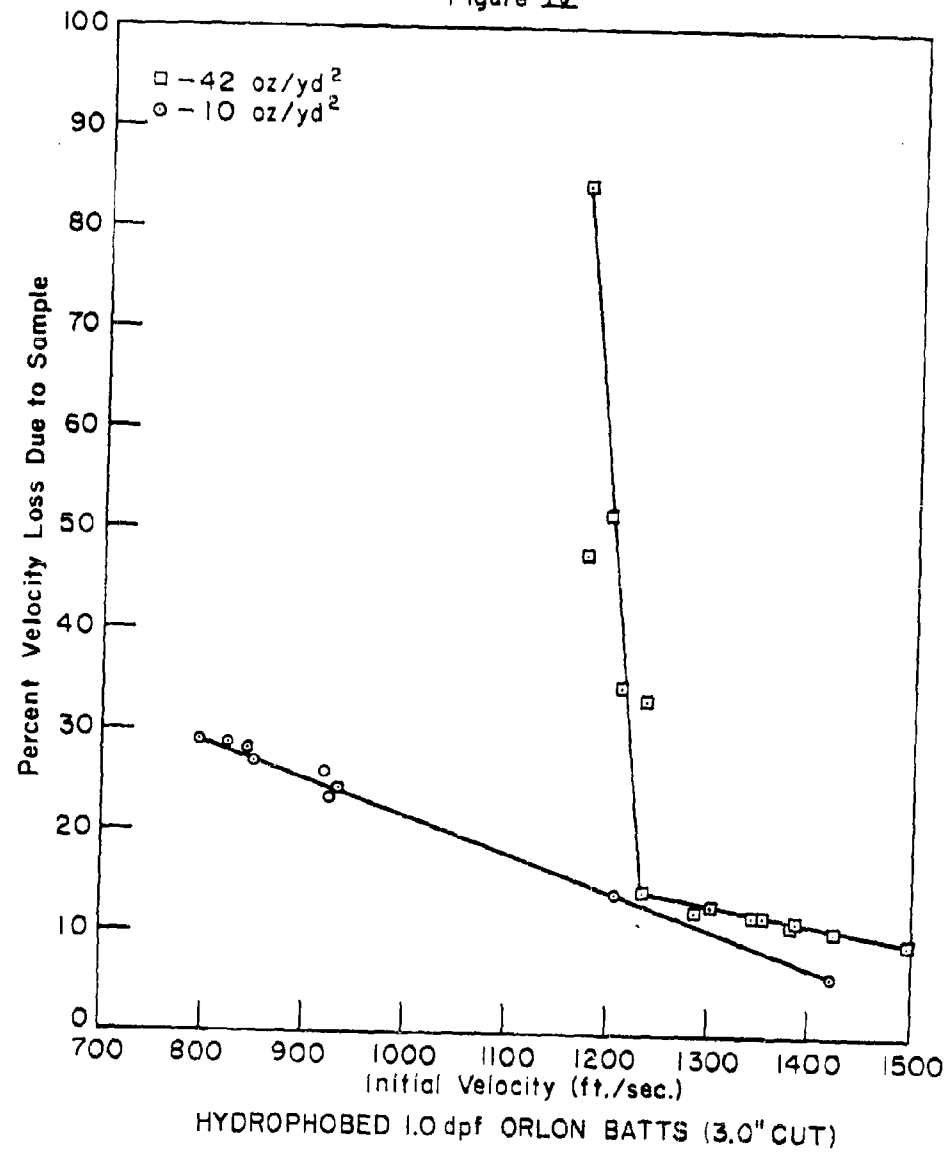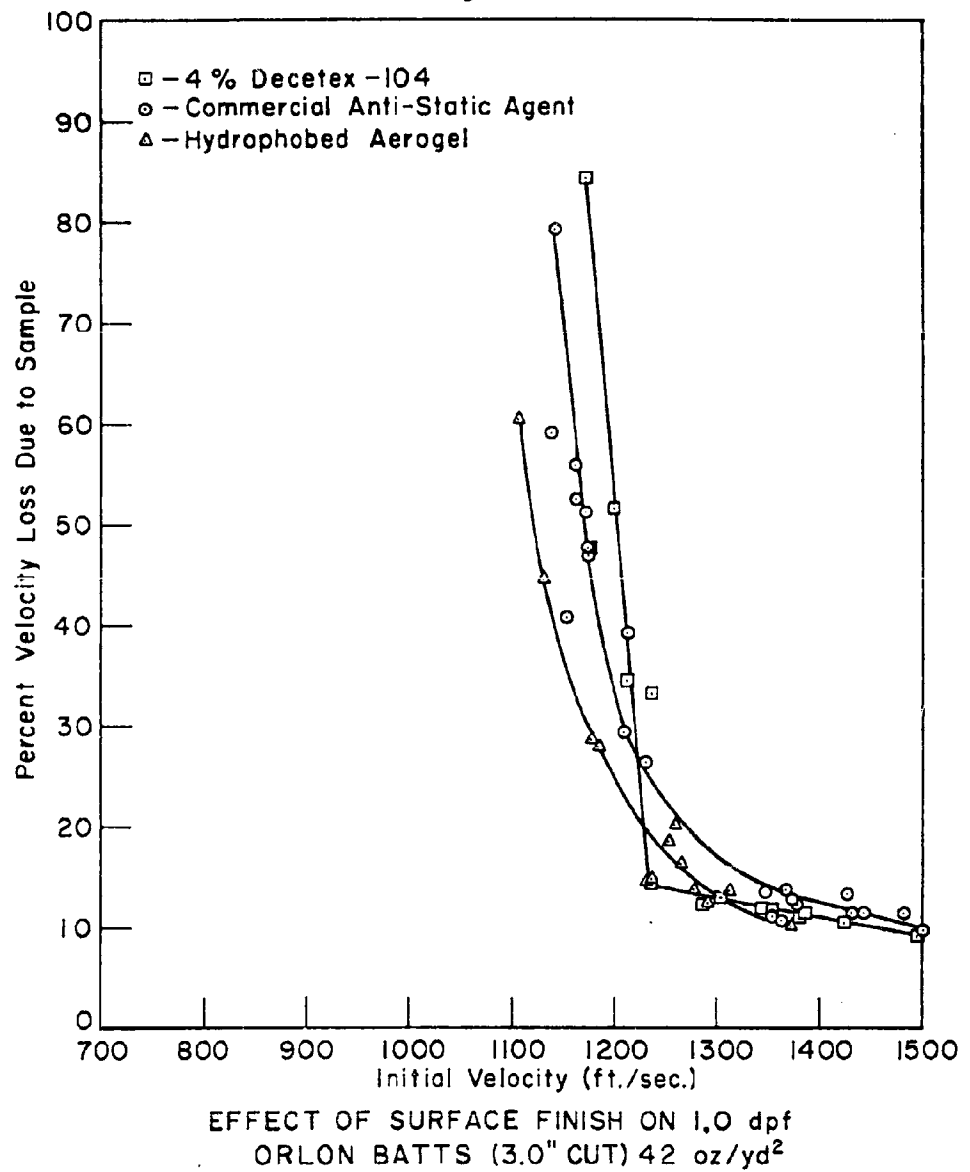 armor capable of protecting the wearer from 17 grain projectiles traveling at velocities up to 1600 ft/sec. Only if these materials were positioned properly could this protection be achieved. If the Orlon batt were used as the outside layer which would be struck first by the projectile traveling 1600 ft/sec, it would be easily penetrated with the residual velocity of the projectile being greater than 1350 ft/sec. This residual value far exceeds the limiting velocity of the Doron, resulting in complete penetration of the composite. However, if the Doron were placed outside to encounter the projectile first, the initial velocity would be lowered by 36 - 37% during its passage through the Doron. The residual velocity would be slightly in excess of 1000 ft/sec. This value is less than the limiting value of the Orlon batt. The projectile would be completely contained.

94
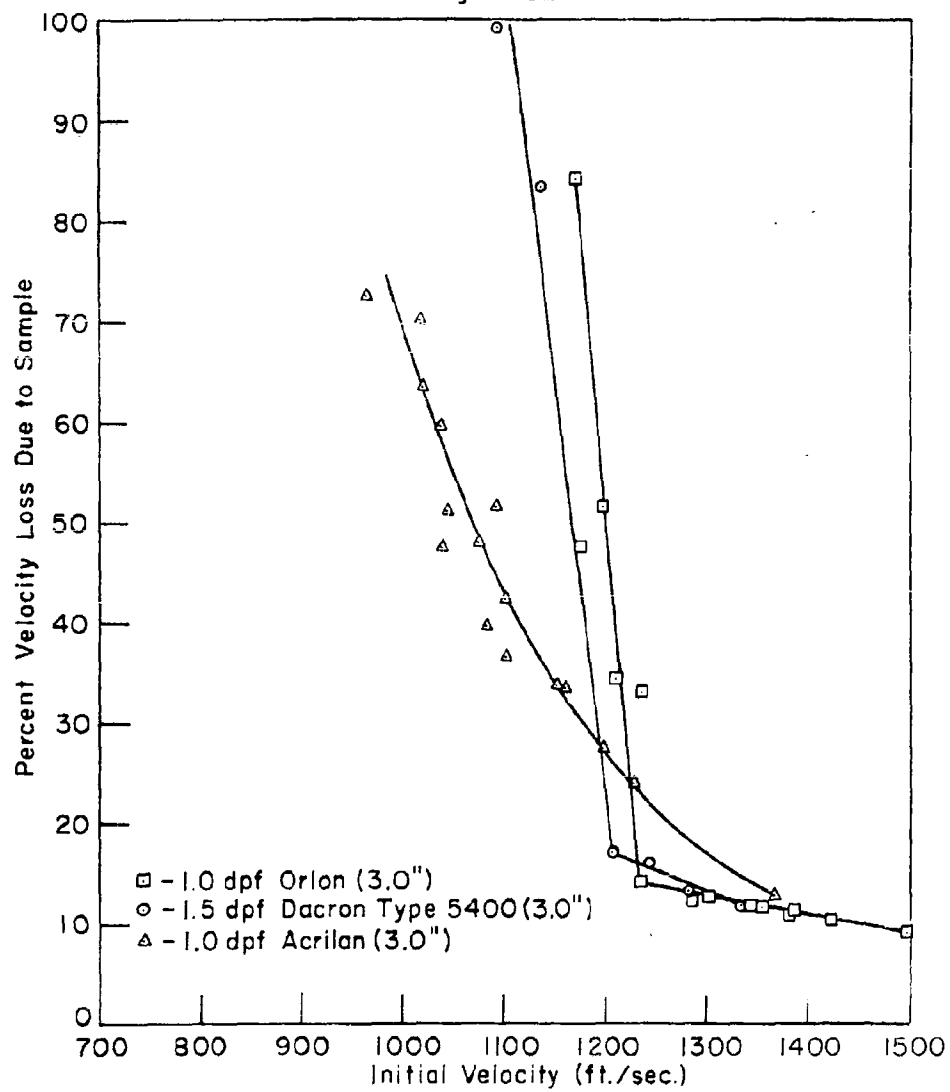
Figure VI

COMPARISON BETWEEN COMMERCIALLY –
AVAILABLE FINE STAPLE FIBERS 42 oz/yd²

Figure VII

VARIATION IN COMMERCIAL DACRON STAPLE FIBERS 42 oz/yd^2

96

Figure VIII

- ⊙ – 0.5 dpf Acrilan (3.0" Cut)
- ⊡ – 1.5 dpf Dacron Type 64 (2.5" Cut)
- △ – 50/50 Blend
- ▽ – 50/50 Composite with Acrilan in Front

FIBROUS BLENDS 42 oz/yd^2

Figure IX

Percent Velocity Loss Due to Sample

Initial Velocity (ft./sec.)

1/8" DORON, 175 oz/yd^2

Figure X

NYLON ARMOR CLOTH, 168 oz/yd²
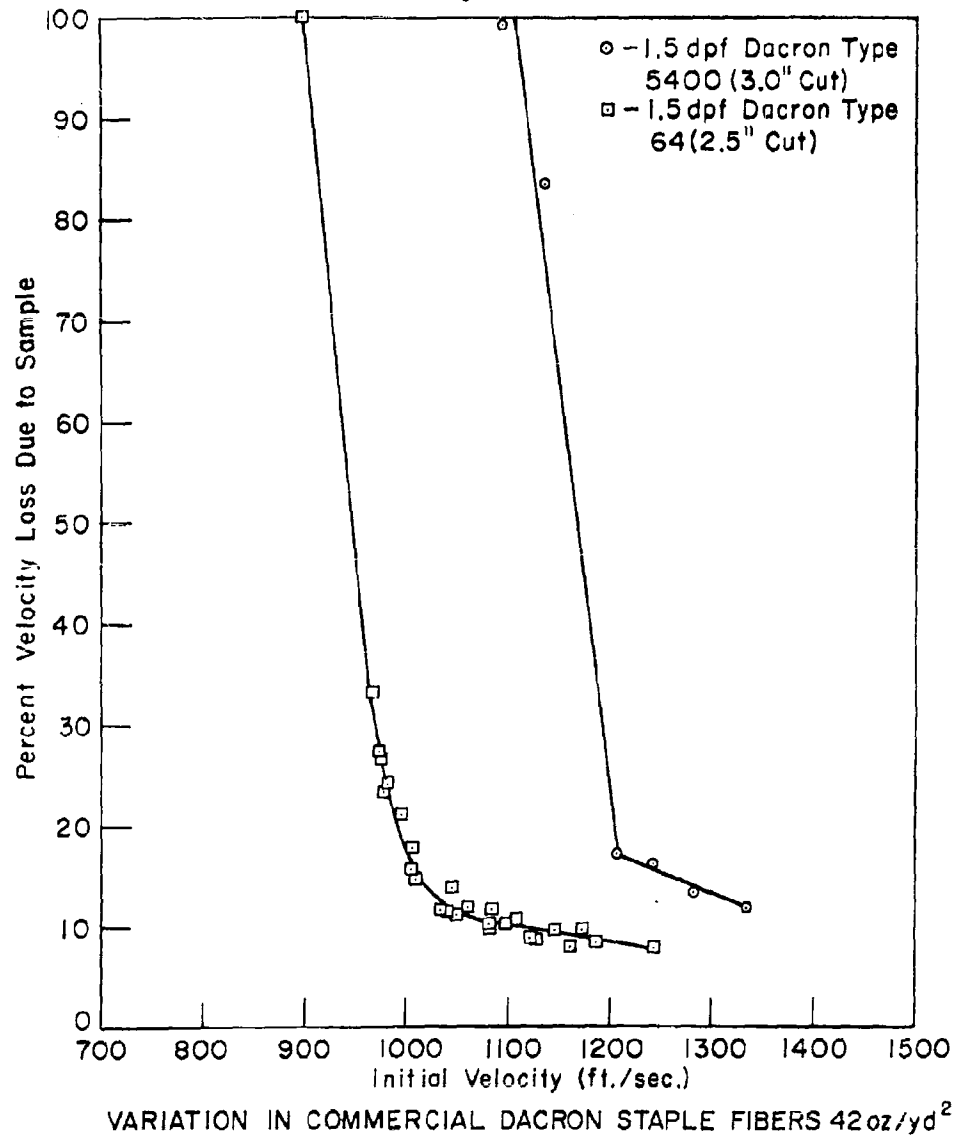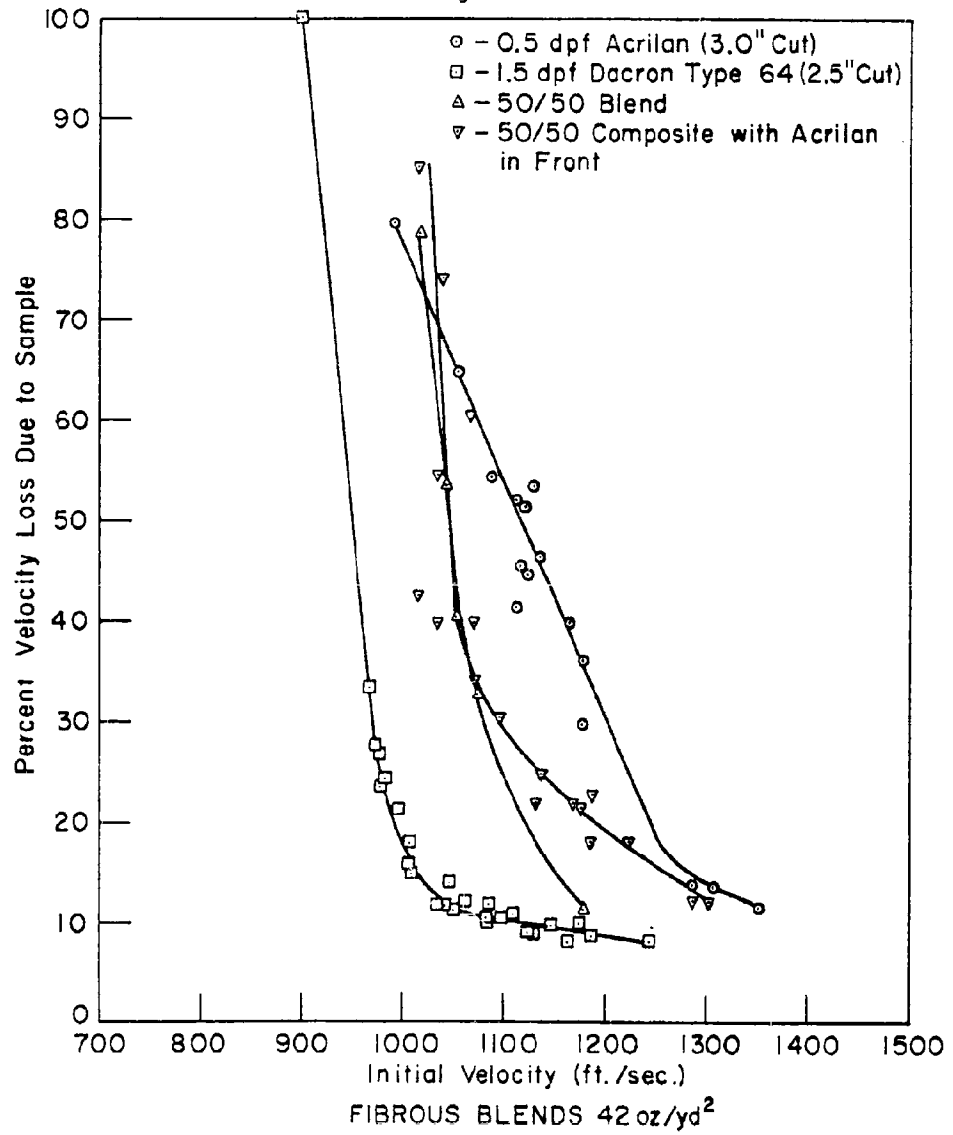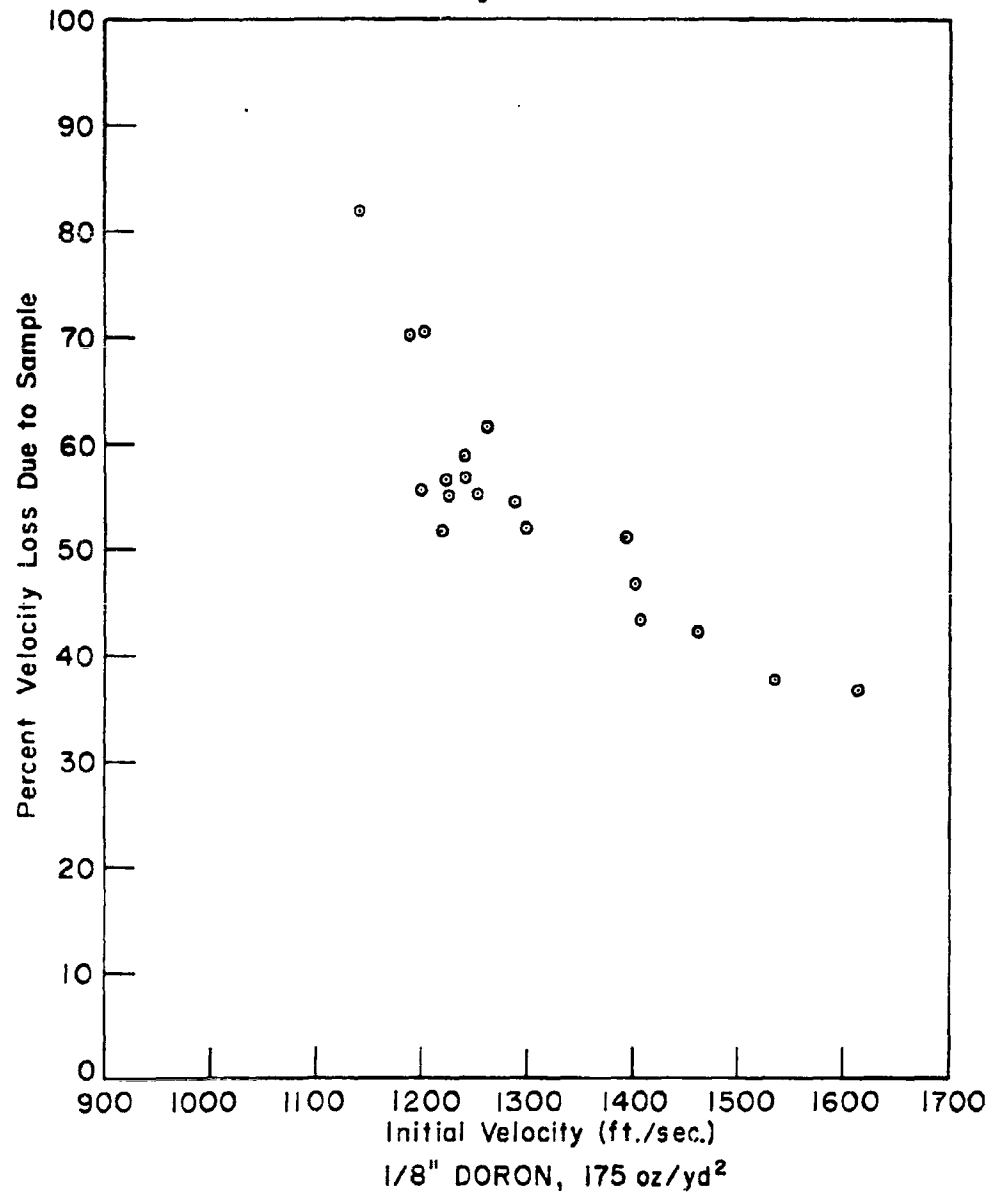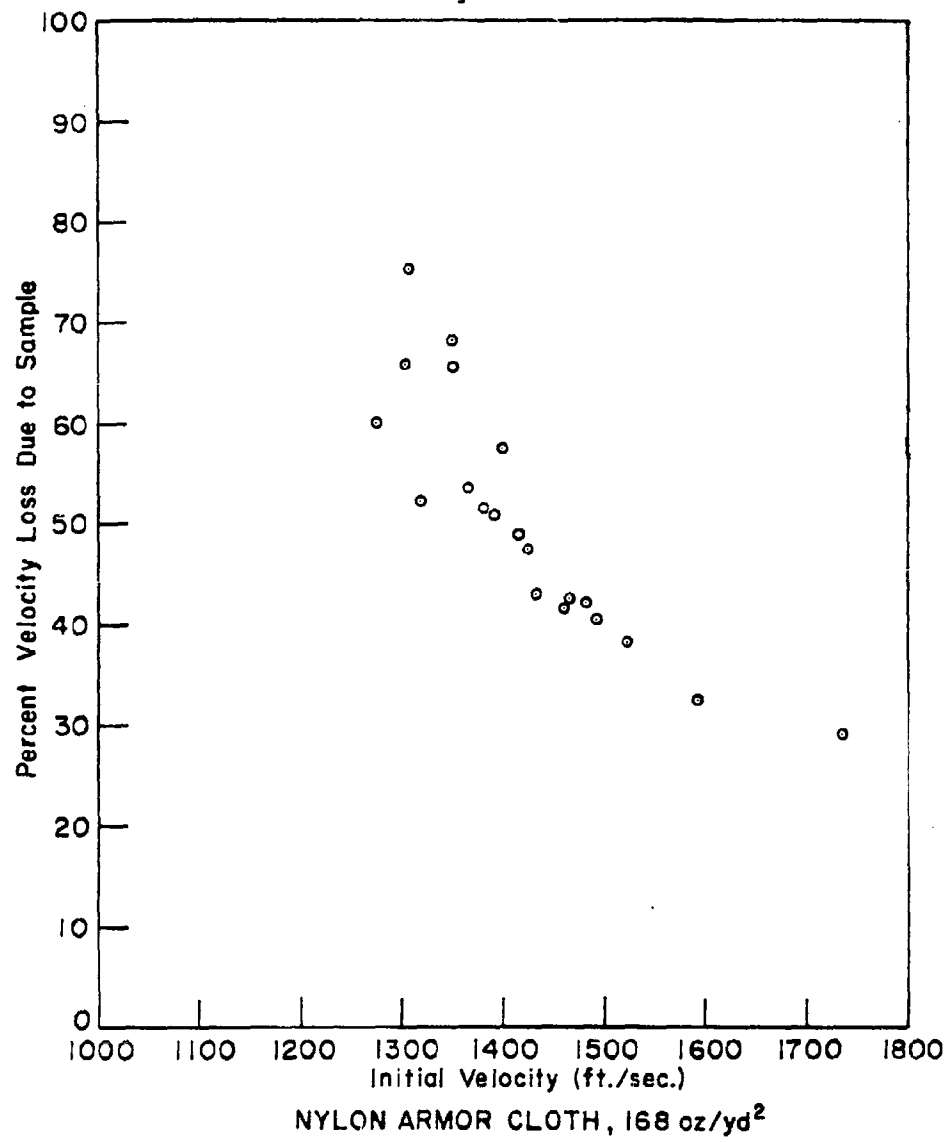
In closing, I wish to emphasize the over-all contributions of buoyancy and thermal insulation to personnel body armor. Our tests have shown that batts composed of these hydrophobed "fine" fibers are vastly superior to many thermal insulating liners presently in use, such as both solid and perforated Polyvinylchloride foams.

SOME U. S. ARMY RESEARCH OFFICE SPONSORED RESEARCH

Dr. Sherwood Githens, Jr.
Deputy Chief Scientist
U. S. Army Research Office
Box CM, Duke Station, Durham, N. C.

Selected basic research projects sponsored by the U. S. Army Research Office having possible applications to the development of body armor were discussed by Dr. Githens.

Identification of these projects by proposal number and title with a brief of the scope of the projects is given below. A compilation of the projects including bibliographies may be obtained upon request to Dr. Githens at the address given above.

1235-E STUDY OF THE MECHANISMS OF THE INITIATION OF PLASTIC FLOW AND FRACTURE IN METALS

Scope: Investigations will be made of the initiation of: (1) brittle fracture in steel in the presence of notches; (2) fracture in single crystals of zinc; and (3) yielding in zinc single crystals associated with the initiation of fracture.

1253-E RESEARCH AND DEVELOPMENT AND THEORETICAL ANALYSIS OF SCABBING IN MATERIALS

Scope: (1) Studies will be continued on scabbing damage in materials and on stress wave propagation and dynamic properties of materials affecting scabbing; (2) theoretical analysis of stress waves in hardened steel plates, effect of backing materials, elasto-plastic and shock-type disturbances, and delay-time effects will also be studies; and (3) an experimental program will be set up to study brittle fracture in metals using plaster-of-Paris models.

1283-E A STUDY OF PHOTOELASTICITY, PHOTOPLASTICITY, AND PHOTOELASTIC
        MATERIALS

Scope: The study is being continued on (a) three-dimensional photo-
elasticity of non-spherical objects; (b) dynamic photoelasticity;
(c) improvement of photoelastic materials; and (d) photoplasticity.

1325-E PROPAGATION OF ELASTIC AND PLASTIC STRAIN PULSES IN BOUNDED
        SOLIDS

Scope: (1) An attempt will be made to analyze theoretically the
effect of the lateral inertia of a bar on the dispersion of a plastic
strain pulse in a cylindrical bar; (2) experimental studies will be
extended on the propagation of plastic strain in a lead bar, particu-
larly with the use of single crystal or extruded specimens; and
(3) preliminary studies will be made with geometrical shapes other
than that of a uniform cylindrical bar to determine the feasibility
of obtaining extremely high stresses in solids by implosion.

1740-E ULTRASONIC MODEL STUDY OF ELASTIC WAVES IN LAYERED MEDIA

Scope: By the utilization of ultrasonic elastic waves, a study will
be made of the physical properties of layered media. Specific ob-
jectives will include: (1) the flexual wave propagation in plates
of varying thickness; and (2) the study of the radiation pattern of
compressional and shear waves originating in certain types of ruptures
such as fault slips. Attempts will be made to separate effects at the
source from those of propagation.

1892-E STRESS ANALYSIS IN VISCOELASTIC MATERIALS

Scope: Studies will be made of: (1) use of generalized operators in
viscoelastic stress analysis; (2) development of methods of stress
analysis; (3) investigation of the more general mixed types of
boundary value problems; and (4) effect of unload boundaries which
offer particular difficulties in applying the method of functional
equations.

1929-E RELAXATION SPECTRA OF HIGH POLYMERS AND THEIR EFFECT ON
        VISCOELASTIC RESPONSE

Scope: Research will be concerned with (1) providing spectra of
relaxation times for certain typical cross-linked and linear
polymers; (2) studying the effect of polymer structure and filler on
dynamic behavior as well as on stress relaxation; (3) studying the
effect of temperature with respect to mechanical behavior, particu-
larly with respect to the inhomogeneity produced by temperature
gradients; and (4) establishing rational methods of viscoelastic
analysis for types of polymers based on the experimental results.

102

2573-E   RESEARCH IN FINITE AMPLITUDE WAVE PROPAGATION IN SOLIDS

Scope: Studies will be made of (1) the compression behavior of
aluminum to the point where the stress-strain curve begins to turn
upward; (2) strain rate effects in lead and copper, particularly
with reference to the Malverne theory of strain rate wave propagation;
and (3) dimetral effects in aluminum for the first one and one-half
diameters from the impact face. The method of measuring Poisson's
ratio and dilatation will be applied in all cases.

2589-C   DYNAMIC MECHANICAL PROPERTIES OF POLYMERS AND THEIR SOLUTIONS
         AND GELS

Scope: A study will be made of certain polymers and polymer-plasti-
cizer systems by a double transducer apparatus and other experimental
methods to measure, in each case, the in-phase and out-of-phase
components of the dynamic shear modulus and other time-dependent
properties over a wide range of temperatures and frequencies. The
data will be analyzed to provide certain basic time-dependent and
temperature-dependent functions.

2998-E   STUDIES OF PLASTIC WAVE PROPAGATION

Scope: The research is to consist of both theoretical and experi-
mental studies of flexural waves and of longitudinal waves. In the
theoretical studies, the effects of lateral inertia and shear will
be incorporated in the equations and the experimental work will be
in direct support of the theoretical work. The studies of longitu-
dinal waves will be an extension of the work reported at the Second
Plasticity Symposium at Brown University and sponsored previously by
the University of Texas Research Institute.

3055-E   EFFECT OF RATE OF LOADING AND UNLOADING ON THE DEFORMATIONAL
         BEHAVIOR OF ROCKS

Scope: The dynamics of rock deformation can best be studied through
controlled laboratory experiments in which the important natural
environmental conditions are simulated as realistically as possible.
Such experiments not only provide the basis for valid interpretation
of deformational features in rock, i.e., geologic structure, and a
means of determining the conditions which obtained during the
development of that structure, but they also make possible the pre-
diction of rock behavior under a variety of physical conditions, a
factor of vital importance to many engineering problems. In most
engineering studies of rock properties, the rocks are tested only at
atmospheric pressure. As the behavior of rock under even low con-
fining pressure is often quite different from that under atmospheric
pressure, experimental data obtained at atmospheric pressure may be
misleading, if not meaningless, when applied to situations where
confining pressure must be considered. All rocks beneath the earth's

103

surface are, in effect, subjected to confining pressure, owing to the weight of the overburden and to the restriction of the surrounding medium. Therefore, whenever subterranean construction is to be undertaken, the effect of confining pressure on rock behavior must be considered. The anticipated increase in subterranean construction owing to both improved engineering techniques and necessity (e.g., aquaducts and other tunnels, intelligence centers and nuclear bomb blast caverns or shelters) will require knowledge of the behavior of rocks under confining pressure and a variety of loading conditions in order to construct the safest engineering structure with least difficulty and least expense. The ability to predict the behavior of rock under certain imposed conditions will not only be of value during construction, but will also enable the engineer to design the structure to withstand imposed loads of tectonic or man-made (e.g., nuclear bomb, rocket thrust) origin. Of particular importance to the military is the deformational behavior of foundation rock at rocket launching sites. Non-elastic deformation of the foundation rock at the moment of departure from the launching pad could affect missile trajectory. Geologists have long been aware of the fact that rocks, ordinarily brittle when deformed in the engineering laboratory, commonly undergo flowage when deformed in the earth's crust. The research here outlined will provide geologists and geophysicists with a better understanding of the processes and mechanisms of deformation in rocks and the factors which control individual processes, as well as provide geologists with a basis for the valid interpretation of geologic structure.

3134-E   AN EXPERIMENTAL INVESTIGATION OF DYNAMIC MATERIAL PROPERTIES

Scope: The objective is to determine experimentally the dynamic response of several selected types of material to large amplitude pulse type loading. The experimental techniques have been developed previously by the investigator. A secondary objective of the program will be the determination of the effect of dynamic plastic preloads of known amplitude on the subsequent static behavior of strain-hardening metals.

3176-E   DEVELOPMENT OF A MODEL MATERIAL OF LOW POISSON'S RATIO FOR THREE-DIMENSIONAL EXPERIMENTAL STRESS ANALYSIS

Scope: It is believed that the material exhibiting a low Poisson's ratio could be a material completely different from the ones commonly used at present, or could be one of the materials used at present with transformed properties. In the first case the cooperation of people familiar with the chemistry of resins should be obtained. For the second approach some experience has already been gathered by the investigator by enclosing air bubbles or micro-balloons in the liquid resin before casting it. The results obtained have not been conclusive, but show that the approach is feasible.

It is proposed to approach the solution of the problem following the two ways mentioned above and to determine the mechanical properties of various plastics. One of the plastics exhibiting the desired properties will be singled out, and used to solve a pre-selected three-dimensional elastic problem, either photoelastically or by means of grids.

3263-E MECHANICS OF CREEP AND IMPACT FOR PLASTICS

Scope: This research includes experimental and theoretical studies on the mechanical behavior of selected plastics; covering the creep and impact stress-strain-time behavior for simple and combined stresses. The scope of the studies includes:

1. creep studies

2. high strain rate (impact) studies

3. "equation of state" studies

3267-E STRESS-STRAIN CHARACTERISTICS OF MATERIALS AT HIGH RATES OF STRAIN

Scope: Three materials will be included in the study: copper, aluminum, and iron. Each of these materials will be at least 99.95 percent pure. These particular materials have been selected because a great deal of information is available concerning them, they are relatively simple in molecular structure, and a fairly wide variation in strain-rate sensitivity is expected between them. Strains will be measured as a function of time and distance from the impact end of a semi-infinite bar (12 in. long) of each material at impact velocities of 100 and 400 fps. Stresses and strains will be measured using specimens 1/2-in. and 1 in. long using the pressure bar technique to measure the stresses and resistance strain gages for the strain. The best of all the techniques which have been developed by the investigator during the past ten years for making these measurements will be employed. Specimens of small diameter will be used to reduce the effects of lateral inertia. Stresses and strains corresponding to the conditions of the experimental measurements will be computed.

DEVELOPMENT OF QMC COMPOSITE ARMOR VEST

E. R. Barron
Quartermaster Research & Engineering Command, U. S. Army
Natick, Massachusetts

Man has been on earth but a minute fraction of time in relation to the age of the earth. During this time he has created defenses for his protection that are as unusual as any devised by nature, and are in many instances often remarkably similar. Undoubtedly the animal armor developed in nature must have inspired him to create his own body armor.

Progress in his armor from the rough shield of tanned skins stretched on a wooden frame, came when he found out how to use metal. For many centuries before Christ, the principle of body armor was employed by warriors to strengthen armies and lead them to victory.

Such body armor was adapted to combat conditions and tactics of the times and was of course limited to the available natural materials of sufficient hardness to deflect a blow, the velocity, and intensity of which were limited to human force. He also discovered that the toughness and strength of metals created other problems since a sheet of iron or bronze was rigid.

Rigidity in an armored garment was obvious to the armorer, limiting body movement, causing discomfort, and affecting the combat efficiency of the warrior. The same problems face the designer of present day body armor. The designers imagination is stimulated by the work and experience of the Medieval armorer, who was in essence a technical expert.

One usually envisions armor as the ornate armor of the Knights and the wealthy, used mainly for jousting tournaments and parade, made to order by an army of skilled workers. However contrary to this consensus was the large quantities of armor also developed and used by the common foot soldier, made on a mass production basis.

The Battle of Wisby, which was fought between the Danes and Gottlanders in 1361 demonstrates quite vividly the armorers technical skills and efforts to obtain maximum mobility. A mass grave of 1800 soldiers (see Figure 1) was uncovered accidentally in 1905, which presented the pathetic picture of the horrors that accompanied a war of those days. The army was made up of peasants who patched up and donned old suits of armor for the hand to hand struggle. Twenty-five complete sets of different armor were found. It appeared that different detachments wore different kinds of armor.

The Swedish Museum of Antiquities undertook a comprehensive study of these finds which was finally published in 1941 and may well serve as a primary design handbook for the present day armor technologist involved with rigid materials. The progression of armor at that time, from a small number of large rigid plates to a large number of small plates in order to obtain maximum mobility are illustrated in Figures 2-5.

Among the finds were six different designs and two basic constructions. (See Figure 2.) The coat of plates which is of French and German origin, consisting of from six to 600 plates, using a rivet construction and the llamelar armor of Tibetian origin, (also up to 600 plates) using a leather thong construction (Type VI). Note the use of both horizontal and vertical plates and the three types of openings, the back (Type III), the sides (Type IV), and the front (Type V).

Figure 3 is a typical coat of plates of Type I, found at Wisby using 22 plates with a one piece rigid pivot-type shoulder and opening in the back. Note the extent to which the armorer went to have the plates conform to body contour.

Figure 4 represents the extreme to achieve maximum articulation, a Type V, coat of plates. This armor is unique among the finds, consisting of 495 plates and is a short armless coat open in front where it was held together with buckles. The reinforcing consisted of small narrow plates fastened to the inside of a leather covering by rivets.

The actual dimensions and pattern layout of type V armor are shown in Figure 5. At the bottom, the front is longer than the back by two rows of plates to form a pendent skirt.

Figure 6 illustrates the extent to which shoulder protection and mobility was achieved and which has been utilized in the latest QMC Composite Armor Vest.

By the time of the Middle ages, suits of armor were developed, intricate and ingenious and capable of withstanding shattering blows or vicious sword thrusts. With the coming of firearms, the use of body armor kept declining and with it, the resultant lost art.

107

Even in the Civil War there is valid data that metal body armor was used to protect the thorax and abdomen. Experimentation with various metals and designs was sponsored by the Germans and Allies in World War I. Towards the end of the war fairly large numbers of thoraco abdominal vests were made, but never satisfactorily tried upon the field of battle. Even when reinforced plastics were developed, the same problem of garment rigidity was inherent with all designs.

World War II saw the adaptation of body armor soley for protection of flight personnel in a static and seated position. This was mainly for the reason that the materials with good ballistic resistance were stiff and heavy. The infantryman could not wear it without affecting his efficiency.

Body armor followed an erratic path after World War II. Recognition of the inherent problems had to be determined, in order to provide protection against missiles of various velocities and sizes, in such a manner that the materials and design would not immobilize the soldier.

In modern warfare, top priority has been given to mobility and a vigorous campaign has been waged to reduce the weight of equipment. Increases in fire power greatly augmented the density of wounding agents. Wound ballistic studies and field research under combat conditions directed by the SGO, established the anatomic regional frequency and distribution of wounds. Studies were made which indicated the maximum energy loads that soldiers could carry. It was quite obvious that each additional pound of garment weight reduced proportionately the individual soldier's combat efficiency.

Reaction and the behavior of soldiers, burdened with the weight of body armor, which, as yet, had not proved itself, insofar as inspiring confidence, resulted in the soldier throwing his vest away or refusing to wear it.

During 1947 the QMC developed Body Armor which covered the torso from the base of the neck to just below the waist. The ballistic material consisted of laminated fiberglass composition (Doron). This composition was in the form of flat, square or oblong shaped rigid plates, held in place by a jacket type garment with seamed pockets to hold the plates in position. The plates were arranged in an overlapping manner in order that there would not be unprotected areas due to separation of the plates while the wearer was moving. The rigidity of the "Doron" plates restricted movements and caused discomfort. Bending from the waist was difficult and shifting of the plates aggravated the possibility of unprotected areas.

The Korean War and its high mortality rate emphasized the need for armor. Certain Marine Corps troops were provided a "Doron" plate vest. The QMC considering "Doron" rigid plates as restrictive and heavy, developed a vest utilizing its application of available research information. The progress that was new was the

108

fabrication of body armor of multiple layers of 12 oz. nylon fabric weighing 8 lbs. The weight allowed the soldier to perform his mission without immediate fatigue or discomfort.

This was a first step to provide practical protection to the combat soldier. The reduction in mortality rate, and the reaction to the feeling of safety wearing an armored vest, was dramatic in its effect upon troops in contact with the enemy. The keen acceptance of ballistic protection for the vital areas of the body stimulated several approaches to provide a still more efficient, nylon-type, armored vest.

In the preliminary work conducted by the QMC on the nylon vest, it became evident that even though it consisted of cloth, there were some major problems, regarding; rigidity in certain areas, bulk, compatibility with other field clothing and weapons and the articulation requirements.

Limited studies were conducted by the QMC of the musculature which takes place when the body assumes different typical combat positions.

The gross body dimensional changes in back length of a man in the prone firing position are shown in Figure 7. The back length is diminished some 3" as the arms are placed forward the shoulders are raised and shows the wide range of dynamic changes that take place in seven areas of the back.

Upper torso distortion, Figure 8 shows the torso distortion and how the shoulder breadth is greatly reduced and contraction of the distance between the base of the neck and the end of the shoulder is three inches. The length of the torso on one side is 15-1/2 inches and is changed to 17 inches.

It became evident that because of these gross body dimensional changes, major design changes were required in the nylon vest to compensate for these changes within the vest by using articulating ballistic panels. A definition of articulation is a joining or joint between two separable parts or a moving joint between parts.

Articulation was provided in the back by an action back construction located approximately at the lower tip of the scapular. (See figure 9.) This action compensates for the increase in body dimensions when the scapular is rotated or the shoulder is elevated as shown in this slide. By this simple design technique, two major things were accomplished.

First, minimum lifting of the vest which reduces protection. Note the lower edge of the vest in both slides. There is a minimum of loss of coverage when the soldier is in the firing position.

109

Second, the articulation or overlap at the back also compensates for the excess material caused by the decrease in back measurements and by the ballistic panels overlapping so the helmet will not be pushed forward or off.

Finally, the action principle was also extended to the side openings where an overlapping of the front and back pieces fully protects the wearer from the armpits to the waist during all body movements. This was accomplished without bulkiness or discomfort, and was a considerable advancement over earlier vests which opened and thus exposed the sides of the body.

Figure 10 illustrates that we were not able to fully articulate the shoulder area and chest, resulting in a bunching up of the material and impinging of the material against the neck.

With the advances in ballistic material research and the use of titanium and other rigid metals being considered, the problem of incorporating these materials was evident. A pre-design study of Free Moving Body Armor systems was conducted to further study the work originally initiated by the QMC during development of the Korean Vest.

The surface of the human body twists and stretches, changing its curvature from very concave to very convex, either separately or all at once. Figure 11 illustrates that at any given location it contorts differently and its mode of contortion is different from that of an adjacent location.

The technique used in this initial study was to mark the center line of the back and front of a typical torso, with dots, each separated three inches. When the torso is bent forward, the first three inch space is shortened by one half inch, the second three inches remains constant whereas there is a gradual shrinkage or compression from three inches to three quarters of an inch in the segment of the lower part of the torso. The distortion in bending backward is the reverse and represents a one quarter to one half inch increase in space between dots. At the same time the back center line has a shrinkage of from one quarter to one half inch between segments except in two areas where the dimensions are constant. Bending forward the back line is expanded from one half to one and one quarter inches between dots. Bending to the left and right shows the largest change, from 10 inches to 25 inches. This information was applied in the development of the composite armor vest.

Using newly designed articulating panels consisting of four plies of ballistic nylon and .032 Titanium, a prototype composite armor vest was designed by the QMC, utilizing initially 249 Titanium plates. (See Figure 12.) As the overlap area represents 20 per cent of the total weight, 3-1/4 square and 2-1/4 square size plates were found to provide the least amount of overlap weight, consistent

with required articulation. Plates were attached by either stitching, stapling or in individual cloth pockets. This vest weighed 10 lbs.

The final prototype weighing 8 lbs. 15 ozs. (See figures 13 and 14) selected for field testing has 149 plates, a Velcro front closure system. Note the articulating armored pivot shoulder pad which appears to solve one of the major obstacles in applying rigid metal plates to the shoulder is considered to be a vital medical re-quirement. The vest is considered to be capable of mass production at a cost of approximately $60-$80 per vest. Tests conducted at Mt. Washington, and at Fort Lee from June to August, 1961, using standard cold-wet, cold-dry, hot weather clothing and the new QMC integrated clothing ensembles indicated that of the four models tested, the 8 lb. 15 oz. Vest, with 129 plates did not interfere with test subjects performance in simulating combat activities and was pre-ferred by all test subjects. A user test of this model is planned during FY 62, with type classification scheduled for FY 63.

Now, the question arises, can the newer nylon felt or batting materials be used in this same vest design? Vests of Felt/ Titanium using the same construction have been made leading to the conclusion that the bulk is materially increased, and the articula-ting panels do not function as well as the ballistic nylon because of the nature of the felt type materials. Enlarging the plate size, reducing the number of plates and overlap may solve some of these problems. Progress in this area has been made as a result of more detailed recent study of the body dimension changes associated with movement, so as to deliniate those areas which did not require articulation. This study may well serve as a design criteria hand-book for modern day rigid armor systems.

Instead of merely marking off the center line as in our previous studies, the torso is marked off in two inch squares. A series of motions, with subsequent measurement of the grid dimensional changes indicates the plate size and articulating requirements. (See Figure 15.)

Significant changes are reflected when the arms are raised. The lower third of the torso remains fairly constant whereas the chest and shoulder grids change from horizontal to curved lines. The center line however remains fairly constant.

The back is representative of these changes and indicates the complexity of providing major dimensional and shape changes with rigid materials in the shoulder area. (See Figure 16.)

Figures 17 and 18 shows first the mathematical grid distor-tion which takes place when the hands are raised and Figure 19 the gross dimensional change. As the center line in this position remains fairly constant, it appears that by studying all positions, a variety of stabilizing areas is evident. By hanging or pivoting

plates from these areas, larger plates and improved articulation will be provided. Included in this new effort is the objective of incorporating "graded levels" of ballistic protection. The SGO has indicated this can be accomplished and we are currently working out the levels of protection in terms of material thickness and different materials for the entire torso to provide a more balanced armor vest.

The culmination of all research is an end item. It is thus the responsibility of the armor designer to not only apply the findings of the material researcher, but he must be thoroughly familiar with the combat soldiers activities and assure compatibility of the item with the spectrum of hot and cold weather clothing.

Figure 1

Grave Uncovered in 1905
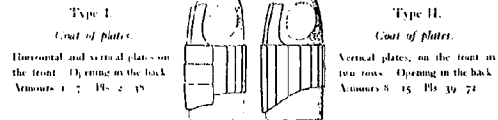
Figure 2   Typical Armor

Figure 3   Type I--Coat of Plates
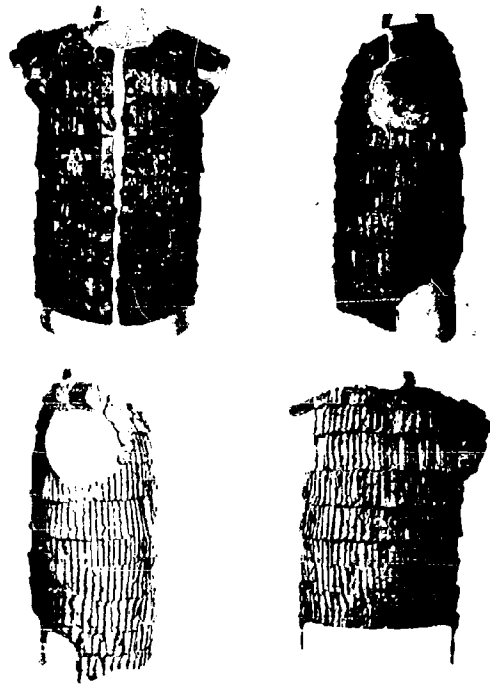
Figure 4
Type V--Coat of Plates
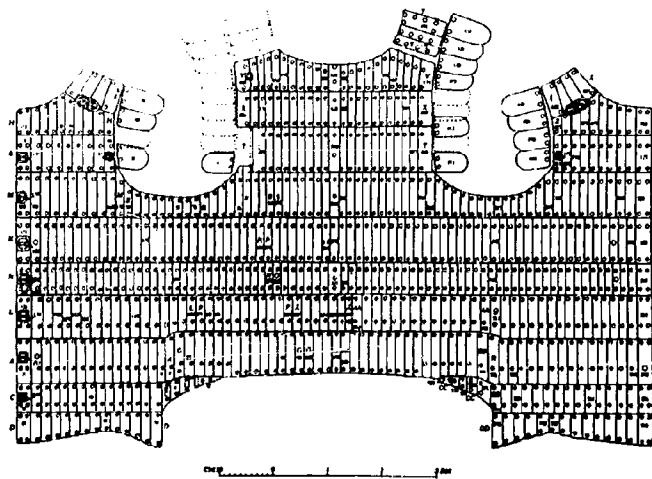
Figure 5
Pattern Layout--Type V Armor

Figure 6

QMC BODY ARMOR DESIGN
BODY DIMENSIONAL CHANGES

	STANDING POSITION	PRONE POSITION
A	FROM 3" TO 1½"	
B	2½	2
C	2½	2¾
D	2½	2½
E	5	4½
F	4½	4
G	6	5

Figure 7

QMC BODY ARMOR DESIGN

DISTORTION IN UPPER TORSO

COMPARATIVE SHADED AREAS
EMPHASIZE SHOULDER BREADTH
REDUCTION, AND CHEST DEPTH
EXPANSION, AND DISAPPEARANCE
OF UPPER CHEST INTO NECK AREA.
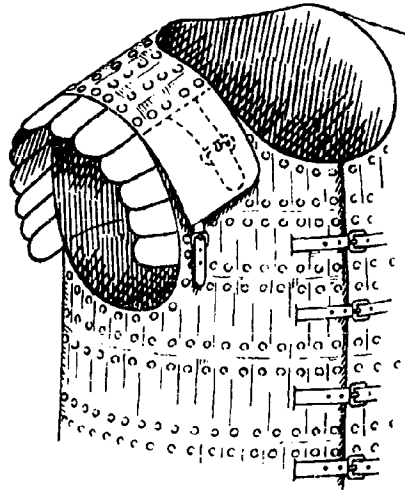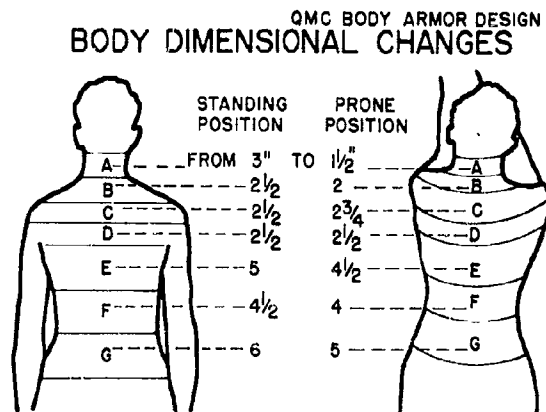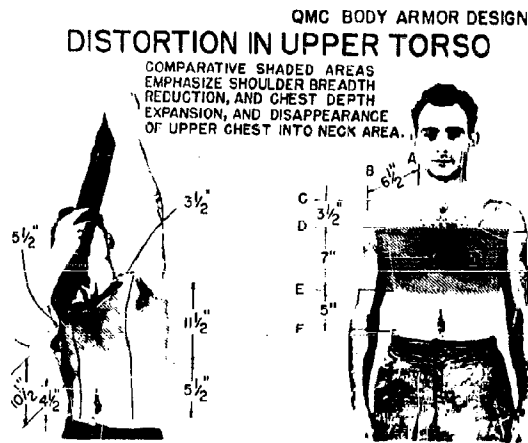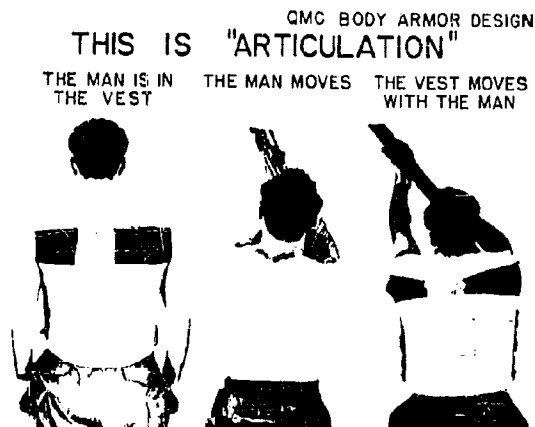
Figure 8

QMC BODY ARMOR DESIGN

THIS IS "ARTICULATION"

THE MAN IS IN THE VEST   THE MAN MOVES   THE VEST MOVES WITH THE MAN

Figure 9

Figure 10

Figure 11

117
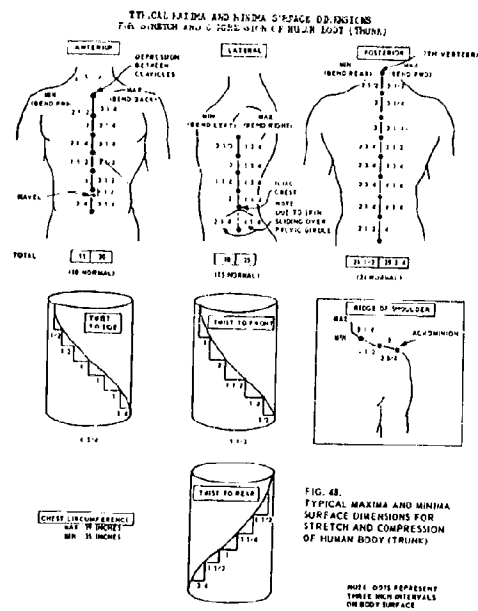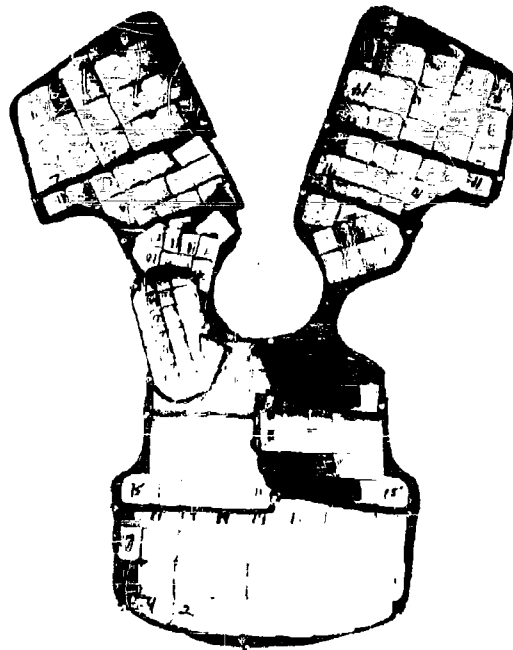
Figure 12

Figure 13
QMC Composite Armor Vest

Figure 14
QMC Composite Armor Vest

Figure 15

Figure 16

Grid Distortion when Raising Arms

Figure 17

121
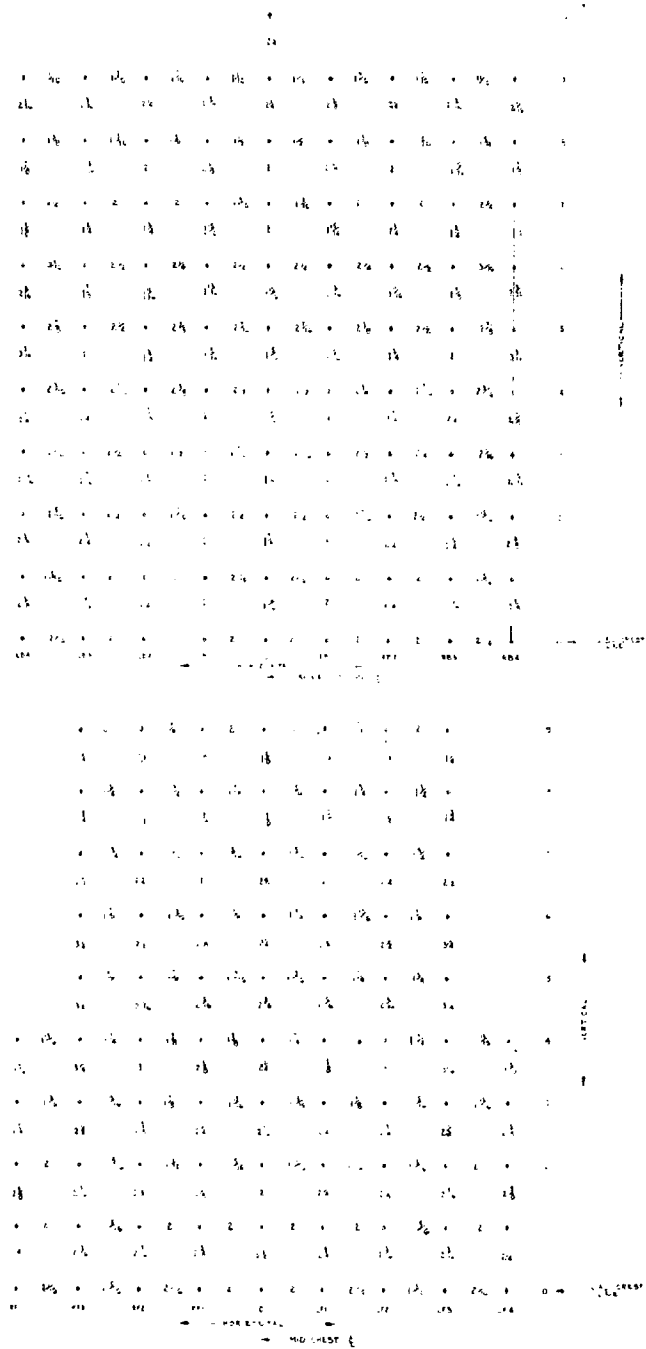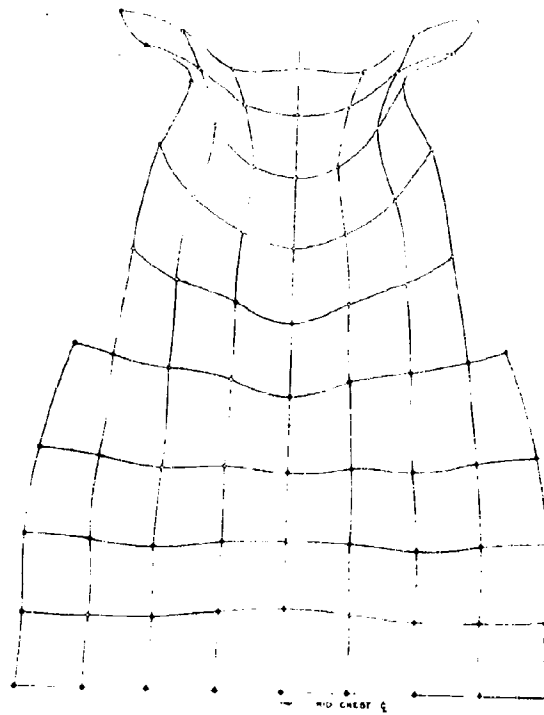
Figure 18

Grid Distortion Raising
Hands
Front & Back View

POSITION IV : FRONT VIEW
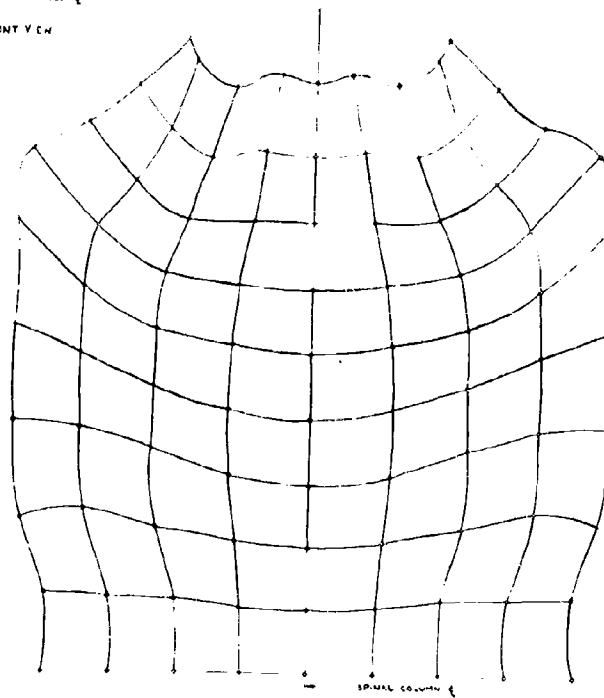
POSITION IV - BACK VIEW

THE EFFECT OF RESIN CONCENTRATION ON PHYSICAL PROPERTIES OF A LAMINATED STRUCTURE FOR A CRASH AND BALLISTIC PROTECTIVE FLIGHT HELMET

Abraham L. Lastnik & John W. Gates
US Army Quartermaster R & E Command
Natick, Mass.

The Quartermaster Corps recently initiated a study to improve the crash protective characteristics of a helmet for Army aircraft crewmen. This report is concerned with the effect of resin concentration on physical properties of a nylon fabric laminated structure.

The present Army aircraft crewman's helmet has a hard shell constructed of glass fiber fabric laminated with polyester resin. This helmet provides good crash protection but very little ballistic protection. Nylon fabric laminated with resin is known to possess ballistic resistance and good energy absorption properties when impacted by missiles. Therefore, it was decided to investigate nylon structures as possible materials in helmet applications, where both ballistic resistance and protection against low speed impact in the event of a crash were essential.

In the preliminary investigations, a ballistic resistant helmet (1), in the shape of a conventional flight helmet with 15 - 18 percent resin content, was impacted with 160 ft-lbs of energy by a striking mass with a velocity of 25 feet per second. The helmet appeared to absorb the energy. High speed motion pictures, however, revealed excessive transient deformation in the impact area which caused the helmet to bottom. Transient deformation is the deflection of a material under load, which recovers rapidly when the load is removed. This deformation is of extremely short duration and usually cannot be detected visually.

Although a helmet structure may appear to absorb impact energy effectively, the occurrence of transient deformation may at the point of impact, cause skull damage. In order to reduce this deformation the rigidity of the helmet was increased by increasing the percent resin from 15 - 18 percent to 35 - 40 percent. This more rigid shell was impacted with 225 ft-lbs of energy by a striking mass with a velocity of 30 feet per second. Though this

123

helmet shell was impacted with approximately 40 percent more energy than the first shell, it did not bottom.

Since energy absorption of the helmet shells appeared to be a function of their rigidity, this study was undertaken to determine the effect of resin concentration (a determining factor on rigidity of the laminated structure) on:

1. flexural modulus
2. energy absorption.

The effect of resin concentration on the resistance to ballistic penetration was also determined. A resume of test results are contained in Table 1.

Table 1

Effects of Resin Concentration on Properties of Test Panels

Sample Number	Resin Content percent	Areal Density oz/ft^2	V50 fps	Flex Mod. $1x10^5$ psi	Energy Absorb. $in-lbs/in^3$
1	15.8	16.83	1070	1.26	8.95
2	17.6	16.96	1039	1.55	10.21
3	25.5	17.37	1047	2.18	11.60
4	31.9	18.09	1054	2.13	12.81
5	32.0	18.19	1053	2.07	13.01
6	42.4	20.75	1042	2.91	22.54
7	42.8	20.43	1055	2.85	21.03
8	51.8	21.90	1051	2.32	29.99
9	53.1	22.32	1090	2.72	32.80
10	72.5	24.96	1127	3.08	45.51
11	75.7	25.15	1119	2.90	46.76

Test panels and helmet shells with varying resin concentrations were fabricated with controlled pressure and cure time. Molding conditions are shown in Table 2.

Table 2

Molding Conditions

	Panels (Flat bed press)	Helmet Shells (Bag Mold)
Heating (minutes)	18	90
Temperature (^oF)	330°-355°	330°-355°
Cooling (minutes)	9	90
Pressure (psi)	400	400

124

The panels are made with 9-plies laminated nylon fabric throughout. The helmet shells are made 9-plies of laminated nylon fabric in the crown section tapering to 5-plies in the ear sections [1]. The laminated structures were fabricated from 14 oz. 2x2 basket weave nylon fabric (2) bonded with polyvinyl butyral modified phenolic resin and a straight phenolic resin on the outer surfaces. The resin content of the samples ranged from 15.8 percent to 75.7 percent. The helmet shells were molded into the shape of a standard flight helmet (3) (4) and are now undergoing testing. The results presented in this study were obtained from tests of the laminated panels only.
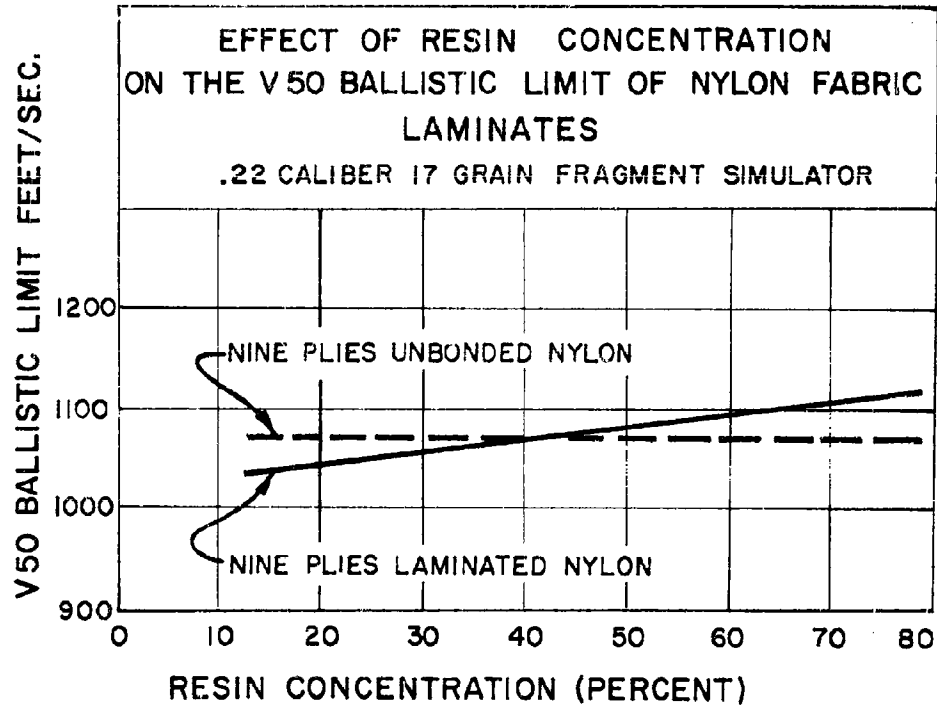
FIGURE 1

Figure 1 and Table 1 show the effect of resin concentration on the V50 ballistic limit of nylon fabric laminate as determined with the .22 caliber, 17 grain fragment simulator. Resin content appears to play a minor role in the ballistic resistance of the laminated structure. The difference in the V50 limit between the high and low resin content structure is approximately ninety feet per second (1039 fps to 1127 fps). Since the V50 limit of unbonded nylon fabric is approximately 1075 feet per second, it is evident that the V50 limit of the laminated nylon is approximately that of the unbonded fabric. Since, in this structure the ballistic resistance is a function of the nylon fabric, increased stiffness can be obtained without penalizing ballistic protection.

An impacted helmet shell appears to dissipate energy by deflecting. Thus, flexural modulus of the test panels and their ability to absorb energy in flexure were studied. Preliminary testing determined that the test specimens would not break during flexural testing. Therefore, a hysteresis type curve was used to determine the flexural modulus as well as the energy absorbed by each specimen.

The flexural modulus of each sample and the energy it absorbed was determined by center beam loading using a 4-inch span. Each specimen, $\frac{1}{2}$-inch by 6-inches and nominally $\frac{1}{4}$-inch thick was loaded and unloaded at the rate of 5-inches per minute. This rate was selected so that all specimens would maintain contact with the load during the unloading phase. Each specimen was deflected 0.74 inches; beyond this point there would have been noticeable slippage at the support beams.
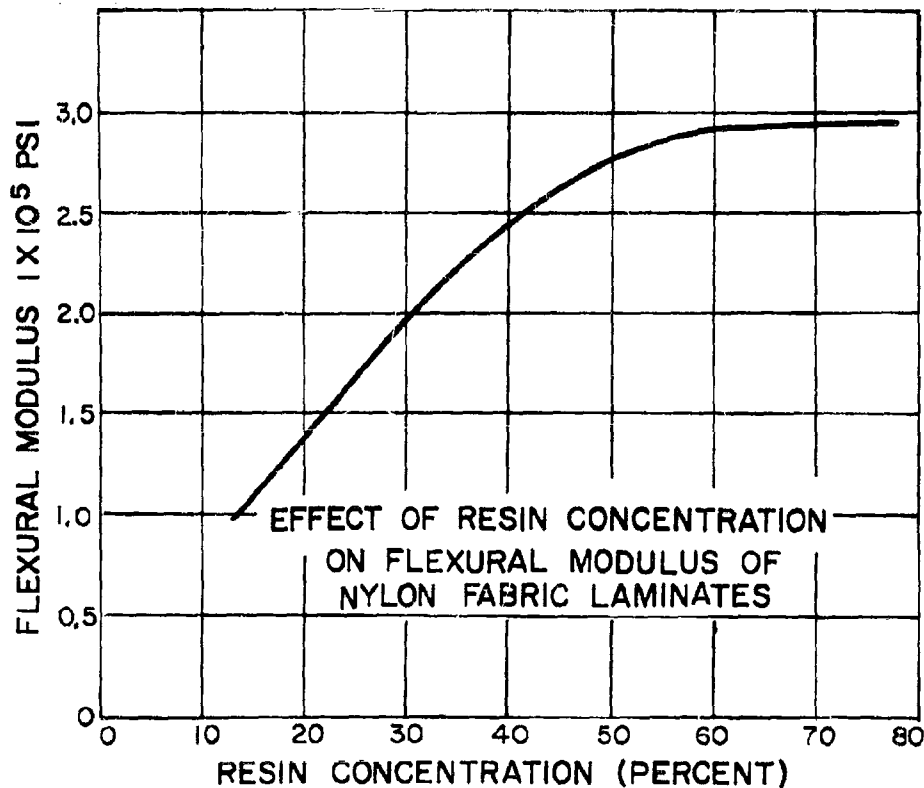
FIGURE 2

Figure 2 and Table 1 show the effect of resin concentration on the flexural modulus of the nylon fabric laminates. The effect of resin concentration on modulus is pronounced between 15 and 40 percent as is shown by the linear portion of the curve. Beyond

40 percent, increased resin concentration will add weight to the structure with no significant effect on flexural modulus. Thus it may be reasonable to assume that nylon fabric laminates with 40 percent resin will provide a helmet structure most suitable for resisting deformation.

Although loading rate will significantly affect flexural strength, it has no apparent effect on flexural modulus (5). Thus, if flexural data can be obtained from helmet structures in a crash situation, it may be possible to relate these data with flexural moduli of similarly constructed panels at lower rates of loading. Instrumented helmets have been used in controlled crash studies of helicopters; the data are being analyzed.

Figure 3 and Table 1 show the effect of resin concentration on energy absorption on the nylon laminates. Energy absorption was determined by measuring the area formed by the loading and unloading curves. Since creep was not considered, the loading and unloading curves did not form a true hysteresis loop. The energy absorbed by the laminates increased linearly with increased resin concentration and with increased stiffness. This confirms the findings of the first exploratory tests with ballistic resistant helmets.
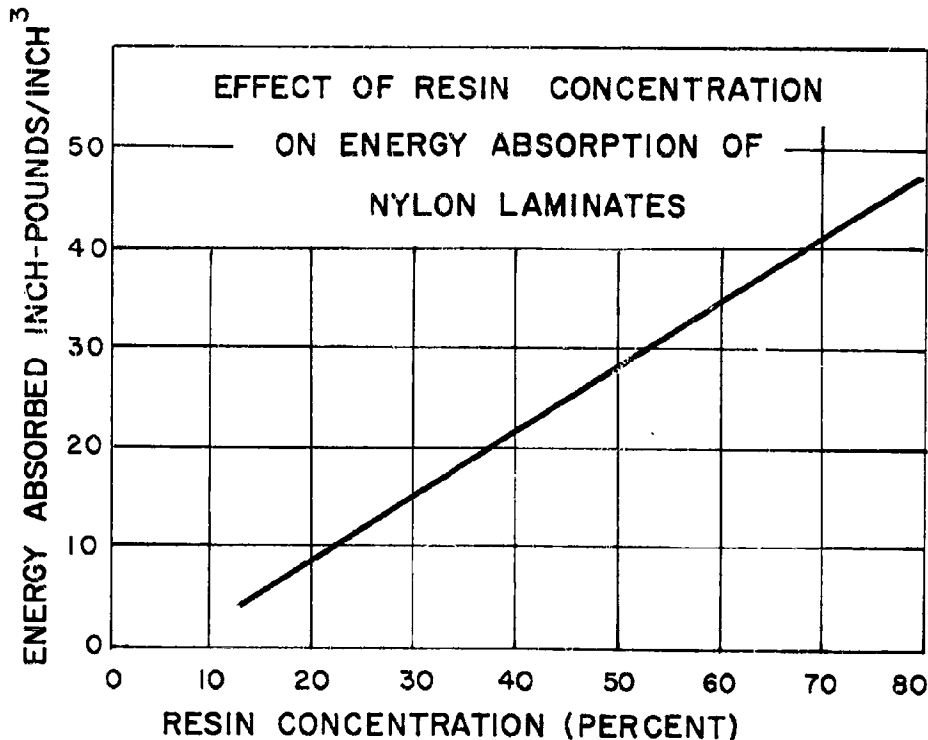
FIGURE 3

The effect of resin concentration on hardness and on tensile properties of the test panels will also be investigated.

The second phase of this study is the investigation of the effect of resin concentration on the crash protective characteristics of laminated helmet shells. Information derived from this series of tests will include energy absorption data and deflection characteristics of the helmet structures.

The findings in this report may be summarized as follows:

1. Resin content has little influence on the ballistic resistance of the laminate.

2. Energy absorbed by the laminate increases with increased resin concentration.

3. Resin content above 40 percent will increase the weight of the laminate without significantly affecting the flexural modulus.

This report is the first of a series of evaluations which will determine the physical characteristics of fabric-resin combinations as they are related to energy dissipation. Those characteristics found to be essential for providing crash protection will be fully exploited in the development of an improved flight helmet.

References

(1) Alesi, A.L. and Landsberg, M.I., Two Unique Plastic Helmets, Technical and Management Conference of the Reinforced Plastics Division, Society of Plastics Industry, Chicago, Illinois. February 1960.

(2) Military Specification MIL-C-12369, Cloth, Nylon, Ballistic for Armor.

(3) Military Specification MIL-H-19366, Helmet: Pilot's Protective, Type APH-5.

(4) Military Specification MIL-H-22995, Helmet: Pilot's Protective, Type APH-6.

(5) Zinzow, W.A., Flexural Properties of Plastics, ASTM Bulletin No. 134, May 1945.

A SET OF ANGLES OF OBLIQUITY FOR USE IN ASSESSING BODY ARMOR

Herbert Maisel, Wallace Chandler, and Gerald DeCarlo
Office of the Quartermaster General
Department of the Army
Washington 25, D. C.

Abstract

Measures of the effectiveness of body armor have been obtained in the past assuming the angle of obliquity is zero, i.e., that the projectiles strike the armor normal to its surface. Since penetrability is a function of the angle of obliquity, it is important to determine the set of angles likely to be encountered to and to use this set when assessing body armor. An estimate of the distribution of the angles of obliquity was obtained for fragments striking the upper torso. It turned out in this situation that the proportion of angles of obliquity less than X degrees is approximately $2X\%$ for $0 \leq X \leq 40$, $(X + 40)\%$ for $40 \leq X \leq 60$ and 100% for $X \geq 60$. The procedure used to obtain this estimate is directly applicable to making similar estimates for other parts of the body.

The paper presented by Mr. Maisel was not reproduced in these proceedings since it is available as a published report and may be obtained upon request from the Office of the Quartermaster General, Department of the Army, Washington 25, D. C.

ATTENDEES

ABBOTT, Kenneth H.   Watertown, Arsenal, Watertown, Mass.

ABERNATHY, Leo   Bureau of Naval Weapons, Department of the Navy, Washington 25, D. C.

AGEN, Helen E.   Quartermaster Research and Engineering Center, Natick, Mass.

ALESI, Anthony L.   Quartermaster Research and Engineering Center, Natick, Mass.

AZRIN, Morris   Quartermaster Research and Engineering Center, Natick, Mass.

BARRON, Edward R.   Quartermaster Research and Engineering Center, Natick, Mass.

BENNETT, Lt Col Robert H.   Army Research Office, Office, Chief of Research and Development, Wash., D.C.

BERMAN, Allen   Ordnance Corps, Picatinny Arsenal, Dover, New Jersey

BEYER, James C.   Office of the Surgeon General, Dept. of the Army, Washington 25, D. C.

BOWE, Jesse C.   U. S. Army Infantry School, Ft. Benning, Ga.

BREISCH, Kenneth E.   Office of Naval Research, Department of the Navy, Washington 25, D. C.

BURNER, Alvin M.   Office of the Surgeon General, Hq, U.S. Air Force, Washington 25, D. C.

COMBS, Carlton E., Jr.   Hq, U. S. Continental Army Command, Fort Monroe, Virginia

COOK, Dudley   Quartermaster Research and Engineering Command, Natick, Mass.

CORCORAN, John W.   Beckman and Whitley, San Carlos, Calif.

CROAN, Leonard S.   Office of Chief of Ordnance (ORDTB),
                                 Department of the Army, Wash., D. C.

CRUGNOLA, Aldo M.   Quartermaster Research and Engineering
                                 Center, Natick, Mass.

DERRICK, LeGrande G.   Naval Medical Field Research Laboratory,
                                 Camp Lejeune, North Carolina

DUNHAM, James V.   Frankford Arsenal, Philadelphia 27, Pa.

FENSTERMAKER, Carl A.   National Bureau of Standards, Wash.,
                                 D. C.

FREDERICK, E. R., Jr.   Mellon Institute, 4400 Fifth Avenue,
                                 Pittsburgh 13, Pa.

FUGELSO, Leif E.   American Machine and Foundry Company,
                                 Niles, Illinois

GARDNER, Charles   Office of the Quartermaster General,
                                 Dept. of the Army, Washington 25, D. C.

GAYDOS, George M.   Picatinny Arsenal, Dover, New Jersey

GITHINS, Sherwood, Dr.   Army Research Office, Durham, N. C.

GRAY, Douglas T.   U. S. Naval Weapons Laboratory,
                                 Dahlgren, Va.

HALL, Warren H.   U. S. Naval Weapons Laboratory,
                                 Dahlgren, Va.

HARRIS, Bravid W. III   Ballistics Research Laboratories,
                                 Aberdeen Proving Ground, Maryland

HENN, Howard Ralph   U. S. Naval Medical Field Research Lab.
                                 Camp Lejeune, North Carolina

HODI, Frank S.   Watertown Arsenal, Watertown, Mass.

JASKOWSKI, Michael C.   Mellon Institute, 4400 Fifth Avenue,
                                 Pittsburgh 13, Pennsylvania

KASDORF, Frank W.   U. S. Naval Weapons Laboratory,
                                 Dahlgren, Va.

KATLIN, Jesse M.   Frankford Arsenal, Philadelphia 27, Pa.

KYMER, James R.   Frankford Arsenal, Philadelphia 27, Pa.

LAIBLE, Roy C.   Quartermaster Research and Engineering
                                 Center, Natick, Mass.

LANDSBERG, Meyer I.   Quartermaster Research and Engineering
                                 Center, Natick, Mass.

LASTNIK, Abraham L.   Quartermaster Research and Engineering
                                 Center, Natick, Mass.

LEOPOLD, Robert S.   U. S. Naval Medical Field Research Lab.,
                                 Camp Lejeune, North Carolina

LEWIS, Frederick J., Jr.   U. S. Naval Medical Research Institute,
                                 Bethesda, Md.

LEY, Herbert L.   Army Research Office, Office, Chief of
                                 Research and Development, Washington, D.C.

MACKLIN, Daniel, K.   Hq, U. S. Marine Corps, Department of
                                 the Navy, Washington, D. C.

MAGRAM, Sidney J.   Office of Chief of Research and
                                 Development, Department of the Army
                                 Washington 25, D. C.

MAISEL, Herbert   Office of the Quartermaster General,
                                 Dept. of the Army, Washington 25, D. C.

MASCIANICA, Francis S.   Watertown Arsenal, Watertown, Mass.

McWHORTER, John C., Jr.   Army Research Office, U. S. Army,
                                 Arlington Hall Station, Arlington 12, Va.

MERRITT, Elmer V.   U. S. Army Transportation Research Command
                                 Fort Eustis, Lee Hall, Va.

MINARD, David   U. S. Naval Medical Research Institute
                                 Bethesda, Md.

MORGAN, Henry M.   National Academy of Sciences, National
                                 Research Council, Washington, D. C.

MURDOCK, John E., Jr.   Quartermaster Board, U. S. Army
                                 Fort Lee, Va.

MYERS, Keith A.   Ballistics Research Laboratories,
                                 Aberdeen Proving Ground, Md.

NOBLE, Richard F.   Marine Corps Landing Force Development
                                 Center, Equipment Board, Quantico, Va.

ODDY, Robert V.   Office of Naval Research, Department of
                                 the Navy, Washington, D. C.

OGILVIE, Bruce C.   Marine Corps Landing Force Development
                                 Center, Marine Corps Schools, Quantico,
                                 Va.

PLESS, William C.   Ballistics Research Laboratories
                                 Aberdeen Proving Ground, Md.

QUINLAN, John F.   U. S. Naval Medical Field Research Lab.
                                 Camp Lejeune, North Carolina

SEERY, Thomas J.   Bureau of Supplies and Accounts, Dept.
                                 of the Navy, Washington 25, D. C.

SCHIEFER, Herbert F.   National Bureau of Standards, Washington,
                                 D. C.

SCHAUB, W. K.   Office of Naval Research, Dept. of the
                                 Navy, Washington, D. C.

SHOUSE, Paul   National Bureau of Standards, Washington,
                                 D. C.

SMITH, Harvey N.   Hq, U. S. Marine Corps, Department of the
                                 Navy, Washington, D. C.

SMITH, Jack C.   National Bureau of Standards, Washington,
                                 D. C.

SPERRAZZA, Joseph   Ballistics Research Laboratories
                                 Aberdeen Proving Ground, Md.

STALLMAN, Arnold S.   U. S. Army Infantry School, Ft. Benning,
                                 Ga.

STEWART, George M.   Army Chemical Center, Edgewood Arsenal,
                                 Maryland

TANEHOLTZ, Stanley D.   Quartermaster Research and Engineering
                                 Center, Natick, Mass.

TARR, Allan L.   Office of Chief of Research and
                                 Development, Department of the Army,
                                 Washington 25, D. C.

134

TERPENNY, Russell

Quartermaster Board, U. S. Army, Fort Lee, Va.

WAREHAM, George B.

Office of Defense Research and Engineering Department of Defense, Washington 25, D.C.

WEINSTOCK, Lionel I.

U. S. Naval Supply Center, Bayonne, N. J.

WITT, David Hampton

Ballistics Research Laboratories Aberdeen Proving Ground, Md.

NAVAL RESEARCH LAB ATTENDEES

Irwin, George R.

Sanders, W. H.

Trent, H. K.

Snipes, T. G., Maj. USMC

Smith, H. L.

McKinney, Karl R.

Ewing, H. O. Jr.

McGogney, D. P.

Ziffer, Arthur

Ferguson, W. J.